12-15-2016

The Interaction of Mercury and Methylmercury with Reduced Sulfur: Implications for the Transformation of Mercury and Methylmercury in the Environment

Nashaat M. Mazrui
University of Connecticut, mzrnash@gmail.com

The Interaction of Mercury and Methylmercury with Reduced Sulfur: Implications for the Transformation of Mercury and Methylmercury in the Environment.

Nashaat M. Mazrui, Ph.D.

University of Connecticut, 2016

Abstract

The formation of mercury sulfide nanoparticles (β-HgS*(s)*$_{nano}$) from inorganic mercury (Hg^{II}), dissolved sulfide, and marine DOM extracted from: Eastern Long Island Sound, Western Long Island Sound and at the shelf break of the North Atlantic Ocean was studied. All the DOM used led to the formation of stable β-HgS*(s)*$_{nano}$ however, DOM extracted from the shelf break was less effective at inhibiting growth of β-HgS*(s)*$_{nano}$ relative to coastal DOM. It is also shown that the β-HgS*(s)*$_{nano}$ are stable in the dark and in the absence of oxygen, but that they slowly aggregate in the presence of light and oxygen. Aside from the precipitation of β-HgS*(s)*$_{nano}$ from dissolved species, we also show that Hg containing nanoparticles can form in the environment from the interaction of Hg^{II} with metal sulfide nanoparticles. Using steady-state and time-resolved fluorescence measurements we show that Hg^{II} forms a strong complex with CdS*(s)* quantum dots.

We further demonstrate that Hg^{II} added to sediment slurries as β-HgS*(s)*$_{nano}$ was methylated by Hg methylating bacteria more than when Hg^{II} was added to the sediment as microparticles of β-HgS*(s)*. Thus, contrary to popular belief, the precipitation of β-HgS*(s)* in sediments does not always limit the availability of Hg^{II} to methylating bacteria. We also found that Hg^{II} added to sediment slurries as Hg^{II} complexed to thiol groups on DOM is more bioavailable for methylation than other complexes of Hg^{II} with reduced sulfur that are commonly found in the environment, and at least 2 times more than Hg^{II} added to the sediment slurries as Hg*(aq)*. The enhanced availability of Hg^{II}-DOM complexes in sediment slurries, shown here, has not been demonstrated before.

Lastly, we show that methylmercury (MeHg) is converted to dimethylmercury (DMeHg) from the adsorption or complexation of MeHg on metal sulfide surfaces or on low molecular weight thiols, respectively. Based on the measured production rates of DMeHg in our experimental solutions and on the saturation level of surface sites of mackinawite, we propose a reaction mechanism involving two MeHg groups adsorbed on reduced sulfur sites. We suggest that our mechanism could be an important source of DMeHg to ocean waters, which remain largely unknown.

The Interaction of Mercury and Methylmercury with Reduced Sulfur: Implications for the Transformation of Mercury and Methylmercury in the Environment.

Nashaat M. Mazrui

B.Sc., University of Nairobi, 2005

M.E.M., Yale University, 2010

A Dissertation

Submitted in Partial Fulfillment of the

Requirements for the Degree of

Doctor of Philosophy

at the

University of Connecticut

2016

APPROVAL PAGE

Doctor of Philosophy Dissertation

The Interaction of Mercury and Methylmercury with Reduced Sulfur: Implications for the Transformation of Mercury and Methylmercury in the Environment

Presented by

Nashaat M. Mazrui, B.Sc., M.E.M.

Major Advisor _____
Robert Mason

Associate Advisor _____
Jing Zhao

Associate Advisor _____
Penny Vlahos

Associate Advisor _____
Michael Hren

Associate Advisor _____
Fatma Selampinar

University of Connecticut
2016

Dedicated to my parents,

My husband,

And my Sisters.

ACKNOWLEDGMENTS

I would like to thank my advisor Dr. Robert Mason for his guidance and support for as long as I have been his graduate student. He has been a patient, understanding and concerned advisor and I'm humbled to have gotten the opportunity to work with him. His generosity, partying nature and good humor contributed to a relaxed atmosphere in the laboratory and made my life as a graduate student far more interesting. I would also like to thank my associate advisors, Drs. Jing Zhao, Penny Vlahos, Michael Hren and Fatma Selampinar for availing themselves when I needed them. Their criticism and advice during my exam time was valuable and made for a well-crafted research.

Many thanks to Dr. Sofi Jonsson (my awesome collaborator!). In many ways, Sofi has been like my second advisor and no words can convey my sincere gratitude towards her. I have learnt a lot from working beside her for the past two years and I'm truly lucky to have had that opportunity. I am also deeply grateful to the Baumann family. Their good nature and warm house provided not only a supportive and encouraging atmosphere for myself but also a platform to discuss and brainstorm on research ideas in an informal setting. I'm going to miss the many times we cooked and ate together at their residence.

I would also like to thank various graduate students and their advisors, notably, Sravan Thota and Dr. Jing Zhao; Drs. Joseph Awino and Jessica Rouge; John Macharia, Andrew Meguerdichian and Dr. Steven Suib, for assisting me with the expertise and instrumentation necessary for analyzing some of my samples. Many thanks to Dr. Celia Chen, Dr. Kate Buckman, Dr. Vivene Taylor and Amanda Curtis for their help during our field sampling expeditions and their advice during our meetings. Special thanks to Prentiss Balcom, Claudia Koerting and Bridget Holohan for their laboratory support and to Debra Schuler, Janet Laflamme, Patricia Evans, Emilie Hogrebe, and Ashley Orcutt for their administrative support. To past and present members of the Mason lab including, Brian Dimento, Veronica Ortiz, Kathleen Gosnell, Emily Seelen and Amina Schartup, thanks for your assistance every now and then. I'd also like to acknowledge the funding organizations: The National Science Foundation, The Swedish Research Council,

The Marine Science department and the Graduate School at the University of Connecticut for their financial support.

To my family and friends, living abroad and in the US, who have been supportive and encouraging. My parents, especially my mother, for instilling discipline and hard work in her daughters. To my sisters, Luby and Niha, my family in Binghamton, NY and New Brunswick, NJ and many others whom I cannot all mention here, thank you very much for your support and encouragement during my graduate career. To my dear loving husband, you bore the brunt of my frustrations in grad school and have been my punching bag throughout this period. Thank you for the love and support that you have given me and for always being there when I needed you.

List of Selected Abbreviations

MeHg	Methylmercury
DMeHg	Dimethylmercury
DOM	Dissolved Organic Matter
SRB	Sulfate Reducing Bacteria
β-HgS$(s)_{nano}$	Nanoparticles of the mercury sulfide phase, metacinnabar
CdS$(s)_{nano}$	Nanoparticles of cadmium sulfide
SUVA	Specific Ultra Violet Absorption
FeS$(s)_{m}$	The iron sulfide phase, mackinawite
POM	Particulate Organic matter
ELIS	Eastern Long Island Sound
WLIS	Western Long Island Sound
SB	The shelf break of the North Atlantic Ocean
DLS	Dynamic Light Scattering
TEM	Transmission Electron Microscopy
β-HgS$(s)_{micro}$	Microparticles of the mercury sulfide phase, metacinnabar
HOC	High Organic Carbon
LOC	Low Organic Carbon
k_m	Rate constant for the methylation of Hg^{II} to MeHg
DOC	Dissolved Organic Carbon
XRD	X-ray Diffraction Crystallography
BET	Brunauer–Emmett–Teller
NPs	Nanoparticles
SRHA	Suwanee River Humic Acid

Table of Contents

1. Introduction

1.1. Background and Rationale

1.1.1 Exposure and Toxicity of Mercury in the Environment

Mercury (Hg) is a naturally occurring element existing primarily as cinnabar (α-HgS*(s)*) in the earth's crust. It is released to the water, land and air naturally from the weathering of minerals and from volcanic and hydrothermal emissions. With the industrial revolution came intense use of fossil fuels, mining activities and waste incineration. Due to such activities, the anthropogenic sources of Hg to the atmosphere significantly increased and today, the concentration of Hg in the atmosphere is enriched by up to 500% relative to the pre-industrial era.[1-3] Anthropogenic Hg is mostly released to the atmosphere in gaseous form as elemental mercury (Hg^0). The residence time of Hg^0 in the atmosphere is about one year; hence it can be transported over long distances before it is oxidized to Hg^{II} and deposited to land and water by wet and dry deposition.[2,4]

In anoxic environments, mainly in the sediment, Hg^{II} is intracellularly converted to methylmercury (MeHg) by sulfate and iron reducing bacteria.[5-8] The bacteria are suggested to take up dissolved neutral Hg^{II} complexes by passive diffusion across the cell membrane.[9] It has also been suggested that Hg-thiol complexes are taken up accidentally by the bacteria via active transport using a divalent metal ion transporter for essential elements like Zn.[10] The mechanism for the bacterial transformation of Hg^{II} to MeHg was recently shown to involve two types of proteins: a coronoid HgcA protein (the methyl carrier) encoded by the hgcA gene and a 2[4Fe-4S] ferrodoxin HgcB protein encoded by the hgcB gene.[11] Why the bacteria methylate Hg^{II} is unclear, however, it has been hypothesized that the bacteria methylate Hg^{II} to facilitate its transport out of the cell. Thus, Hg methylation by the methylating bacteria would be a detoxification mechanism for the bacteria.[10,12] The MeHg released by the bacteria can be taken up by phytoplankton via passive or active transport from the water column and by benthic organisms from the sediment.[13-16] Inside organisms, MeHg accumulates in lean tissues due to its high affinity for sulfhydryl groups on proteins.[17] As methylation mostly occurs in aquatic ecosystems and because MeHg bioaccumulates and biomagnifies

up the food web, aquatic organisms contain high levels of MeHg relative to terrestrial organisms.[18] Thus, human exposure to MeHg mainly occurs through the consumption of fish, with more than 90% of the US fish eating population consuming marine and estuarine fisheries.[3,18,19]

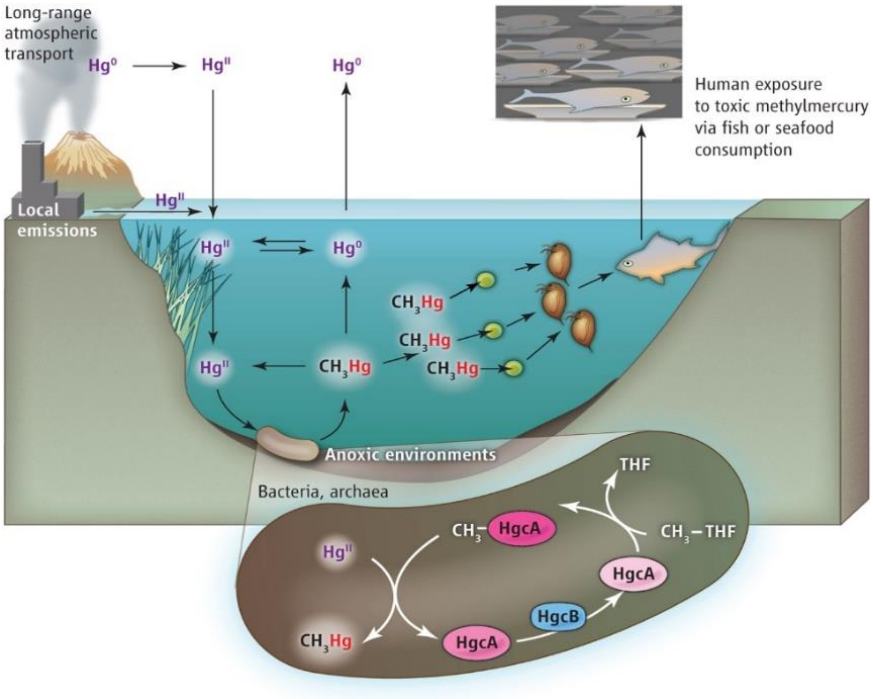

Fig. 1: A simplified illustration of the biogeochemical cycling of mercury in the environment. Adapted from 'Cracking the Mercury Methylation Code' by A.J. Paulain and T. Bakar, 2013, *Science.* 339:1280-1281. Copyright (2013) American Association for the Advancement of Science.

The toxicity of MeHg became widely known after the poisoning event in Minamata Japan, when a chemical company (Chisso Corporation) released their waste water containing MeHg into Minamata Bay. The MeHg was inadvertently produced during the production of acetaldehyde from acetylene gas and H_2SO_4 using HgO as a catalyst. Following increased production of acetaldehyde in the 1950's and 1960's, severe neurological effects were observed in fish, cats, birds and humans.[20] For humans, MeHg poisoning led to a disease now called the Minamata disease, whose effects include difficulty walking and speaking, blindness, fetal abnormalities, microcephaly and death.[21] Today, exposure to lower levels of MeHg is more common with the effects augmented in developing fetuses and children. The neurodevelopmental effects

of chronic low level exposure to MeHg include delays in neurocognitive development, losses in IQ, impaired motor development, cardiovascular effects and endocrine disruption.[21,22] About 6.92 million women of child-bearing age in the US are estimated to have Hg levels of concern.[23] In fact, the most common reason for fish consumption advisories in the US and EU countries today, is the concern for Hg contamination in fish.

In addition to the severe toxicity posed by exposure to MeHg in fish, the long-range transport of Hg^0 across the globe raises ethical questions on issues of transboundary pollutants. A case in point is that of the pristine Arctic ocean where the source of anthropogenic mercury to the ocean is predominantly from long-range transport.[24] In addition, the diet of the Northern Peoples in the Arctic is composed mostly of seafood, including marine mammals.[24] A study by the Arctic Monitoring and Assessment Program (AMAP), reported that more than 50% of mothers and women of child-bearing age have blood levels that exceed 5.8 µg/L—EPA's safe limit.[24] In some Northern communities, mercury levels as high as 40 µg/L have been recorded for mothers, pregnant women, and women of child bearing age.[24] Limiting sea food consumption in these communities and others is not a viable solution as this not only interferes with cultural practices and traditions, but also denies people of the economic and nutritional benefits of consuming fish.

To address the low level chronic exposure to Hg that many fish-eating populations across the world face, the United Nations Environmental Program (UNEP) has promoted negotiations that have led to a multilateral agreement (the Minamata Convention) between nations, requiring them to limit Hg use and emissions to the environment. One challenge in the implementation of the Minamata Convention has to do with the lack of a good understanding of the factors that influence the transformation of one mercury form to another.[25] Relating changes in Hg emissions to MeHg concentrations in fish, is thus a challenge. The forms of Hg commonly encountered in the environment include Hg^0, Hg^{II}, MeHg and dimethylmercury (DMeHg). Apart from reactions responsible for the interconversion of one form to another; the biogeochemistry of each differs. For example, Hg^{II} can be converted to $HgS_{(s)}$, effectively reducing the concentration of mercury in the environment; MeHg is the form of Hg that bioaccumulates in organisms; and Hg^0 and DMeHg are volatile species that are evaded from land and water and transported across the

globe. The conversion of one form to another changes the biogeochemistry of Hg and determines the exposure level and toxicity to populations.

As a soft acid, mercury binds strongly to reduced sulfur (a soft base). Many of the transformation reactions therefore, involve the association of Hg to reduced sulfur compounds. A good understanding of the biogeochemistry of mercury requires knowledge of its reactions with reduced sulfur species. In aquatic systems, mercury forms stable complexes with inorganic sulfide and thiol containing ligands (represented here as RS^-) in dissolved organic matter (DOM).[18,26-28] The stability constants of the complexes formed between mercury and these ligands is much higher than for other mercury complexes, as shown in Table 1. Consequently, in sediment pore water where DOM and inorganic sulfide concentrations are substantial, mercury is found predominantly bound to these ligands.[18,27,29]

Table 1. The thermodynamic stability constants for common complexes of mercury and methylmercury found in natural waters[30]

Reaction	**log K**
$MeHg^+ + RS^- = MeHgSR$	16.50
$MeHg^+ + HS^- = MeHgSH$	14.50
$MeHg^+ + OH^- = MeHgOH$	9.37
$MeHg^+ + Cl^- = MeHgCl$	5.25
$Hg^{2+} + 2\ Cl^- = HgCl_2$	14.00
$Hg^{2+} + 2\ OH^- = Hg(OH)_2$	22.23
$Hg^{2+} + 2\ HS^- = Hg(HS)_2$	37.71
$Hg^{2+} + HS^- = HgS\ (s) + H^+$	36.81
$Hg^{2+} + 2\ RS^- = Hg(SR)_2$	42.00

1.1.2. The Interactions of Hg^{II} with Reduced Inorganic Sulfur

One of the most studied transformation of mercury is that involving the conversion of Hg^{II} to MeHg by mercury methylating bacteria. The conversion of Hg^{II} to MeHg has been shown to depend on bacterial activity and the bioavailability of Hg^{II} complexes.[31] As sulfate reducing bacteria (SRB) are mostly the

bacteria involved in the methylation process, and because mercury methylation occurs during the degradation of organic matter; one of the most dominant mercury complexes present in these environments are those of mercury and dissolved sulfide which has been generated from the degradation of organic matter (represented here as CH_2O) by SRB (Eqn. 1):

$$2CH_2O + SO_4^{2-} \rightarrow H_2S + 2HCO_3^- \qquad (1)$$

The complexes formed between mercury and reduced sulfur have been shown to differ in their availability for uptake by methylating bacteria.[9] Dissolved complexes that form between mercury and sulfur include HgS^0, $Hg(SH)_2$, $HgHS_2^-$, and HgS_2^{2-}. Studies that have modelled the speciation of Hg^{II} in porewater and in pure bacterial cultures, have found a positive relation between the concentration of neutral mercury-sulfide complexes and the production of MeHg in sediment and in the bacterial cultures.[9,30,32,33] It has thus been suggested that it is the neutral complexes that are taken up by mercury methylating bacteria via passive transport across the cell wall of the bacteria.[9]

Under conditions where the precipitation of $HgS(s)$ is favorable, Hg^{II} is sequestered from the dissolved phase as a metal sulfide solid of extremely low solubility. Recent studies suggest that in the presence of organic matter, Hg^{II} precipitates as metacinnabar nanoparticles (β-$HgS(s)_{nano}$), which have been shown in pure cultures to be more bioavailable than the bulk precipitates.[34] β-$HgS(s)_{nano}$ have been detected in natural waters and their formation confirmed in laboratory studies. Deonarine *et al.*, found that the precipitation of $HgS(s)$ in solutions containing Hg^{II}, S^{II-} and thiol ligands or Suwanee River Humic Acid (a model terrestrial DOM isolate) resulted in smaller sized particles and diminished particle growth rates relative to hydroxyl containing ligands or to controls where no organic matter was added.[35] Reduced growth and aggregation rates of $ZnS(s)_{nano}$ and $CdS(s)_{nano}$ have also been observed when precipitation occurs in presence of thiol containing ligands or DOM solutions.[36,37,35,38,39] DOM was found to further prevent aggregation of particles by inducing electro steric repulsive forces. The rate of particle growth in presence

of different freshwater DOM components differed, with variations between them best explained by macromolecular effects such as molecular weight and aromaticity.[35,38-40]

The bioavailability of β-HgS*(s)*$_{nano}$ to methylating bacteria has been studied in pure cultures and in sediment slurries. In both cases, the rate of methylation was enhanced in experiments containing β-HgS*(s)*$_{nano}$ relative to experiments containing commercially available β-HgS*(s)* microparticles.[34,41] Additionally, when different DOM isolates were added with Hg^{II} to pure bacterial cultures of sulfate reducing bacteria, the production of MeHg correlated with the sulfur content and Specific Ultra Violet Absorbance (SUVA) at λ= 254 nm of the DOM isolates (where SUVA is correlated to DOM size and aromaticity).[41] It was suggested that β-HgS*(s)*$_{nano}$ of different sizes and bioavailability precipitated in the pure cultures and contributed to the different rates of MeHg production observed in the experiment.[41] Since methylating bacteria are not known to take up nanoparticles directly, the increased bioavailability of the nanoparticles is suggested to be due to lattice and surface imperfections which are more pronounced for smaller particles.[34]

Previous studies on β-HgS*(s)*$_{nano}$ have focused on low molecular weight thiols and freshwater and soil-derived DOM, and there has been little study of the ability of marine-derived DOM in influencing HgS*(s)* precipitation.[42-45] Dissolved organic matter (DOM) is a complex mixture of organic compounds originating from the exudation and degradation of organisms. Only 20% of DOM has been characterized, and is known to include identifiable compounds such as carboxylic acids, amino acids, and hydrocarbons.[26] The remaining 80% is composed of humic substances of complex structures and various functional groups, with carboxylic and phenols groups as the most abundant and sulfur containing groups found in lower concentrations.[26] It has been shown that DOM from the marine environment is different from DOM in the terrestrial environment and this is bound to affect the precipitation of β-HgS*(s)*$_{nano}$ and impact the bioavailability of mercury to methylating bacteria.[44,46]

Mercury is also known to interact with nanoparticles of other metal sulfide solids present in the environment. For example, nanoparticles of mackinawite (FeS_m*(s)*) have been shown to immobilize Hg^{II}. The sorption of Hg^{II} on FeS_m*(s)* was found to involve the dissolution of FeS_m*(s)* and precipitation of β-

$HgS_{(s)}$ at high Hg^{II}:$FeS_{m(s)}$ ratios, while mixed precipitates of Hg^{II} were formed on the surface of $FeS_{m(s)}$ at low Hg^{II}:$FeS_{m(s)}$ ratios.[47,48] Studies have also shown that cubic $ZnS_{(s)nano}$ can be completely transformed to β-$HgS_{(s)nano}$ by the addition of Hg^{II} to $ZnS_{(s)nano}$ solutions.[49] It is also possible to synthesize mercury doped or mixed mercury cadmium chalcogenide quantum dots for industrial applications.[50-52] The co-precipitation of Hg^{II} with engineered metal sulfide nanoparticles ending up in aquatic systems is thus possible and will change the speciation of Hg^{II} and impact its biogeochemistry.

1.1.3. The Interactions of Hg^{II} with Reduced Organic Sulfur

In the presence of organic matter, mercury forms Hg^{II}-thiol complexes with reduced sulfur groups on DOM in the dissolved phase and on particulate organic matter (POM) in the solid phase. Pure bacterial culture studies, using sulfate reducing and iron reducing bacteria, have shown that Hg^{II} is more bioavailable for methylation when complexed to some low molecular weight thiols and not others; and that the configuration of the thiol also affected the rate of methylation.[10,53] These studies suggest a specific mechanism is involved in the uptake of the Hg^{II}-thiol complexes. Schaefer *et al*., using a series of experiments demonstrated that the uptake of Hg^{II}-thiol complexes by methylating bacteria is likely accidental via a mechanism for the uptake of essential divalent metal ions (e.g. Zn^{II}) by the bacteria.[10,54] As Hg^{II}-thiol complexes are stronger than Zn^{II}-thiol complexes, Hg^{II} easily competes with Zn^{II} for the thiols. Reduced sulfur groups on DOM bind Hg^{II} with a similar affinity as that of the low molecular weight thiols.[29] The effect of Hg^{II} complexation to DOM on methylmercury production in the sediment has however, not been investigated.

It has also been suggested that the availability of Hg^{II} to methylating bacteria is reduced when Hg^{II} binds to reduced sulfur groups on particulate organic matter. Indeed, Jonsson *et al*., showed using isotope enriched mercury tracers that Hg^{II} added to sediment slurries as Hg^{II} bound to terrestrial POM was less available for methylation than when Hg^{II} was added as a $HgCl_2$ complex.[31] In the marine system, organic matter can be of two sources: allochthonous organic matter is from outside sources while autochthonous is produced from within the system by primary producers (e.g. phytoplankton) or from the degradation of

organic matter by bacteria in the sediment.[55] Allochthonous organic matter typically has a higher molecular weight and aromaticity than autochthonous organic matter.[55] In systems with high organic matter content, the % of allochthonous organic matter is higher than that of autochthonous. It has been suggested that the autochthonous organic matter (characterized by more proteins and less humic substances), binds Hg^{II} less strongly than allochthonous organic matter and contributes to the higher methylation rates recorded for low organic matter sites.[30,56-59] While this is true, it has also been shown that bacterial activity is enhanced more in presence of autochthonous organic matter than in presence of allochthonous organic matter.[60] The former organic matter is rich in labile and more easily degraded material thus it stimulates bacterial activity. Whether the binding affinity of Hg^{II} to the two types of organic matter or the effect of the organic matter on bacterial activity is the controlling factor for methylation in the marine environment is yet to be determined.

1.1.4. The Interactions of MeHg with Reduced Sulfur

The net production of MeHg is a net sum of methylation and demethylation processes. The demethylation process is less studied than the methylation; however, it is known to occur in many environments and via both biotic and abiotic mechanisms. Two major pathways for biotic demethylation are oxidative and reductive demethylation. In oxidative demethylation, MeHg is degraded to Hg^{II} while in reductive demethylation, it is degraded to Hg^{0}. The involvement of reduced sulfur species in biotic demethylation is less known but it has been suggested that neutral complexes of MeHg and inorganic sulfur are taken via passive diffusion by demethylating bacteria.[61,62] In a study where seven different freshwater and estuarine sediments in Sweden were included, the dominant complexes of MeHg modelled in the porewater were determined to be MeHgSH, $MeHgS^{-}$, and MeHg-thiol.[61] The demethylation rates in the sites with low mercury concentrations correlated positively with the MeHg complexes of inorganic sulfide.[61] In another study done in pure bacterial cultures of iron reducing bacteria, low concentrations of cysteine were found to inhibit the demethylation process while higher concentrations did not.[63] The

complexation of MeHg with reduced sulfur species thus affects the biotic demethylation process, though the effect is not well understood.

The abiotic demethylation of MeHg though even less studied than biotic demethylation, is known to occur via the reaction of MeHg with reduced sulfur species.[64-66] In the 1970's, scientists discovered that H_2S can demethylate MeHg by forming dimethylmercury (DMeHg) and β-HgS*(s)* via the intermediate bismethylmercury sulfide ($(CH_3Hg)_2S$).[64] More recently studies have found that cysteine and selenocysteine can demethylate MeHg in marine mammals to form HgS/HgSe*(s)* and DMeHg, and it has been suggested that the intermediate steps here are similar to the demethylation of MeHg by H_2S shown in earlier years.[66,67] The intermediate product of the reaction between MeHg and H_2S or cysteine (i.e. $(CH_3Hg)_2S$), is suggested to be unstable and thus spontaneously degrades to DMeHg and β-HgS*(s).* As the overall reaction involves the degradation of two MeHg groups to form one DMeHg and one Hg^{II}, the process both demethylates and methylates MeHg. Thus, the term demethylation of MeHg to describe the degradation pathway of MeHg by reduced sulfur species can be misleading

Just like Hg^{II}, MeHg also adsorbs on FeS_m*(s)*, though the complexation of MeHg with surface sites of FeS_m*(s)* is less strong (log K = 6) than the complexation of Hg^{II} with the FeS_m*(s)* surface sites (log K = 29.6).[68] FeS_m*(s)* in the sediment is produced from the reaction of H_2S and Fe^{II}, with about 10-25% of the H_2S produced by SRB during the degradation of organic matter (Eqn. 1), precipitating as iron sulfide solids.[69-71] As mentioned earlier, the adsorption of Hg^{II} on FeS_m*(s)* has been shown to lead to the precipitation of β-HgS*(s).*[48] No studies have yet determined if MeHg adsorbed on FeS_m*(s)* will also transform to another mercury compound.

1.2. Aims, Goals and Experimental Approach

In light of the above discussion on the interactions of Hg^{II} and MeHg with reduced sulfur species, the aim of this work was to fill the knowledge gaps that exist for the reactions of Hg^{II} and MeHg with reduced sulfur species; and discuss how these reactions impact the conversion of one mercury form to

another. The specific aims of the subsequent chapters in this thesis and associated goals and experimental approach used to fulfill each aim are discussed below.

Specific Aims:

1. To study the formation of β-$HgS_{(s)nano}$ in solutions containing DOM extracted from the marine environment and from the overall dynamics of the interaction of Hg^{II} with metal sulfide nanoparticles.

2. To study the methylation rates, in multiple estuaries, for Hg^{II} complexed to different reduced sulfur species that are commonly found in the sediment.

3. To study if MeHg adsorbed onto $FeS_{m(s)}$, other metal sulfide minerals, as we all as on low molecular weight thiols, can degrade to form DMeHg, similar to the known reaction of MeHg with H_2S.

1.2.1. *Goals for Specific Aim One*:

a) Compare β-$HgS_{(s)nano}$ formed in solutions containing marine dissolved organic matter and in mono and dithiols.
b) Determine the stability of the formed β-$HgS_{(s)nano}$ over time and under light and oxygenated/deoxygenated conditions.
c) Elucidate the interaction of Hg^{II} with $CdS_{(s)nano}$ to understand the potential for Hg^{II} to be incorporated into nanoparticles in the environment

Experimental approach for Specific Aim One:

Marine DOM was extracted using solid phase extraction techniques from 20–50 L of surface waters collected from the eastern and western side of Long Island Sound (ELIS and WLIS, respectively) and at the shelf break of the North Atlantic Ocean (SB). Following the procedure described by Dittmar *et al*., seawater was filtered through a 0.45 µm Meissner cartridge filter and a 0.2 µm glass fiber filter (both pre-rinsed with 0.01 M HCl, > 1 L of ultrapure UV treated water and 1 L of sample water), before loading onto a modified benzene styrene polymer cartridge (pre-rinsed with 6 ml of methanol and 1 L of ultrapure UV treated water) at a rate of < 4ml/min.[72] The cartridge was then rinsed with 40 ml of 0.01 M HCl and dried with Argon gas before the DOM was eluted with methanol followed by acetone.

β-HgS*(s)*$_{nano}$ were formed in the lab from the reaction of 150 µM Hg^{II} with 150 µM HS^- in presence of 10 mg C/L marine DOM or 300 µM monothiols (cysteine, mercaptophenyl acetic acid) or 150 µM dithiols (1,2-ethanedithion and 1,3-propanedithiol). Particle size of the formed β-HgS*(s)*$_{nano}$ was determined by Dynamic Light Scattering (DLS) and UV-Vis measurements. Transmission Electron Microscopy (TEM) was also performed to confirm the diameter and presence of particles in solution. We also compared the formation of β-HgS*(s)*$_{nano}$ using different ratios of Hg^{II}:DOM from where the concentration of reduced sulfur on DOM is lower than the concentration Hg^{II} (1.5 nmol Hg^{II}/mg C), to 150 µmol Hg^{II}/mg C, where particles settled 1 hour after the reaction. To determine the stability of the particles in anoxic conditions, the formed β-HgS*(s)*$_{nano}$ were monitored for over one month. The stability of β-HgS*(s)*$_{nano}$ under different environmental conditions was determined by purging the β-HgS*(s)*$_{nano}$ solutions with air and nitrogen as well as exposing them to light or dark conditions.

To study the interaction between Hg^{II} and CdS*(s)*$_{nano}$, CdS*(s)*$_{nano}$ were formed from the reaction of 150 µM Cd^{II} with 75 µM HS^- in presence of 600 µM cysteine. The optical properties of CdS*(s)*$_{nano}$ were analyzed by UV-Vis and steady state fluorescence measurements. Dissolved mercury was then added to the CdS*(s)*$_{nano}$ solution and the mixture analyzed using UV-Vis, steady state and time resolved fluorescence measurements. CdS*(s)*$_{nano}$ was chosen to represent other metal sulfide nanoparticles/quantum dots that can be found in the marine environment. CdS*(s)*$_{nano}$ were chosen as a model for metal sulfide nanoparticles

species as they are easy to synthesize in the laboratory, are stable to oxidation and can be characterized from their well-studied optical properties. Additionally, unlike iron and copper, cadmium is not complicated by multiple redox states allowing for the examination of the interactions without potential redox reactions occurring.[37]

1.2.2. Goals for Specific Aim Two:

a) Synthesize isotopically enriched Hg^{II} tracers of Hg^{II} complexes commonly found in coastal marine sediments.

b) Compare the methylation rates of prepared solid, adsorbed and dissolved Hg^{II} tracers in sediment slurries, and the potential role of DOM and nanoparticles in influencing methylation.

c) Determine the controlling factor driving differences in the methylation rates between high and low organic carbon sites.

Experimental approach for Specific Aim Two:

Isotopically enriched Hg^{II} tracers were prepared in house from $^{200}HgCl_2$ and $^{199}HgCl_2$ dissolved in 0.1 M HCl followed by a dilution in ultra-pure water. The tracers included ELIS DOM capped β-$HgS(s)_{nano}$, β-$HgS(s)_{micro}$, Hg^{II} complexed to dissolved and particulate organic matter of marine origin (Hg^{II}-POM and Hg^{II}-DOM respectively), Hg^{II} adsorbed on freeze-dried sediments of high and low organic carbon content (Hg^{II}-$HOC_{sediment}$ and Hg^{II}-$LOC_{sediment}$ respectively), and Hg^{II} added as chloride complexes ($HgCl_2$, $HgCl_3^-$ and $HgCl_4^{2-}$) here referred to as $Hg^{II}(aq)$. Hg^{II}-POM, Hg^{II}-DOM, Hg^{II}-$HOC_{sediment}$ and Hg^{II}-$LOC_{sediment}$ were prepared by equilibrating Hg^{II} with POM, DOM, $HOC_{sediment}$ and $LOC_{sediment}$ respectively, for 24 h to allow for strong thiol bonds to form between Hg^{II} and the complexing agent. Both POM and DOM were collected from surface waters of Eastern Long Island Sound. DOM was extracted using a solid phase extraction method (PPL cartridges) as described above. POM was collected by filtering surface waters of ELIS using a 1.0 µm plankton net, after which the collected particles were rinsed, freeze-dried and re-suspended in

ultra-pure water. $HOC_{sediment}$ and $LOC_{sediment}$ were obtained from freeze-dried sediment cores collected during the summer of 2013 from Barn Island high and low organic carbon sites in Connecticut, USA. β-$HgS(s)_{nano}$ and β-$HgS(s)_{micro}$ were synthesized from equimolar concentrations of Hg^{II} and HS^- with and without the presence of ELIS DOM respectively. The particles were aged for 3 days before being added to sediment slurries. Control experiments were performed to determine if added DOM or POM increased Hg^{II} methylation by e.g. altering the activity of Hg^{II} methylating bacteria. In the control experiments, Hg^{II} and DOM/POM were added to sediment without prior equilibration

Fresh sediment slurries were collected in the summer of 2015 from four locations in Connecticut, USA. Acid cleaned polycarbonate core samplers (diameter of 4.8 cm) were used to manually extract 3 cores from each location. Sediment was collected from the top 4 cm of each core, pooled and homogenized in the lab under low oxygen conditions using a N_2 flushed glove bag. Sediment slurries were added to tubes containing the Hg^{II} tracers (n=3 per set) that had been frozen at -80°C. The Hg^{II} spiked sediments were incubated for 0 and 12 h in a water bath at ambient temperature (±2°C), and incubations terminated by freezing the sample tubes in dry ice. Frozen Hg^{II} incubation samples (methylation assays) were freeze-dried and MeHg double extracted into purified water using $CuSO_4/KBr/H_2SO_4$ followed by CH_2Cl_2 before being analyzed using Inductively Coupled Mass Plasma Spectroscopy (ICP-MS). An internal standard of $Me^{201}Hg(aq)$ was equilibrated with 0.5–2 g of freeze-dried sediment before MeHg was extracted from the samples. As the Hg^{II} tracers, the internal standard and ambient mercury are not 100% pure in one Hg isotope, the concentration of MeHg from the Hg^{II} tracers, from the internal standard added and from ambient mercury was determined mathematically using a signal deconvolution matrix. In our calculations, we used the ICP-MS signals for each isotope of Hg in the sample together with the relative isotopic abundance of Hg in the tracers, in the internal standard and in ambient mercury. The methylation rate was the determined using the following equation:

$$k_m\,(d^{-1}) = \Delta[MeHg] \cdot ([Hg^{II}]_{t0} \cdot t(d))^{-1}$$

where k_m is the methylation rate, Δ[MeHg] is the difference in the concentration of MeHg in samples incubated for 12 h and those incubated for 0 h, Hg^{II}_{t0} is the concentration of Hg^{II} in the tracers and t is the time of incubation.

We also determined the natural concentrations of total Hg (HgT) and organic matter (measured as % carbon loss on ignition at 550 °C) in the bulk un-spiked sediments; and analyzed the concentration of HgT, MeHg, dissolved sulfide and organic carbon (DOC) in pore water samples. Fluorescence measurements were also performed on pore water samples extracted from the sites.

1.2.3. Goals for Specific Aim Three:

a) Determine if DMeHg is formed from the reaction between MeHg and metal sulfide solids (FeS_m *(s)*, CdS*(s)* and β-HgS*(s)*).
b) Determine the mechanism for the formation of DMeHg from the reaction of MeHg and FeS_m *(s)*.
c) Compare the formation of DMeHg from the reaction of MeHg and FeS_m *(s)* to that of the reaction between MeHg and dissolved reduced sulfur (thiols and S^{-II}).

Experimental approach for Specific Aim Three:

FeS_m*(s)* was prepared in the laboratory alongside CdS*(s)* and HgS*(s)*. The synthesis involved the addition of 0.6 M sodium sulfide to 0.6 M $(NH_4)_2Fe(II)(SO_4)_2{\cdot}6H_2O$, $Cd(NO_3)_2{\cdot}4H_2O$, and $HgCl_2$, respectively in a N_2 filled glove bag. The particles were purified by washing in ultra-pure water then stored in smaller vials at -80°C until use. Particle characterization was done by X-ray Diffraction Crystallography (XRD) and Brunauer–Emmett–Teller (BET) on freeze-dried metal sulfide vials. In the intital experiments, MeHg was added to FeS_m*(s)* slurries, to the filterate of the FeS_m*(s)* slurry, or to MQ water to confirm that the DMeHg produced was from the adsorption of MeHg on FeS_m*(s)* and not due to any reaction happening in solution.

To elucidate the mechanism of the reaction, a series of experiments were performed to determined the rate of DMeHg formation at different MeHg:FeS_m*(s)* ratios. The ratios were obtained by first holding

the amount of FeS_m*(s)* constant and varying the concentration of MeHg; and then later holding the MeHg concentration constant and varing the amount of FeS_m*(s)* added. Adsorption studies were also performed at the different ratios of MeHg:FeS_m*(s)* and the concentration of MeHg immobilized on the binding sites of the FeS_m*(s)* mineral determined. Experiments were also conducted with the other metal sulfide solids prepared here (CdS*(s)* and HgS*(s)*), with FeS_m*(s)* aged for 1 h, 1 d and 7d; and at different pH and ionic strength. For the reaction between MeHg and metal sulfide solids, the amount of metal sulfide added to the reaction vial was equalized to obtain the same ratio of MeHg:sulfide surface area for all the three solids.

The reaction between MeHg and FeS_m*(s)* was compared to the reaction of MeHg with dissolved inorganic sulfide (added as an aqueous solution of Na_2S) and with thiols (cysteine, mercaptopropionic acid, 1,2-ethanedithiol, and 1,3-propanedithiol). Similar to the procedure describe above, MeHg was added to solutions containing one of the reduced sulfur forms and the amount of DMeHg produced was determined. In all experiments, the MeHg:S ratio was equal to or greater than the ratio of MeHg:FeS_m*(s)*. We also determined the activation energy for the reaction between MeHg and FeS_m*(s)*, and for the reaction between MeHg and dissolved inorganic sulfide. In these experiments, vials were incubated for 0, 40, and 60°C, and DMeHg produced from each reaction determined.

1.3. Summary

The experiments and approaches outlined above were designed to provide further insight into the mechanisms controlling the formation of MeHg in marine sediment. We have studied the role that reduced sulfur has in controlling the form and bioavailability of Hg^{II} to methylating bacteria, and therefore the potential for its methylation to the more toxic and bioaccumulative MeHg. As the net concentration of MeHg in any environment is determined by both its rate of formation and degradation, the studies also provided new insights into the potential for MeHg to be degraded by metal sulfide soilds and low molecular weight thiols. In addition, these studies highlighted a potential pathway for the formation of DMeHg in marine waters. Of all the forms of Hg found in the environment, the pathways for the formation of DMeHg are least understood. While other pathways for its formation may exist, the results presented in this thesis

provide one avenue for its formation. Overall, the results outlined here contribute to a better understanding of the cycling of Hg and methylated Hg in the marine environment.

References

1. Mason, R.P.; Fitzgerald, W.F.; Morel, F.M.M. The biogeochemical cycling of elemental mercury: Anthropogenic influences. *Geochim. Cosmochim. Acta* **1994,** *58* (15), 3191-3198; 10.1016/0016-7037(94)90046-9.

2. Mason, R.P.; Sheu, G.-. Role of the ocean in the global mercury cycle. *Global Biogeochem. Cycles* **2002,** *16* (4), 40-1.

3. Sunderland, E.M.; Mason, R.P. Human impacts on open ocean mercury concentrations. *Global Biogeochem. Cycles* **2007,** *21* (4).

4. Selin, N.E.; Jacob, D.J.; Yantosca, R.M.; Strode, S.; Jaeglé, L.; Sunderland, E.M. Global 3-D land-ocean-atmosphere model for mercury: Present-day versus preindustrial cycles and anthropogenic enrichment factors for deposition. *Global Biogeochem. Cycles* **2008,** *22* (2); 10.1029/2007GB003040.

5. Gilmour, C.C.; Elias, D.A.; Kucken, A.M.; Brown, S.D.; Palumbo, A.V.; Schadt, C.W.; Wall, J.D. Sulfate-reducing bacterium Desulfovibrio desulfuricans ND132 as a model for understanding bacterial mercury methylation. *Appl. Environ. Microbiol.* **2011,** *77* (12), 3938-3951; 10.1128/AEM.02993-10.

6. Gilmour, C.C.; Henry, E.A.; Mitchell, R. Sulfate stimulation of mercury methylation in freshwater sediments. *Environmental Science and Technology* **1992,** *26* (11), 2281-2287.

7. Yu, R.-.; Flanders, J.R.; MacK, E.E.; Turner, R.; Mirza, M.B.; Barkay, T. Contribution of coexisting sulfate and iron reducing bacteria to methylmercury production in freshwater river sediments. *Environ. Sci. Technol.* **2012,** *46* (5), 2684-2691; 10.1021/es2033718.

8. Yu, R.-.; Adatto, I.; Montesdeoca, M.R.; Driscoll, C.T.; Hines, M.E.; Barkay, T. Mercury methylation in Sphagnum moss mats and its association with sulfate-reducing bacteria in an acidic Adirondack forest lake wetland. *FEMS Microbiol. Ecol.* **2010,** *74* (3), 655-668; 10.1111/j.1574-6941.2010.00978.x.

9. Benoit, J.M.; Gilmour, C.C.; Mason, R.P.; Heyes, A. Sulfide controls on mercury speciation and bioavailability to methylating bacteria in sediment pore waters. *Environ. Sci. Technol.* **1999,** *33* (6), 951-957; 10.1021/es9808200.

10. Schaefer, J.K.; Rocks, S.S.; Zheng, W.; Liang, L.; Gu, B.; Morel, F.M.M. Active transport, substrate specificity, and methylation of Hg(II) in anaerobic bacteria. *Proc. Natl. Acad. Sci. U. S. A.* **2011,** *108* (21), 8714-8719; 10.1073/pnas.1105781108.

11. Parks, J.M.; Johs, A.; Podar, M.; Bridou, R.; Hurt Jr., R.A.; Smith, S.D.; Tomanicek, S.J.; Qian, Y.; Brown, S.D.; Brandt, C.C.; Palumbo, A.V.; Smith, J.C.; Wall, J.D.; Elias, D.A.; Liang, L. The genetic basis for bacterial mercury methylation. *Science* **2013,** *339* (6125), 1332-1335; 10.1126/science.1230667.

12. Poulain, A.J.; Barkay, T. Cracking the mercury methylation code. *Science* **2013,** *339* (6125), 1280-1281; 10.1126/science.1235591.

13. Mason, R.P.; Reinfelder, J.R.; Morel, F.M.M. Uptake, toxicity, and trophic transfer of mercury in a coastal diatom. *Environ. Sci. Technol.* **1996,** *30* (6), 1835-1845; 10.1021/es950373d.

14. Moye, H.A.; Miles, C.J.; Phlips, E.J.; Sargent, B.; Merritt, K.K. Kinetics and uptake mechanisms for monomethylmercury between freshwater algae and water. *Environ. Sci. Technol.* **2002,** *36* (16), 3550-3555; 10.1021/es011421z.

15. Lawrence, A.L.; Mason, R.P. Factors controlling the bioaccumulation of mercury and methylmercury by the estuarine amphipod Leptocheirus plumulosus. *Environ. Pollut.* **2000,** *111* (2), 217-231; 10.1016/S0269-7491(00)00072-5.

16. Bowling, A.M.; Hammerschmidt, C.R.; Oris, J.T. Necrophagy by a benthic omnivore influences biomagnification of methylmercury in fish. *Aquat. Toxicol.* **2011,** *102* (3-4), 134-141; 10.1016/j.aquatox.2011.01.006.

17. Seewagen, C.L.; Cristol, D.A.; Gerson, A.R. Mobilization of mercury from lean tissues during simulated migratory fasting in a model songbird. *Sci. Rep.* **2016,** *6*; 10.1038/srep25762.

18. Fitzgerald, W.F.; Lamborg, C.H.; Hammerschmidt, C.R. Marine biogeochemical cycling of mercury. *Chem. Rev.* **2007,** *107* (2), 641-662; 10.1021/cr050353m.

19. Chen, C.Y.; Serell, N.; Evers, D.C.; Fleishman, B.J.; Lambert, K.F.; Weiss, J.; Mason, R.P.; Bank, M.S. Meeting report: Methylmercury in marine ecosystems - From sources to seafood consumers. *Environ. Health Perspect.* **2008,** *116* (12), 1706-1712; 10.1289/ehp.11211.

20. Balogh, S.J.; Tsui, M.T.-.; Blum, J.D.; Matsuyama, A.; Woerndle, G.E.; Yano, S.; Tada, A. Tracking the fate of mercury in the fish and bottom sediments of Minamata bay, Japan, using stable mercury isotopes. *Environ. Sci. Technol.* **2015,** *49* (9), 5399-5406; 10.1021/acs.est.5b00631.

21. Karagas, M.R.; Choi, A.L.; Oken, E.; Horvat, M.; Schoeny, R.; Kamai, E.; Cowell, W.; Grandjean, P.; Korrick, S. Evidence on the human health effects of low-level methylmercury exposure. *Environ. Health Perspect.* **2012,** *120* (6), 799-806; 10.1289/ehp.1104494.

22. Antunes dos Santos, A.; Appel Hort, M.; Culbreth, M.; López-Granero, C.; Farina, M.; Rocha, J.B.T.; Aschner, M. Methylmercury and brain development: A review of recent literature. *J. Trace Elem. Med. Biol.* **2016,** *38*, 99-107; 10.1016/j.jtemb.2016.03.001.

23. Mahaffey, K.R.; Clickner, R.P.; Jeffries, R.A. Adult women's blood mercury concentrations vary regionally in the United States: Association with patterns of fish consumption (NHANES 1999-2004). *Environ. Health Perspect.* **2009,** *117* (1), 47-53; 10.1289/ehp.11674.

24. Kirk, J.L.; Lehnherr, I.; Andersson, M.; Braune, B.M.; Chan, L.; Dastoor, A.P.; Durnford, D.; Gleason, A.L.; Loseto, L.L.; Steffen, A.; St. Louis, V.L. Mercury in Arctic marine ecosystems: Sources, pathways and exposure. *Environ. Res.* **2012,** *119*, 64-87; 10.1016/j.envres.2012.08.012.

25. Mason, R.P.; Choi, A.L.; Fitzgerald, W.F.; Hammerschmidt, C.R.; Lamborg, C.H.; Soerensen, A.L.; Sunderland, E.M. Mercury biogeochemical cycling in the ocean and policy implications. *Environ. Res.* **2012,** *119*, 101-117; 10.1016/j.envres.2012.03.013; 10.1016/j.envres.2012.03.013.

26. Ravichandran, M. Interactions between mercury and dissolved organic matter--a review. *Chemosphere* **2004,** *55* (3), 319-331; 10.1016/j.chemosphere.2003.11.011.

27. Miller, C.L.; Mason, R.P.; Gilmour, C.C.; Heyes, A. Influence of dissolved organic matter on the complexation of mercury under sulfidic conditions. *Environ. Toxicol. Chem.* **2007,** *26* (4), 624-633.

28. Graham, A.M.; Aiken, G.R.; Gilmour, C.C. Dissolved organic matter enhances microbial mercury methylation under sulfidic conditions. *Environ. Sci. Technol.* **2012,** *46* (5), 2715-2723; 10.1021/es203658f; 10.1021/es203658f.

29. Skyllberg, U. Competition among thiols and inorganic sulfides and polysulfides for Hg and MeHg in wetland soils and sediments under suboxic conditions: Illumination of controversies and implications for MeHg net production. *Journal of Geophysical Research: Biogeosciences* **2008,** *113* (G2), - G00C03; 10.1029/2008JG000745.

30. Hollweg, T.A.; Gilmour, C.C.; Mason, R.P. Mercury and methylmercury cycling in sediments of the mid-Atlantic continental shelf and slope. *Limnol. Oceanogr.* **2010,** *55* (6), 2703-2722.

31. Jonsson, S.; Skyllberg, U.; Nilsson, M.B.; Westlund, P.-.; Shchukarev, A.; Lundberg, E.; Björn, E. Mercury methylation rates for geochemically relevant HgII species in sediments. *Environmental Science and Technology* **2012,** *46* (21), 11653-11659.

32. Drott, A.; Lambertsson, L.; Björn, E.; Skyllberg, U. Importance of dissolved neutral mercury sulfides for methyl mercury production in contaminated sediments. *Environmental Science and Technology* **2007,** *41* (7), 2270-2276.

33. Benoit, J.M.; Gilmour, C.C.; Mason, R.P. Aspects of bioavailability of mercury for methylation in pure cultures of Desulfobulbus propionicus (1pr3). *Appl. Environ. Microbiol.* **2001,** *67* (1), 51-58.

34. Zhang, T.; Kim, B.; Levard, C.; Reinsch, B.C.; Lowry, G.V.; Deshusses, M.A.; Hsu-Kim, H. Methylation of mercury by bacteria exposed to dissolved, nanoparticulate, and microparticulate mercuric sulfides. *Environmental Science and Technology* **2012,** *46* (13), 6950-6958.

35. Deonarine, A.; Hsu-Kim, H. Precipitation of mercuric sulfide nanoparticles in NOM-containing water: Implications for the natural environment. *Environmental Science and Technology* **2009,** *43* (7), 2368-2373.

36. Gondikas, A.P.; Jang, E.K.; Hsu-Kim, H. Influence of amino acids cysteine and serine on aggregation kinetics of zinc and mercury sulfide colloids. *J. Colloid Interface Sci.* **2010,** *347* (2), 167-171; 10.1016/j.jcis.2010.03.051; 10.1016/j.jcis.2010.03.051.

37. Mullaugh, K.M.; Luther III, G.W. Growth kinetics and long-term stability of CdS nanoparticles in aqueous solution under ambient conditions. *Journal of Nanoparticle Research* **2011,** *13* (1), 393-404.

38. Deonarine, A.; Lau, B.L.; Aiken, G.R.; Ryan, J.N.; Hsu-Kim, H. Effects of humic substances on precipitation and aggregation of zinc sulfide nanoparticles. *Environ. Sci. Technol.* **2011,** *45* (8), 3217-3223; 10.1021/es1029798; 10.1021/es1029798.

39. Slowey, A.J. Rate of formation and dissolution of mercury sulfide nanoparticles: The dual role of natural organic matter. *Geochim. Cosmochim. Acta* **2010,** *74* (16), 4693-4708.

40. Nason, J.A.; McDowell, S.A.; Callahan, T.W. Effects of natural organic matter type and concentration on the aggregation of citrate-stabilized gold nanoparticles. *Journal of Environmental Monitoring* **2012,** *14* (7), 1885-1892.

41. Graham, A.M.; Aiken, G.R.; Gilmour, C.C. Effect of dissolved organic matter source and character on microbial Hg methylation in Hg-S-DOM solutions. *Environ. Sci. Technol.* **2013,** *47* (11), 5746-5754; 10.1021/es400414a; 10.1021/es400414a.

42. Murphy, K.R.; Stedmon, C.A.; Waite, T.D.; Ruiz, G.M. Distinguishing between terrestrial and autochthonous organic matter sources in marine environments using fluorescence spectroscopy. *Mar. Chem.* **2008,** *108* (1-2), 40-58.

43. Boyd, T.J.; Osburn, C.L. Changes in CDOM fluorescence from allochthonous and autochthonous sources during tidal mixing and bacterial degradation in two coastal estuaries. *Mar. Chem.* **2004,** *89* (1-4), 189-210.

44. Koprivnjak, J.-.; Pfromm, P.H.; Ingall, E.; Vetter, T.A.; Schmitt-Kopplin, P.; Hertkorn, N.; Frommberger, M.; Knicker, H.; Perdue, E.M. Chemical and spectroscopic characterization of marine dissolved organic matter isolated using coupled reverse osmosis-electrodialysis. *Geochim. Cosmochim. Acta* **2009,** *73* (14), 4215-4231.

45. Schmidt, F.; Elvert, M.; Koch, B.P.; Witt, M.; Hinrichs, K.-. Molecular characterization of dissolved organic matter in pore water of continental shelf sediments. *Geochim. Cosmochim. Acta* **2009,** *73* (11), 3337-3358.

46. L. Malcolm, R. The uniqueness of humic substances in each of soil, stream and marine environments. *Anal. Chim. Acta* **1990,** *232* (C), 19-30; 10.1016/S0003-2670(00)81222-2.

47. Jeong, H.Y.; Klaue, B.; Blum, J.D.; Hayes, K.F. Sorption of mercuric ion by synthetic nanocrystalline mackinawite (FeS). *Environ. Sci. Technol.* **2007,** *41* (22), 7699-7705.

48. Jeong, H.Y.; Sun, K.; Hayes, K.F. Microscopic and spectroscopic characterization of Hg(II) immobilization by mackinawite (FeS). *Environ. Sci. Technol.* **2010,** *44* (19), 7476-7483; 10.1021/es100808y.

49. Jaiswal, A.; Ghsoh, S.S.; Chattopadhyay, A. Quantum dot impregnated-chitosan film for heavy metal ion sensing and removal. *Langmuir* **2012,** *28* (44), 15687-15696; 10.1021/la3027573.

50. Smith, A.M.; Nie, S. Bright and compact alloyed quantum dots with broadly tunable near-infrared absorption and fluorescence spectra through mercury cation exchange. *J. Am. Chem. Soc.* **2011,** *133* (1), 24-26; 10.1021/ja108482a.

51. Mews, A.; Eychmueller, A.; Giersig, M.; Schooss, D.; Weller, H. Preparation, characterization, and photophysics of the quantum dot quantum well system CdS/HgS/CdS. *J. Phys. Chem.* **1994,** *98* (3), 934-941.

52. Taniguchi, S.; Green, M.; Lim, T. The room-temperature synthesis of anisotropic CdHgTe quantum dot alloys: A "molecular welding" effect. *J. Am. Chem. Soc.* **2011,** *133* (10), 3328-3331; 10.1021/ja200132d.

53. Schaefer, J.K.; Morel, F.M.M. High methylation rates of mercury bound to cysteine by Geobacter sulfurreducens. *Nat. Geosci.* **2009,** *2* (2), 123-126; 10.1038/ngeo412.

54. Schaefer, J.K.; Szczuka, A.; Morel, F.M.M. Effect of divalent metals on Hg(II) uptake and methylation by bacteria. *Environ. Sci. Technol.* **2014,** *48* (5), 3007-3013; 10.1021/es405215v.

55. Zhang, Y.; Liang, X.; Wang, Z.; Xu, L. A novel approach combining self-organizing map and parallel factor analysis for monitoring water quality of watersheds under non-point source pollution. *Sci. Rep.* **2015,** *5*; 10.1038/srep16079.

56. Yamashita, Y.; Tanoue, E. Chemical characterization of protein-like fluorophores in DOM in relation to aromatic amino acids. *Mar. Chem.* **2003,** *82* (3-4), 255-271.

57. Mayer, L.M.; Schick, L.L.; Loder III, T.C. Dissolved protein fluorescence in two maine estuaries. *Mar. Chem.* **1999,** *64* (3), 171-179; 10.1016/S0304-4203(98)00072-3.

58. Para, J.; Coble, P.G.; Charrière, B.; Tedetti, M.; Fontana, C.; Sempéré, R. Fluorescence and absorption properties of chromophoric dissolved organic matter (CDOM) in coastal surface waters of the northwestern Mediterranean Sea, influence of the Rhône River. *Biogeosciences* **2010,** *7* (12), 4083-4103; 10.5194/bg-7-4083-2010.

59. Hammerschmidt, C.R.; Fitzgerald, W.F.; Balcom, P.H.; Visscher, P.T. Organic matter and sulfide inhibit methylmercury production in sediments of New York/New Jersey Harbor. *Mar. Chem.* **2008,** *109* (1-2), 165-182.

60. Kim, M.; Han, S.; Gieskes, J.; Deheyn, D.D. Importance of organic matter lability for monomethylmercury production in sulfate-rich marine sediments. *Sci. Total Environ.* **2011,** *409* (4), 778-784; 10.1016/j.scitotenv.2010.10.050.

61. Drott, A.; Lambertsson, L.; Björn, E.; Skyllberg, U. Potential demethylation rate determinations in relation to concentrations of MeHg, Hg and pore water speciation of MeHg in contaminated sediments. *Mar. Chem.* **2008,** *112* (1-2), 93-101; 10.1016/j.marchem.2008.07.002.

62. Barkay, T.; Miller, S.M.; Summers, A.O. Bacterial mercury resistance from atoms to ecosystems. *FEMS Microbiol. Rev.* **2003,** *27* (2-3), 355-384; 10.1016/S0168-6445(03)00046-9.

63. Lu, X.; Liu, Y.; Johs, A.; Zhao, L.; Wang, T.; Yang, Z.; Lin, H.; Elias, D.A.; Pierce, E.M.; Liang, L.; Barkay, T.; Gu, B. Anaerobic Mercury Methylation and Demethylation by Geobacter bemidjiensis Bem. *Environ. Sci. Technol.* **2016,** *50* (8), 4366-4373; 10.1021/acs.est.6b00401.

64. Craig, P.J.; Bartlett, P.D. The role of hydrogen sulphide in environmental transport of mercury. *Nature* **1978,** *275* (5681), 635-637.

65. Baldi, F.; Parati, F.; Filippelli, M. Dimethylmercury and dimethylmercury-sulfide of microbial origin in the biogeochemical cycle of HG. *Water Air Soil Pollut.* **1995,** *80* (1-4), 805-815; 10.1007/BF01189732.

66. Khan, M.A.; Wang, F. Chemical demethylation of methylmercury by selenoamino acids. *Chem. Res. Toxicol.* **2010,** *23* (7), 1202-1206; 10.1021/tx100080s; 10.1021/tx100080s.

67. Asaduzzaman, A.M.; Schreckenbach, G. Degradation mechanism of methyl mercury selenoamino acid complexes: a computational study. *Inorg. Chem.* **2011,** *50* (6), 2366-2372; 10.1021/ic1021406; 10.1021/ic1021406.

68. Miller, C.L. The role of organic matter in the dissolved phase speciation and solid phase partitioning of mercury. , University of Maryland, 2005.

69. Bottrell, S.H.; Newton, R.J. Reconstruction of changes in global sulfur cycling from marine sulfate isotopes. *Earth-Sci. Rev.* **2006,** *75* (1-4), 59-83.

70. Morse, J.W.; Luther III, G.W. Chemical influences on trace metal-sulfide interactions in anoxic sediments. *Geochim. Cosmochim. Acta* **1999,** *63* (19-20), 3373-3378.

71. Suits, N.S.; Arthur, M.A. Sulfur diagenesis and partitioning in Holocene Peru shelf and upper slope sediments. *Chem. Geol.* **2000,** *163* (1-4), 219-234.

72. Dittmar, T.; Koch, B.; Hertkorn, N.; Kattner, G. A simple and efficient method for the solid-phase extraction of dissolved organic matter (SPE-DOM) from seawater. *Limnol. Oceanogr. Methods* **2008,** *6* (JUN), 230-235.

2. The Formation of β-HgS Nanoparticles in Presence of Marine DOM and the Interaction of Hg^{II} with Metal Sulfide Nanoparticles.

2.1. *Introduction*

The production of Methylmercury (MeHg) from inorganic mercury (Hg^{II}) has spurred concern over anthropogenic mercury emissions worldwide and prompted research into the processes of MeHg formation. Hg^{II} is converted to MeHg (the more toxic and bio-accumulative form commonly found in the environment) during the mineralization of organic matter by bacteria carrying the methylating gene.[1-3] A major hotspot for MeHg production is the coastal sediment, owing to the active degradation of organic matter by Sulfate Reducing Bacteria — one of the main methylators of Hg^{II}.[1,4-11] The MeHg produced accumulates up the food chain causing neurodegenerative diseases in both humans and wildlife.[12,13] Substantial progress in understanding the biogeochemistry of Hg^{II} in coastal areas has been made thus far; however, it is still difficult to predict the production of MeHg across ecosystems. This is partly because Hg^{II} speciation (a factor that influences MeHg production) is not well understood contributing to much controversy.[14-18] The speciation of Hg^{II} refers to the forms of Hg^{II} found in the environment. Mercury forms complexes with different ligands in solution including chlorides, hydroxides, thiols, and inorganic sulfides. As Hg^{II} is a soft acid, its complexes with reduced sulfur groups are the most thermodynamically stable. The bioavailability of the different complexes to methylating bacteria differs. It has been suggested that bacteria take up neutral complexes of Hg^{II} by passive diffusion and Hg-thiol complexes by active uptake.[14,19,20]

One of the neutral complexes suggested to form in the environment is a hydrated HgS*(aq)* complex. Though computational calculations support the formation of the aqueous complex and propose the structure to be HOHgSH, experimental data and thermodynamics don't concur fully with the quantum calculations and there is no evidence of its existence.[21,22] It has been suggested that the aqueous complex in question is actually a HgS nanoparticle (diameter between 1-100 nm), which passes through conventional filters of 0.45 µm and is erroneously considered as a dissolved mercury complex.[23] Contrary to the lack of evidence for the existence of HgS*(aq)*, recent research confirms the formation of HgS nanoparticles (NPs) in natural

settings.[24-26] While the importance of the NPs to Hg^{II} speciation is gaining ground, little data exists on the formation and persistence of these particles under different conditions. The objective of this work was to gain knowledge on the formation and behavior of HgS nanoparticles (β-HgS*(s)*$_{nano}$) forming in the environment. Results from our study will provide a better understanding of Hg^{II} speciation, ultimately improving estimates on MeHg production rates in coastal environments.

Nanoparticles in the environment have been detected in wastewater effluents, hydrothermal vents, pore waters, and mine tailings.[27-31] Since up to 50% of the atoms reside on the surface, these nanometer sized particles have high surface energy which the particle tends to compensate for by rearranging surface and near surface atoms.[32] As such, NPs (especially those < 30 nm) have size-dependent properties affecting their reactivity, mobility, solubility and bioavailability, and which differ substantially from their bulk counterparts.[32-35] Due to their high surface energy, NPs are unstable and tend to aggregate, coalesce when possible and settle out of solution.[36,37] The interaction of two particles — described by the Derjaguin-Landau-Verwey-Overbeek (DLVO) theory — depends on the sum of two opposite forces; the attractive van der Waals forces and the repulsive forces that exist between like charged particles. When particles are in close proximity, attractive van da Waals forces dominate and the particles are likely to aggregate unless conditions exist that hinder the aggregation process.[36,38]

Organic molecules have been shown to hinder the aggregation of particles by forming coordinate covalent bonds between functional groups on the organic molecule and metal ions on the surface of the particle.[39,40] Fourier Transform Infra-red spectroscopy (FTIR) of β-HgS*(s)*$_{nano}$ stabilized by bovine serum albumin (BSA) suggests that the surface of β-HgS*(s)*$_{nano}$ is bound to amide and carboxyl groups of the BSA.[41] As Hg has a higher affinity for S (a soft base) than O or N, binding to reduced sulfur groups is also expected. Indeed, low molecular weight thiol ligands have been shown to inhibit the growth of β-HgS*(s)*$_{nano}$ relative to their hydroxyl containing analogues.[42] Nonspecific hydrophobic interactions between humic fractions of natural dissolved organic matter (DOM) and β-HgS*(s)*$_{nano}$ have also been noted to slow down the growth of particles.[38] The adsorption of negatively charged organic matter present in the environment to the β-HgS*(s)*$_{nano}$ surface enhances electrostatic repulsive forces and induces electrosteric forces especially

when humic substances are involved.[25,38,42-46] Both these forces have been reported to stabilize β-HgS*(s)*$_{nano}$ forming in presence of organic matter. Nanoparticles forming in DOM isolated from a terrestrial environment (Suwanee River Humic Acid (SRHA)), were observed with Transmission Electron Microscopy (TEM) to have a diameter of less than 10 nm.[24,44] Such particles are considered metacinnabar-like as they have an average bond length and coordination number similar to β-HgS*(s)*, but are less crystalline and possess a higher degree of disorder.[24-26] Mercury containing NPs can also form when Hg^{II} replaces or co-precipitates with other metal ions.[47-49]

Most studies on β-HgS*(s)*$_{nano}$ have focused on fresh water and soil-derived DOM; yet the binding affinity of Hg^{II} to DOM changes with DOM character and this is likely to impact particle formation. Also, the binding strength of Hg^{II} to DOM changes with Hg^{II}:DOM ratio.[50] At ratios lower than 1 μg Hg^{II} /mg C (common in the environment) Hg^{II} binds strongly to reduced sulfur groups, while at higher ratios, weaker binding to the more prevalent hydroxyl and amide functional groups occurs.[50] Few studies have investigated β-HgS*(s)*$_{nano}$ formation at environmental ratios of Hg^{II}:DOM. Thirdly, even fewer studies have looked at persistence of the β-HgS*(s)*$_{nano}$ under different environmental conditions or at the interaction of Hg^{II} with other metal sulfide solids. Here we investigated the formation and stability of β-HgS*(s)*$_{nano}$ forming in the presence of various thiols and organic matter extracted from three marine environments: Eastern Long Island Sound (ELIS), Western Long Island Sound (WLIS), and offshore at the shelf break of the North Atlantic Ocean (SB). We expanded on previous work by looking at the fate of the particles when exposed to oxygen and sunlight. Using CdS*(s)*$_{nano}$ as a model metal sulfide species, we also investigated the interaction of Hg^{II} with other metal sulfide nanoparticles forming in aquatic systems or with engineered quantum dots ending up in natural waters. We hypothesized that (1) Coastal DOM is better at inhibiting the growth of β-HgS*(s)* nanoparticles than DOM from the open ocean; (2) The size of β-HgS*(s)* nanoparticles increases with decreasing relative DOM concentration; (3) The stability of β-HgS*(s)* nanoparticles is reduced in light and oxic environments; and (4) Hg^{II} forms a stable complex with CdS*(s)*$_{nano}$ similar to complexes of Hg^{II} with reduced sulfur.

2.2. Methodology

2.2.1. Extracting Dissolved Organic Matter from Seawater

Dissolved organic matter was isolated from surface waters collected at Eastern Long Island Sound (ELIS), Western Long Island Sound (WLIS), and at the shelf break of the North Atlantic Ocean (SB) as shown in the map (Fig. 1). Surface water from each of the locations was collected using Teflon-coated acid cleaned Go-Flo bottles deployed down to the chlorophyll maximum zone. The water was filtered on board immediately after collection using a 0.45 and a 0.2 µm cartridge filters and then stored in ultra-clean cubitainers and brought back to the lab. The filtered seawater (20–50 L) was acidified to pH 2 just before the extraction and then passed through a modified benzene styrene polymer cartridge at a rate of < 4 mL/min using a peristaltic pump. Following the recommendation by Dittmer *et al.*, no more than 5 L were loaded on one cartridge at a time.[51] All cartridges were pre-rinsed with 6 mL of methanol and 1 L of ultrapure UV treated water just before use. Extracted DOM was desalted by rinsing the cartridge with 40 mL of 0.01 M HCl before drying the cartridge with argon/nitrogen gas. DOM was eluted from the dry cartridge using methanol and acetone and then stored in the freezer. An aliquot of the DOM solution was dried using a Nitrogen evaporator (N-EVAP 111) at 40^{o}C, re-dissolved in purified water and analyzed for the dissolved organic carbon (DOC) concentration using a Shimadzu TOC analyzer (TOC-VCPN). The absorbance and fluorescence measurements of the extracted DOM were also performed as described further below.

Fig. 1. Map showing the location where dissolved organic matter used in the synthesis of β-HgS*(s)*$_{nano}$ was extracted from surface waters using a modified styrene divinyl polymer cartridge.

2.2.2. Preparation of Experimental Solutions

All solutions were prepared using UV oxidized deionized water (18.4 MΩ), degassed by boiling and purging with nitrogen for at least 20 min. Preparation and synthesis was done in a glove box. The mercury stock solution was prepared by dissolving 0.26 g of mercury nitrate monohydrate in 25 mL of 0.1 M HCl. The sulfide stock solution was prepared by dissolving 10 g sodium sulfide nanohydrate (Acros) in 5 mL of degassed water. The crystals of the sulfide salt were washed to remove oxidation products and dried under nitrogen before weighing. The concentration of the sulfide standard was determined by titrating an aliquot of the sulfide preserved in Sulfide Anti-Oxidant Buffer (SAOB) with $Pb(NO_3)_2$ using an ion selective electrode. The SAOB solution contained 2 M NaOH for converting H_2S to S^{2-} thereby preventing the evasion of H_2S *(g)* from the solution; 0.1 M ascorbic acid for minimizing the oxidation of S^{2-}; and EDTA for binding metal ions that catalyze the oxidation of S^{2-}.[52] Thiol capping agents consisting of 1,2-ethanedithiol, 1,3-propanedithiol, 4- mercaptophenyl acetic acid, glutathione, and L-cysteine were obtained from Alfa Aeser. Stock solutions of the dithiols and 4- mercaptophenyl acetic acid were prepared by dissolving 5 uL and 0.02 g, respectively, in 5 mL methanol. Glutathione and L- cysteine solutions were prepared by dissolving 0.01 and 0.02 g respectively, in 10 mL of 2.2 mM $NaHCO_3$ (with pH 7.8 and

prepared daily). The thiol stock solutions were stored in the glove box and used within 24 h. An aliquot of the DOM solution in methanol was dried under nitrogen, on day of use, then re-dissolved in 2.2 mM $NaHCO_3$, pH 7.8 and filtered through a 0.2 µm syringe filter. Aliquots of all prepared solutions were diluted using the reaction matrix (2.2 mM $NaHCO_3$, pH 7.8) before amending into their respective reaction vials.

2.2.3. Synthesis of β-HgS(s)$_{nano}$ using Different Capping Agents

β-HgS*(s)*$_{nano}$ was synthesized by adding an aliquot of the appropriate capping agent to the solution matrix followed by Hg^{II} addition. The solution of Hg^{II} and capping agent was mixed end to end, and then HS^- was added and the solution mixed again. As the pH of the experimental solution was 7.8 and the pKa1of H_2S is 7, dissolved sulfide existed predominantly as HS^-; thus, we use HS^- to refer to the dissolved sulfide in our experimental solutions. The binding of Hg^{II} to DOM has been shown to increase with equilibration time of Hg^{II} with DOM. Initially, Hg^{II} is bound to the more abundant oxygen and nitrogen containing functional groups on DOM.[53] With equilibration time of between 10–24 h, the more abundant and weaker O and N functional groups are replaced by stronger thiol binding sites.[54-57] To test if the equilibration time of Hg^{II} with DOM, prior to sulfide addition, affects particle size; a subset of the experimental vials were equilibrated with DOM for 24 h before HS^- was added. Particle size with and without Hg^{II}-DOM equilibration was similar. Subsequently, HS^- was added to all vials no more than 5 min after Hg^{II} addition to DOM. For the thiols dissolved in methanol, control solutions were conducted by adding an equivalent amount of methanol to cysteine and glutathione vials prior to Hg^{II} and HS^- addition. Unless otherwise stated, the final concentration of the capping agents was 300 µM for the monothiols, 150 µM for the dithiols, and 833 µM C for DOM. The concentrations of Hg^{II} and HS^- were 150 µM each.

2.2.4 Stability of β-HgS(s)$_{nano}$ under Different Conditions

To determine the stability of the particles under oxic and anoxic conditions, β-HgS*(s)*$_{nano}$ were prepared as described above using ELIS DOM as the capping agent. The solution was divided in to four batches. Each reaction vial contained 3 mL of solution and this was purged with air (oxic) or nitrogen

(anoxic) for 5 min at a rate of about 40 mL/min. Vials purged with N_2 were immediately capped and sealed with parafilm, while the vials under dark conditions were wrapped in foil. All vials were stored in the lab next to the window with direct exposure to sunlight. DLS measurements were performed on the β-HgS*(s)*$_{nano}$ at day 1 before any purging and on day 3 after purging and exposure to light. After 4 weeks, 3 mL of 1 M $CaCl_2$ was added to deoxygenated vials in the dark and oxygenated vials in light to initiate the precipitation of β-HgS*(s)*$_{nano}$ still stable in solution. The mixture was centrifuged at 5000 rpm for 10 min and the supernatant collected and filtered through a 0.2 µm syringe filter. The aromatic content of the filtered solutions was determined by calculating the Specific Ultra Violet Absorption (SUVA) at 254 nm. This was done by measuring the dissolved organic carbon (DOC) concentration and the absorption coefficient, as described further below.

2.2.5. The Interaction of Hg^{II} with CdS(s)$_{nano}$

Cysteine capped CdS particles were synthesized following the same general procedure as the one used to prepare β-HgS*(s)*$_{nano}$. The cadmium stock solution was prepared by dissolving 0.46 g of cadmium nitrate tetrahydrate (Fischer) in 50 mL of 0.1 M HCl. An aliquot of the solution was diluted in 2.2 mM $NaHCO_3$, pH 7.8 before use. The cysteine and $Na_2S.9H_2O$ solutions were prepared as described above. CdS*(s)*$_{nano}$ formed when an aliquot of cysteine was added to the reaction vial containing the matrix followed by the addition Cd^{II} and then HS^-. The concentration of Cd^{II}, HS^-, and cysteine in the final solution was 150 µM, 75 µM, and 600 µM, respectively. Particles were aged for 3 days in the glove box, after which the solution was divided in to five different vials and an aliquot of Hg^{II} was spiked into each vial to give a final concentration of 0–0.3 µM Hg^{II}. The Hg^{II} spiking solution was prepared in $NaHCO_3$, pH 7.8. The UV and FL measurements of the CdS*(s)*$_{nano}$-Hg solutions were performed 1 h after Hg^{II} addition.

2.2.6. Determination of Particle Size

Dynamic Light Scattering (DLS) were performed on a Malvern Zetasizer ZS90. DLS measures particle size in a sample by monitoring changes in the intensity of scattered light after the sample has been

irradiated with a laser light, in our case, of λ = 663 nm. The intensity changes of the scattered light are caused by the Brownian motion of particles; thus, the intensity changes are related to the diffusivity of the particles. Particle size is determined using the Stokes-Einstein's equation as shown below:

$$D_h = (k_B\ T) / 3\pi\ \eta D_t \qquad (1)$$

Where D_h is the hydrodynamic diameter of the particles; k_B is Boltzmann's constant; T is temperature; η is the viscosity of the solution and D_t is the diffusion coefficient which is determined from the scattered light intensity changes when fit to an autocorrelation function.

The solutions containing β-HgS*(s)*$_{nano}$ were transferred to a 1 cm quartz cuvette or a clear disposal zeta cell, and measurements taken at 25^{o}C. The intensity-weighted hydrodynamic diameter was calculated from 20 individual measurements of 10 seconds each. The scattering intensities of the blank solutions consisting of Hg^{II} + matrix, HS^- + matrix, DOM + matrix or Hg^{II} + DOM + matrix, were less than 1.5 kilocounts per sec (kcps). Scattering intensities of experimental solutions containing Hg^{II}, DOM and HS^- were above 5 kcps with most solutions above 10 kcps.

2.2.7. Absorbance and Fluorescence Measurements

Absorbance measurements were conducted using a UV-Vis spectrophotometer (Hitachi U3010). Samples were analyzed in a 1 cm quartz cuvette using the matrix solution as the reference. Fluorescence measurements were performed using a Hitachi F2000 fluorometer with a 1 cm quartz cuvette. The emission spectra for the CdS*(s)*$_{nano}$ solutions were recorded at λ_{ex} of 350 nm. Excitation Emission Matrices (EEMs) of DOM samples used in the β-HgS*(s)*$_{nano}$ synthesis was also recorded. DOM samples were diluted to an absorption of < 0.05 cm^{-1} at 220 nm, using the matrix, prior to fluorescence measurements.[58] FL scans of the DOM were recorded using an excitation wavelength of 220 to 450 nm; every 5 nm. We corrected the FL spectra of the samples by first subtracting the matrix EEM from the sample EEMs and then normalizing the intensity of the sample EEMs to the Raman peak of MQ water recorded at an excitation wavelength of

350 nm and emission wavelength of 371–428, as recommended by Lawaetz and Stedmon.[59] The Raman and Rayleigh scattering peaks were removed from the sample EEMs by excising emission data before λ_{ex} + 40 nm and above twice the excitation wavelength.

For fluorescence lifetime measurements, the samples were excited with a pulsed diode laser (Picoquant) at 405 nm. The emission was collected by a single-photon detector (τ-SPAD, PicoQuant) equipped with a 435 long pass optical filter. Time-dependent single photon counting measurements were performed using PicoHarp 300 (PicoQuant) with a time resolution of 32 ps.

2.3. Results

2.3.1. Formation of β-HgS(s)$_{nano}$ using Different Capping Agents

The formation of β-HgS*(s)*$_{nano}$ was investigated using different thiols and natural organic matter extracted from 3 marine environments. The thiols used in our study included cysteine, glutathione, 4-mercaptophenylacetic acid (4-MAA), 1,2-ethanedithiol, and 1,3-propanedithiol. Dissolved organic matter (DOM) was extracted from offshore at the shelf break of the North Atlantic Ocean (SB), and closer to shore from the west and east of Long Island Sound (WLIS and ELIS, respectively), using a solid phase extraction method with a Bond Elut PPL resin.[51] This method of extraction is easy to use, has a higher extraction efficiency compared to other commercially available cartridges, and also extracts a more representative fraction of the DOM and with low salt content.[51] In our experiments, the extraction efficiency for DOM was 53%, and this is comparable to the extraction efficiency reported for seawater using PPL cartridges.[51,60] β-HgS*(s)*$_{nano}$ formed on addition of 150 µM HS^- to a solution containing 150 µM Hg^{II} and 10 mg C/L (833 µM) DOM or 150 µM Hg^{II} and 300 or 150 µM mono or dithiol, respectively. The hydrodynamic diameter of the particles was determined using Dynamic Light Scattering (DLS).

Particles that formed in the presence of ELIS and WLIS DOM were comparable in size (about 13 nm) and were smaller than those formed in SB DOM, 20 nm (Fig. 2). Among the thiols, the smallest particles were formed in the presence of glutathione and 4-MAA (~ 6.5 nm) and these were about half the

size of particles forming in cysteine (Fig. 3). Cysteine and glutathione vials with and without methanol formed particles of similar size. Hence it was concluded that the methanol added to aid in the dissolution of the dithiols and 4-MAA did not have an apparent effect on particle formation. Particles that formed in the presence of dithiols were much larger (>100 nm) than those formed in the monothiols. DLS measures the hydrodynamic diameter, thus it does not give the diameter of the individual particle. Instead, it uses the diffusion coefficient determined from the data to calculate the diameter of a sphere moving in the same way as the particles. Since the diffusivity of the particles is influenced by the water of hydration, the adsorbed ligand, and the aggregation state; the hydrodynamic diameter is affected by these parameters and can be different from the actual size of the individual particle.

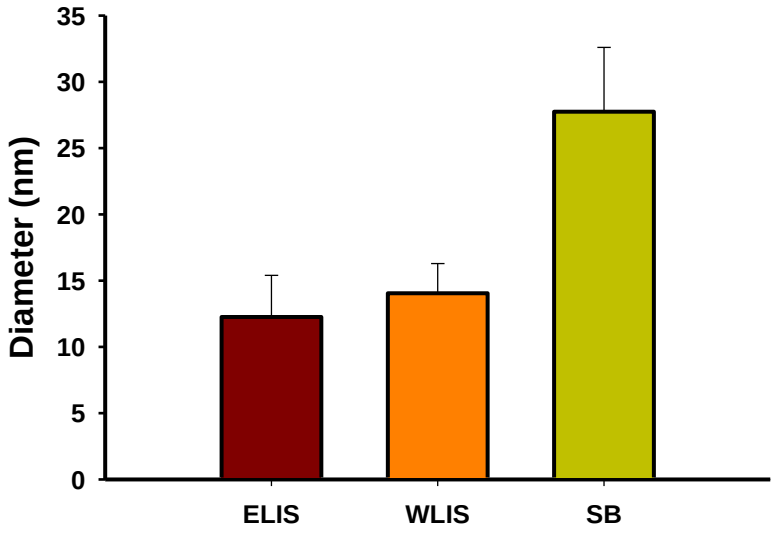

Fig. 2. The hydrodynamic diameter of DOM capped β-HgS*(s)*$_{nano}$. Solutions contained 150 µM $Hg(NO_3)_2$, 150 µM Na_2S and 10 mg C/L DOM extracted from Eastern Long Island Sound (ELIS), Western Long Island Sound (WLIS) and at the SB of the North Atlantic Ocean (SB), in 2.2 mM $NaHCO_3$ (pH 7.8).

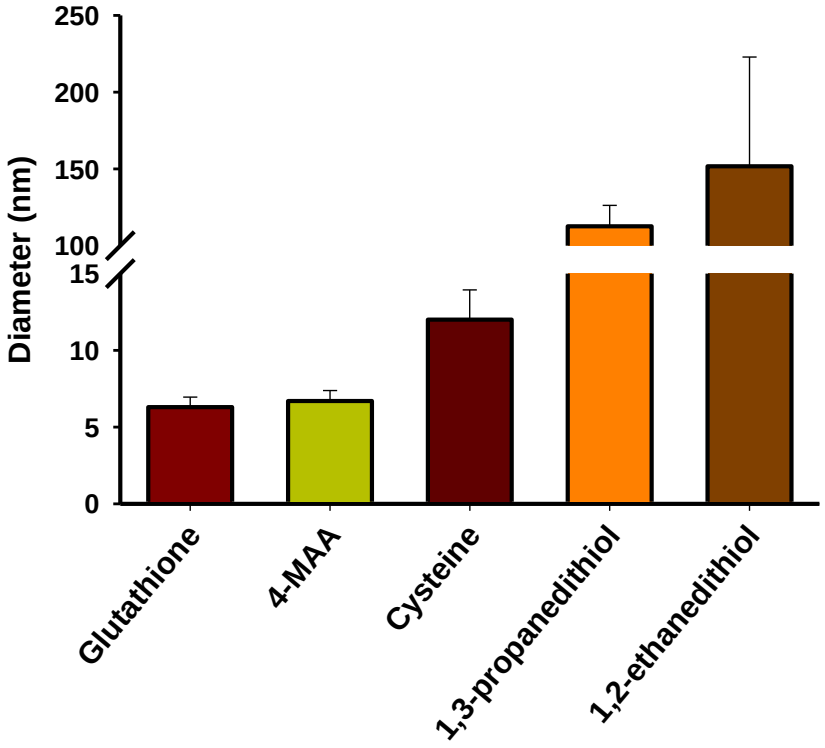

Fig. 3. The hydrodynamic diameter of thiol capped β-HgS*(s)*$_{nano}$. Solutions contained 150 µM $Hg(NO_3)_2$, 150 µM Na_2S and 300 µM monothiol (glutathione, mercaptophenyl acetic acid (4-MAA) or cysteine), or 150 µM dithiol (1,3-propanedithiol or 1,2-ethanedithiol), in 2.2 mM $NaHCO_3$ (pH 7.8).

To determine if the larger diameter of the dithiol capped β-HgS*(s)*$_{nano}$, as determined by DLS measurements, was due to a difference in the core particle size between the monothiols and the dithiols, we used UV-Vis to determine the size of particles formed in presence of cysteine and the dithiols. This was possible because of the quantum confinement effect exhibited by semiconductor nanoparticles with sizes similar to Bohr's radius.[61] The size of the particle is related to the energy difference between the band gap of the nanoparticle and that of the bulk material using the effective mass approximation theory as described in the following equation:

$$\Delta E = E_{NP} - E_{bulk} = \frac{h^2}{8\,R^2}\left(\frac{1}{m_e} + \frac{1}{m_h}\right) - \frac{1.8\,e^2}{4\,\varepsilon\,R\prod\varepsilon_0} \qquad (2)$$

where E is the band gap energy, m_e and m_h are the effective masses of the electron and hole respectively, e is the charge of an electron, ε_0 is the permittivity of a vacuum, ε is the dielectric constant of the material, and R is the radius of the particle.

The band gap energy of a semiconductor is the energy required to excite an electron from the valence band to the conduction band. As the size of the semiconductor decreases, the band gap energy increases, hence nanoparticles have band gap energies larger that their bulk counterparts. The band gap energies of $HgS(s)_{nano}$ and $CdS(s)_{nano}$ lie in the UV-Vis region and can be determined from absorbance measurements of the semiconductor material. The band gap energy of a nanoparticle is obtained by extending a line tangent to the absorption edge (where the peak sharply rises) to the x-axis. As our samples were polydisperse, the peak did not rise as sharply and our calculations are estimates of the average particle size in the sample. The spectra of the β-$HgS(s)_{nano}$ are shown in Fig. 4 and the band gap energy of the cysteine, 1,2-ethanedithiol, and 1,3-propanedithiol capped β-$HgS(s)_{nano}$ were found to be 403, 402, and 417 nm, respectively. The diameter of the dithiol capped particles, calculated using equation 2 above, was similar to that of particles formed in the presence of cysteine (Table 1). This implies that the large hydrodynamic diameter of particles forming in the presence of dithiols, obtained from the DLS measurements, was not due to bigger individual particles.

Table 1: The diameters of β-$HgS(s)_{nano}$ capped with 1,2-ethanedithiol, 1,3-propanedithiol and cysteine determined using the Effective Mass Approximation theory.

Ligand	UV-Vis Diameter (nm)
1,2-ethanedithiol	5.4
1,3-propanedithiol	5.5
Cysteine	5.4

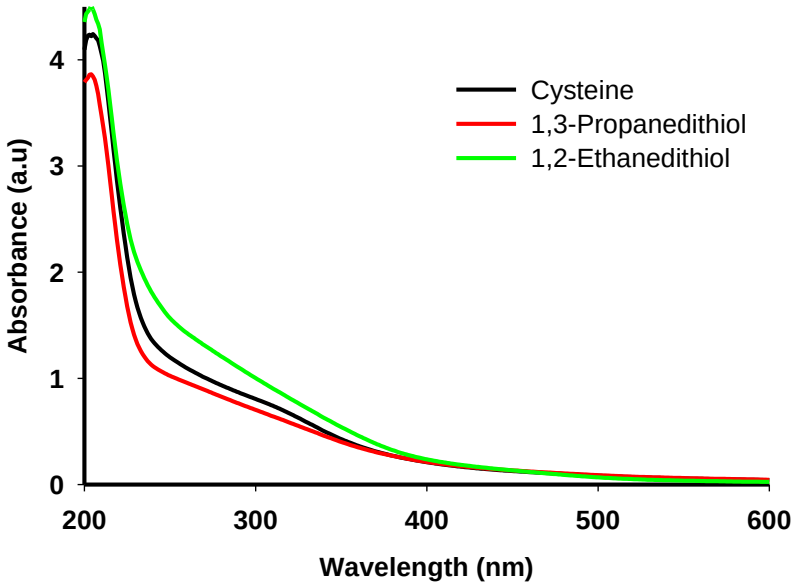

Fig. 4. The UV-Vis spectra of thiol capped β-HgS*(s)*$_{nano}$. The solutions contained 150 µM $Hg(NO_3)_2$, 150 µM Na_2S and 300 µM cysteine or 150 µM dithiol (1,3-propanedithiol or 1,2-ethanedithiol), in 2.2 mM $NaHCO_3$ (pH 7.8).

2.3.2. Stability of β-HgS(s)$_{nano}$ with Time

The growth of the particles was monitored for up to five weeks in experiments where the capping agent was ELIS DOM, SB, DOM or cysteine. As in the previous experiment, β-HgS*(s)*$_{nano}$ were synthesized by adding 150 µM HS^- to a solution containing 150 µM Hg^{II} and 10 mg C/L (833 µM) DOM (ELIS/SB) or 150 µM Hg^{II} and 300 µM (11 mg C/L) cysteine. The DLS measurement of the particles taken immediately after the addition of HS^- (5 min) gave an average particle size of 19.6 ± 3.6 nm for SB; 12.8 ± 1.7 nm for ELIS; and 9.9 ± 1.0 nm for cysteine. Particle size did not change significantly with time when monitored for up to 9 h (Fig. 5).

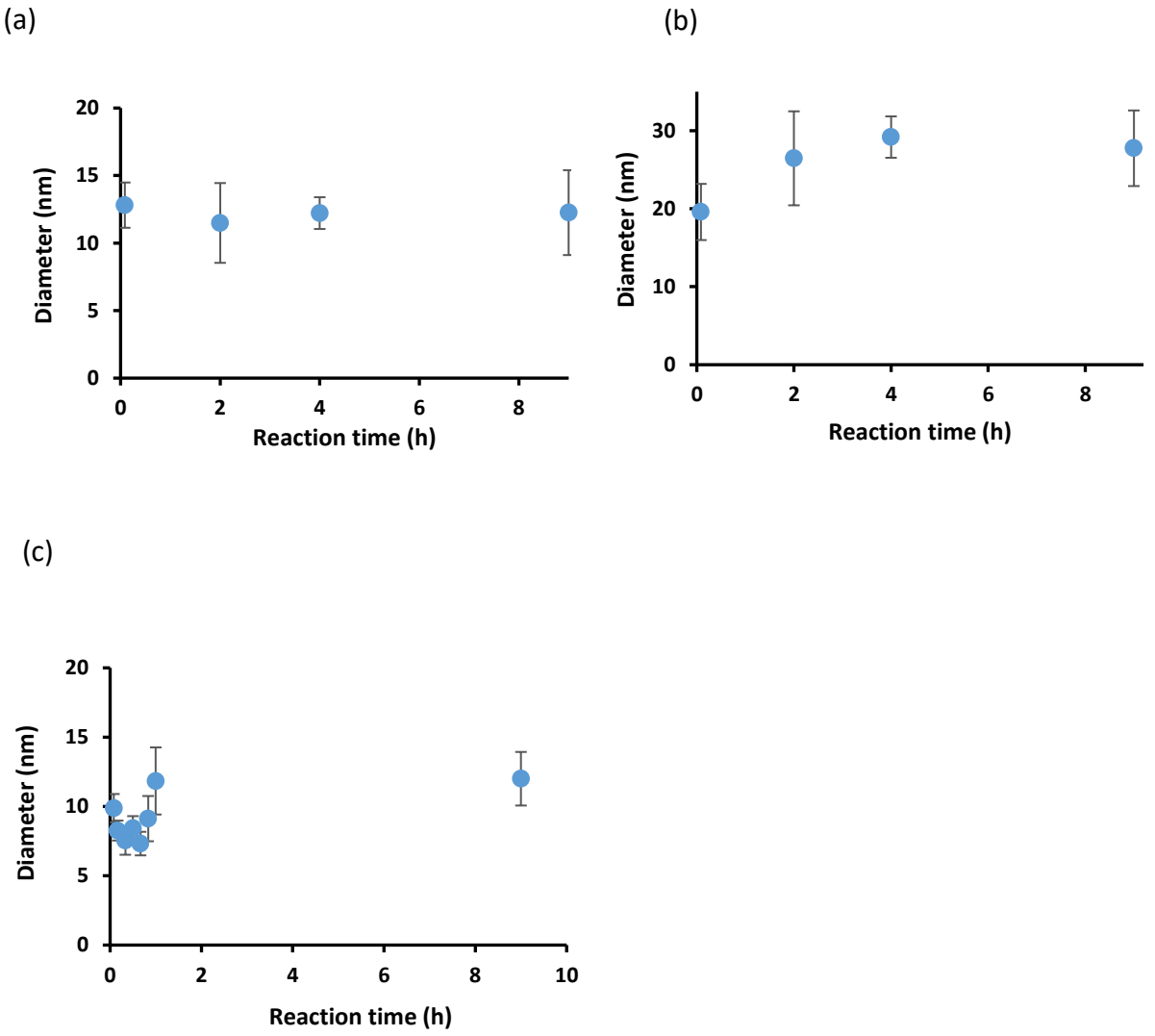

Fig. 5. The hydrodynamic diameter of β-HgS*(s)*$_{nano}$ recorded over time from 0 – 9h of reaction. Solutions contained 150 µM $Hg(NO_3)_2$, 150 µM Na_2S and 10 mg C/L ELIS DOM (a); SB DOM (b); or 300 µM cysteine (c), in 2.2 mM $NaHCO_3$ (pH 7.8).

At longer times (up to 5 weeks), particles capped with ELIS DOM did not show significant growth as they remained about the same size (Fig. 6a) while those capped with SB DOM grew significantly over time (from about 20 to 40 nm), Fig. 6b. Particles formed in presence of cysteine were not monitored by DLS at longer times. In earlier experiments, however, we found that particles forming at the same concentration of reagents, as used here, did not grow appreciably when monitored for 3 weeks using absorbance measurements. The overlaid UV-Vis spectra for the β-HgS*(s)*$_{nano}$ formed in the earlier experiment is shown in Fig.7. The particles had an average particle size of 5.4 ± 0.02 nm.

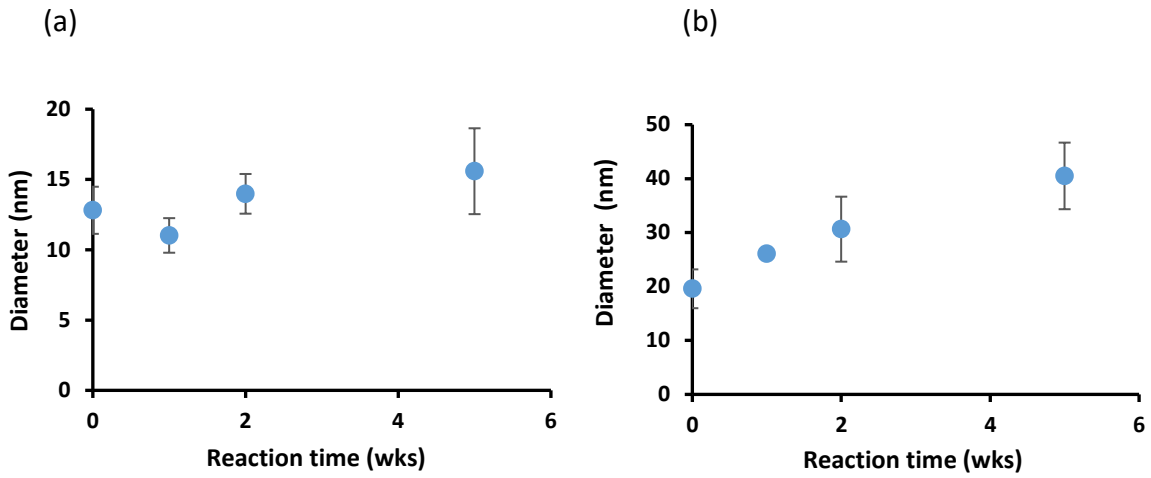

Fig. 6. The hydrodynamic diameter of β-HgS*(s)*$_{nano}$ monitored over time for up to 5 weeks. Solutions contained 150 µM $Hg(NO_3)_2$, 150 µM Na_2S and 10 mg C/L ELIS DOM (a) and SB DOM (b) in 2.2 mM $NaHCO_3$ (pH 7.8).

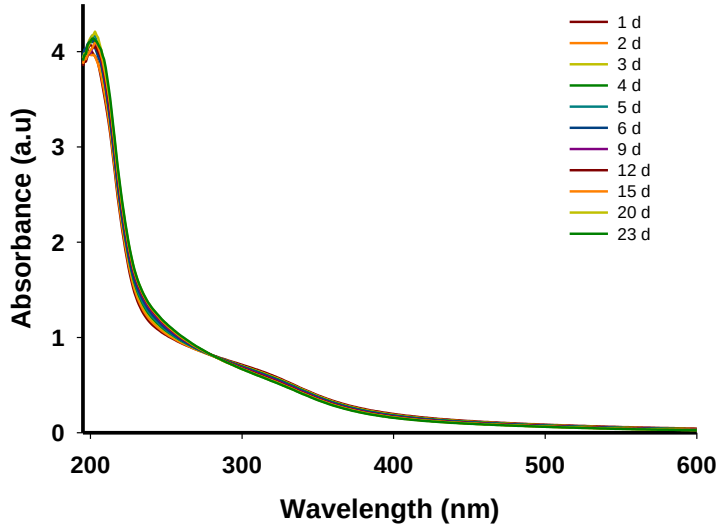

Fig. 7. The overlaid UV-Vis spectra of cysteine capped β-HgS*(s)*$_{nano}$. The solutions contained 150 µM $Hg(NO_3)_2$, 150 µM Na_2S and 300 µM cysteine in 2.2 mM $NaHCO_3$ (pH 7.8).

To understand why the NPs formed in presence of ELIS and SB DOM were different in size, the two DOM were characterized using absorption and fluorescence spectroscopy. The specific ultraviolet absorption (SUVA), calculated by dividing the Naperian absorption coefficient at 254 nm with the

concentration of the DOM in solution, was determined to be 4.9 and 2.5 L $mg^{-1}m^{-1}$ for ELIS and SB DOM, respectively. The 3D excitation and emission matrices of fluorescence scans (Fig. 8) obtained by combining spectra collected at an excitation wavelength of 250 to 450 nm, show that ELIS has a higher fraction of humic-like materials (max emission at a longer wavelength) and a lower fraction of proteinaceous-like materials (max emission at a shorter wavelength) than SB.

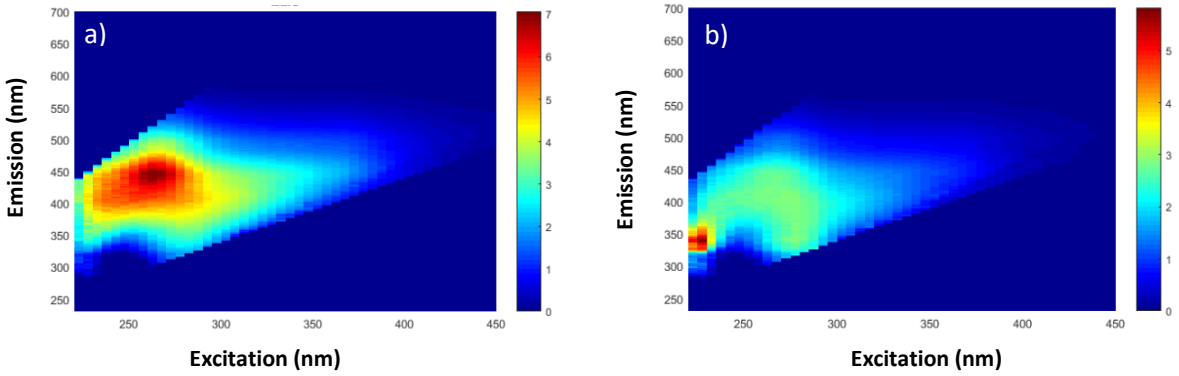

Fig. 8. Excitation and emission matrices (EEM) of dissolved organic matter extracted from surface waters collected from (a) Eastern Long Island Sound (ELIS) and (b) at the shelf break of the North Atlantic Ocean (SB). Fluorescence intensities are given in Raman Units (R.U).

2.3.3. Stability of β-HgS(s)$_{nano}$ under Different Environmental Conditions

To study the stability of particles when exposed to sunlight and oxygenated conditions, β-HgS*(s)*$_{nano}$ were formed at a ratio of 15 µmole Hg^{II} /mg C using ELIS DOM. This was also the ratio used to study the stability of the particles with time. To examine the stability of the particles in sunlit conditions, the formed nanoparticles were exposed to sunlight while to examine the oxidation of the particles in oxic environments, the particles were purged with air. Whereas the particles in dark conditions, whether purged with air or nitrogen, showed no or slight growth over time, exposure to sunlight led to significant increase in particles size, from about 13 nm to up to 71 nm, (Fig. 9). Moreover, the particles that were exposed to both air and light settled out after 2 weeks, while the rest remained stable in solution for at least 1 month. To determine if there was any change in the aromatic content of the DOM in our vials, we added $CaCl_2$ to precipitate the nanoparticles from the solution. After centrifugation, the supernatant was filtered through a 0.2 µm syringe filter; absorbance measurements were taken, and the DOC concentration in the solution analyzed. The

SUVA for the DOM remaining in solution after particles precipitated was calculated to be 2.7 L mg^{-1} m^{-1} for the DOM present in the dark anoxic conditions and 2.3 L mg^{-1} m^{-1} for solutions that were exposed to sunlight and oxygen, compared to the value of 4.9 L mg^{-1} m^{-1} prior to the experiments.

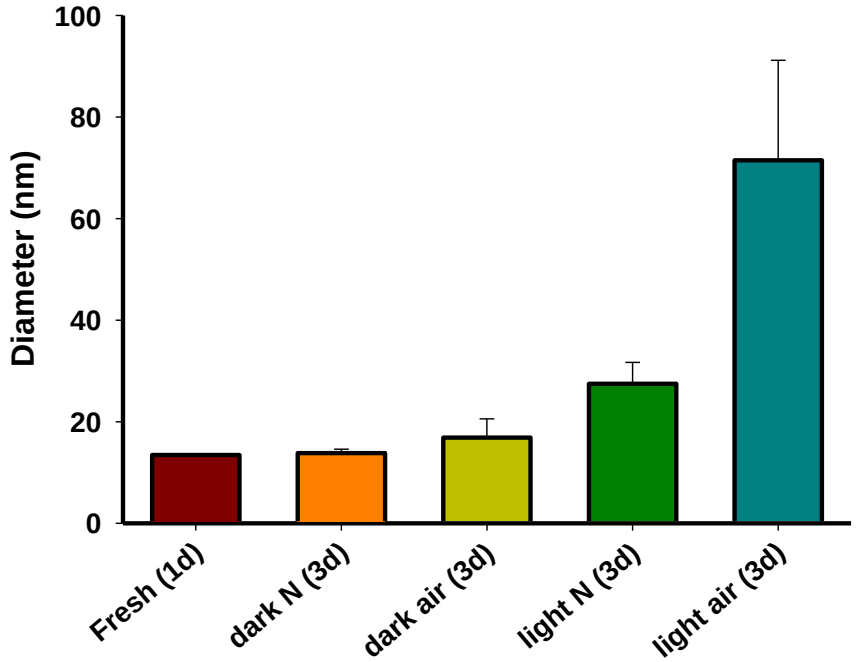

Fig. 9. The hydrodynamic diameter of β-HgS*(s)*$_{nano}$ exposed to different environmental conditions. Solutions contained 150 µM $Hg(NO_3)_2$, 150 µM Na_2S and 10 mg C/L ELIS DOM in 2.2 mM $NaHCO_3$ (pH 7.8).

2.3.4. Formation of β-HgS(s)$_{nano}$ at Different Hg^{II}:DOM Ratios

β-HgS*(s)*$_{nano}$ were also formed in presence of different amounts of ELIS DOM. Dissolved organic matter is composed of a mixture of organic molecules containing phenolic, carboxylic, amino, and thiol functional groups. As a soft acid, Hg^{II} forms stronger complexes with thiol containing moieties of the DOM than with moieties containing the other functional groups. The thiol functional groups on DOM are found however, at a much lower concentration than the O and N containing groups.[53] Thus, as the concentration of Hg^{II} increases, the thiol groups become saturated and Hg^{II} binds to weaker O and N containing groups.[53] The binding affinity of Hg^{II} to DOM therefore increases with a decrease in the Hg^{II}:DOM ratio. Using

aquatic DOM, Haitzer *et al.*, showed that the binding affinity of Hg^{II} to DOM increased with a decrease in DOM concentration up to 5 nmol Hg^{II}/mg C, at which point the researchers did not record a further increase in the binding affinity.[50] Here, we varied the Hg^{II}:DOM ratio from 1.5 nmol Hg^{II}/mg C, where the binding affinity of Hg^{II} to DOM is higher, to 150 µmole Hg^{II} /mg C. The size was found to increase as the ratio increased (Fig. 10). Reaction vials containing a ratio greater than 68 µmole Hg^{II} /mg C precipitated (settled) a few minutes to one hour after the introduction of HS^-.

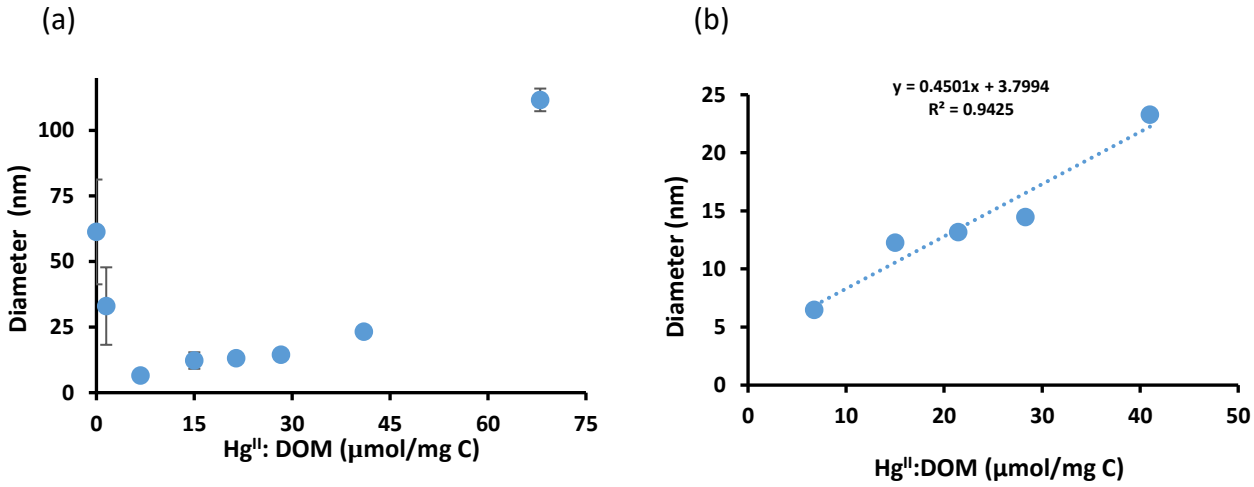

Fig. 10. The hydrodynamic diameter of β-HgS*(s)*$_{nano}$ precipitated at different ratios of Hg^{II}:DOM from 1.5 nmol – 68 µmol/mg C (a); and linear relation between the diameter of the β-HgS*(s)*$_{nano}$ and the Hg^{II}:DOM ratio obtained from 6.8–41 µmol/mg C (b). Solutions contained 150 µM $Hg(NO_3)_2$, 150 µM Na_2S and ELIS DOM in 2.2 mM $NaHCO_3$ (pH 7.8).

Between 6.8 and 41 Hg^{II} µmole/mg C, particle size increased gradually from an average of 6.5 ± 1.8 to 23.3 ± 1.0 nm, after which there was a sharp increase in particle size (Fig. 10a). At the two lowest ratios used (1.5 nmol and 1.5 µmole Hg^{II} /mg C) the particle diameter obtained from DLS measurements was 61.3 and 33 nm, respectively. The TEM images of particles formed at 1.5 nmol Hg^{II} /mg C confirm the presence of particles of ~5 nm in size, (Fig. 11). TEM images of particles formed at a ratio 1.5 µmole Hg^{II} /mg C were not taken in this study, but earlier studies using DOM extracted from Long Island Sound and following the same method of β-HgS*(s)*$_{nano}$ synthesis as used here, show that particles of 4.9 nm in diameter formed at a ratio of 1 µmol Hg^{II} /mg C.[62]

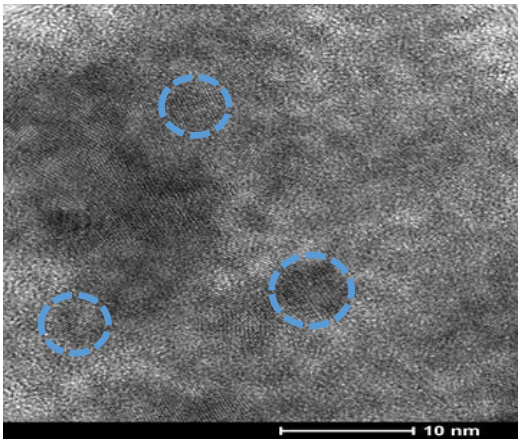

Fig. 11. Transmission Electron Microscopy (TEM) images of β-HgS*(s)*$_{nano}$ precipitated at Hg^{II}:DOM ratio of 1.5 nmol /mg C.

2.3.5. The Interaction of Hg^{II} with CdS(s)$_{nano}$

We also studied the interaction of Hg^{II} with CdS*(s)*$_{nano}$. The CdS*(s)*$_{nano}$ were synthesized using 150 µM Cd^{II}, 75 µM HS^-, and 600 µM cysteine. The absorption spectrum of the CdS*(s)*$_{nano}$ solution shows the typical absorption feature of CdS quantum dots and the particle diameter was calculated using equation 1 to be 3.5 nm (Fig. 12). The diameter calculated from TEM images (Fig. 13) was found to be 3.0 ± 0.4 nm, comparable to the one obtained by absorption measurements.

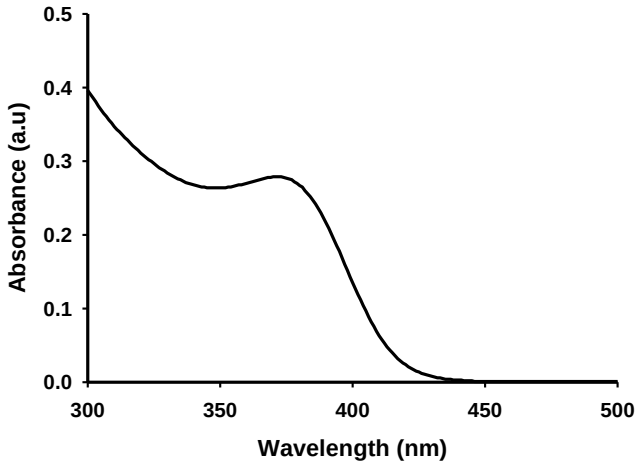

Fig. 12. The UV-Vis spectra of cysteine capped CdS*(s)*$_{nano}$. The solutions contained 150 µM $Cd(NO_3)_2$, 75 µM Na_2S and 600 µM cysteine in 2.2 mM $NaHCO_3$ (pH 7.8).

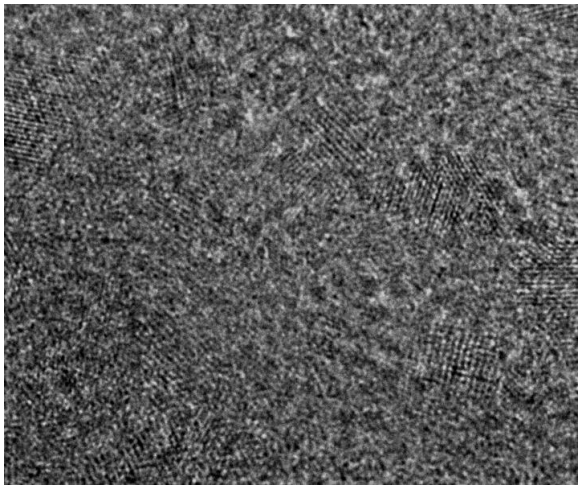

Fig. 13. Transmission electron microscopy (TEM) images of $CdS(s)_{nano}$ precipitated in solutions containing 150 µM $Cd(NO_3)_2$, 75 µM Na_2S and 600 µM cysteine in 2.2 mM $NaHCO_3$ (pH 7.8).

When the $CdS(s)_{nano}$ were excited at λ_{ex} 350 nm, a broad emission centered at 540 nm was observed and this was quenched sequentially on addition of 0.1–0.3 µM Hg^{II} (Fig. 14). Time-resolved fluorescence measurements were performed on all the $CdS(s)_{nano}$ solutions with and without Hg^{II} addition. The measurements were fitted to a biexponential decay curve and the lifetime of the excited state of $CdS(s)_{nano}$ was found not to change with Hg^{II} addition (Fig.15).

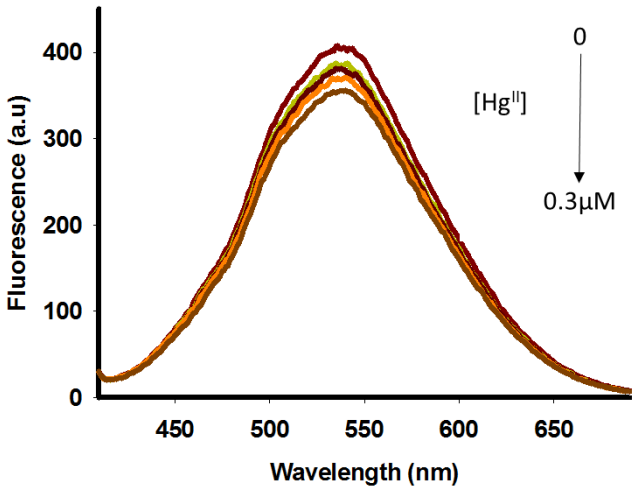

Fig. 14. Fluorescence spectra of $CdS(s)_{nano}$ precipitated in solutions containing 150 µM $Cd(NO_3)_2$, 75 µM Na_2S and 600 µM cysteine in 2.2 mM $NaHCO_3$ (pH 7.8), before and after 0–0.3 µM Hg^{II} addition.

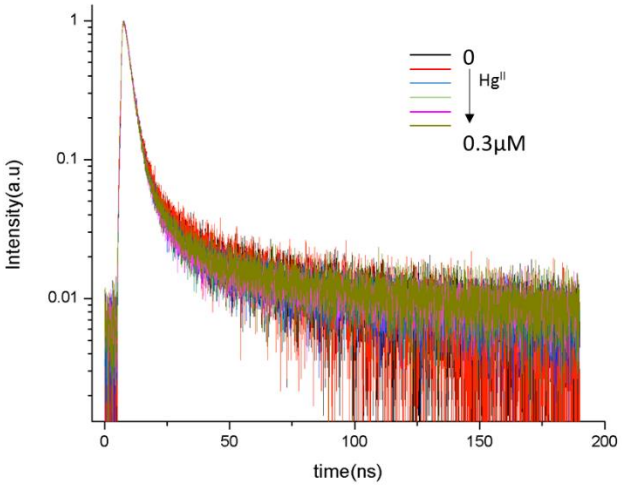

Fig. 15. Overlaid time-resolved fluorescence spectra of CdS*(s)*$_{nano}$ solutions with 0–0.3 μM Hg^{II} added. The CdS*(s)*$_{nano}$ were formed in solutions containing 150 μM $Cd(NO_3)_2$, 75 μM Na_2S and 600 μM cysteine in 2.2 mM $NaHCO_3$ (pH 7.8).

The quenching of CdS*(s)*$_{nano}$ by Hg^{II} was also found to follow the Stern-Volmer relationship, as described in the following equation:

$$F_o/F = 1 + Ka\,Q \qquad (3)$$

Where F_o represents the fluorescence intensity of the pure CdS*(s)*$_{nano}$, F is the fluorescence of particles after addition of Hg^{II}, Q is the concentration of Hg^{II} and Ka is the association constant.

A plot of F_o/F vs. Q, gave a straight line and the log Ka was determined to be 5.7 M^{-1} (Fig. 16). To compare with stability constants in the literature, Ka was converted to K by multiplying with the fraction of the free Hg^{II} present in solution. The fraction of free Hg^{II} is the fraction of Hg^{II} that is not bound to ligands (thiols and sulfide), and was determined by calculating the speciation of Hg^{II} at the conditions of our experiment using the stability constant given in the supporting information. The stability constant for the reaction between Hg^{II} and CdS*(s)*$_{nano}$ was determined to have a log K of 38.

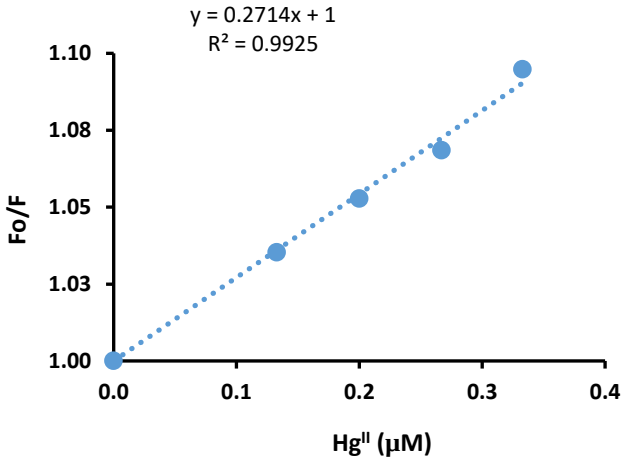

Fig. 16. Stern-Volmer plot for the quenching of CdS*(s)*$_{nano}$ by the addition of 0–0.3 µM Hg^{II}. The CdS*(s)*$_{nano}$ were precipitated in solutions containing 150 µM $Cd(NO_3)_2$, 75 µM Na_2S and 600 µM cysteine in 2.2 mM $NaHCO_3$ (pH 7.8)

2.4. Discussion

2.4.1. Formation of β-HgS(s)$_{nano}$ with Different Capping Agents

Our results show that all the thiols and organic matter used in this study passivated the surface of β-HgS*(s)*$_{nano}$ well enough to prevent sedimentation during the course of the experiment. The passivation can be assumed to be due to Hg^{II}-thiol binding and hydrophobic interactions between the surface of the particle and organic matter in solution, as has been suggested in previous studies.[25,37,42-44,63] The differences in the size of the particles formed imply differences in the ability of the organics to hinder aggregation and growth. Cysteine, a low molecular weight aliphatic molecule, formed particles twice as big as particles formed in 4-mercaptophenyl acetic acid (4-MAA), and glutathione (Fig. 3). Similarly, ELIS DOM and WLIS DOM formed smaller particles than SB DOM (Fig. 2). There was no significant difference between the zeta potentials (Table 2) for particles forming in ELIS DOM, SB DOM, cysteine, and 4-MAA implying the difference in size exhibited by particles capped with ELIS DOM vs SB DOM and particles capped with cysteine vs 4-MAA, is not due to differences in the repulsive forces between like charged particles.

Table 2: The zeta potentials of β-HgS*(s)*$_{nano}$ capped with ELIS DOM, SB DOM, cysteine and 4-mercaptophenylacetic acid (4-MAA).

Ligand	Zeta Potential
ELIS	-34 ± 4.6
SB	-33 ± 9.5
Cyst	-36 ± 8.1
4-MAA	-28 ± 8.8

4-MAA is an aromatic thiol while ELIS DOM and WLIS DOM contain a larger portion of aromatic and humic material than SB (Fig. 8). The capping agents with more aromatic organic matter formed smaller particles than the less aromatic ones, suggesting that steric forces are important in preventing aggregation and growth of nanoparticles. Glutathione, a non-aromatic molecule formed particles smaller than those formed by cysteine possibly because its larger molecular weight than that of cysteine induces steric forces. Our results are in line with previous studies, which found an inverse relation between molecular weight and aromaticity with the size of β-HgS*(s)*$_{nano}$.[25,42,64]

In our experiments, we also found that in addition to molecular weight and aromaticity, multiple thiol groups in a molecule impact the aggregation and growth of particles. Cysteine, an aliphatic monothiol, formed particles with the same core size as the two dithiols used here (Table 1). However, as the hydrodynamic diameter of the dithiol capped particles was much larger than that of particles capped with cysteine, we suggest that one dithiol molecule possibly adsorbed on two neighboring particles causing inter-staple cross-linking. The larger hydrodynamic diameter of the dithiols witnessed in Fig. 3 was thus due to bridged particles diffusing together in solution. This cross-linking behavior has been observed in studies looking at Au, PbS, and CdTe nanoparticles.[65-67] Inter-staple cross-linking reduces the distance between two particles and is known to cause aggregation and precipitation.[65] Here, while the particles capped with monothiols remained suspended in solution; sedimentation occurred within 10 days of reaction when the dithiols were used. The type of organic matter present in aquatic systems thus influences the size and stability of the nanoparticles formed.

2.4.2. Formation of β-HgS(s)$_{nano}$ at Different Hg^{II}:DOM Ratios

β-HgS*(s)*$_{nano}$ were also formed under different ratios of Hg^{II}:DOM from 1.5 nmol – 150 µmole Hg^{II}/mg C. At intermediate ratios (6.8 – 41) of Hg^{II}:DOM used here, a linear relationship between the Hg^{II}:DOM ratio and the size of the particles was observed (Fig. 10b). This linear relationship suggests the size of the particles forming at the intermediate ratios of Hg^{II}:DOM is controlled by the concentration of DOM in solution. To explain this trend, a brief overview on the theory of particle formation is necessary. Nanoparticle formation is described to consist of two steps: nucleation and growth.[36] Prior to nucleation, the high surface energy associated with the creation of a new phase deters particle formation and ions exist in solution as monomers or polynuclear dissolved clusters well beyond the saturation point.[36] At a critical concentration of monomers, a burst of nucleation occurs, creating nuclei of critical size whose high surface energy is balanced by the favorable bonds formed between monomers.[36] Growth follows nucleation and this typically begins with the attachment of new ions to the already formed nuclei.[36,39] The second stage of growth occurs by Oriented Attachment where small particles aggregate and merge to form bigger and more stable particles.[36,37,39] In Oriented Attachment, colliding NPs are first bound by weak van der Waals or electrostatic forces.[37] If the orientation of the two crystals is such that new bonds can be formed between the particles, then surface adsorbed ligands are removed and stronger covalent bonds are formed between the two particles leading to coalescence and growth.[37,68] Growth via Ostwald ripening can also happen, where smaller particles, possessing a higher surface energy than larger particles, dissolve and supply ions that feed the growth of the larger particles.[37] Cysteine capped CdS*(s)*$_{nano}$ forming under similar conditions as used here were found to grow via Oriented Attachment.[37] That is also likely the case for the β-HgS*(s)*$_{nano}$ forming in this study.

In the presence of organic matter, the organic molecules adhere to the surface of the growing nuclei and rapidly undergo adsorption and desorption.[39,69] This process exposes some sections of the surface that become momentarily available for growth by the growth mechanisms mentioned above.[39] We can therefore expect that at a higher concentration of organic matter, more organic molecules compete for the sites on the particle surface; the desorption of one DOM molecule will be more rapidly followed by the adsorption of

another molecule. An increase in the concentration of the organic matter will therefore decrease the accessibility of the particle and hinder growth. In addition, organic molecules also form complexes with metal ions in solution.[39] This complexation hinders the attachment of new ions to the growing nuclei, and the stronger the complex formed the slower the growth of the particle.[39,69] In the same way, an increase in the concentration of organic matter in solution will increase Hg^{II} complexation and inhibit the growth of β-$HgS(s)_{nano}$. The growth of β-$HgS(s)_{nano}$ at the intermediate ratios of Hg^{II}:DOM can be considered to be reaction limited meaning for growth to occur adsorbed molecules need to be removed. The activation energy for growth to occur increases with a decrease in Hg^{II}:DOM ratio, hence the decrease in size with an increase in Hg^{II}:DOM ratio. The rapid increase in size at a Hg^{II}:DOM ratio of 68 μmole Hg^{II} /mg C suggests that the growth of β-$HgS(s)_{nano}$ here is no longer controlled by the DOM concentration. Although the particles did not settle during the course of the experiment, all other ratios used beyond this led to sedimentation within an hour of reaction.

At the lowest two ratios of Hg^{II}:DOM used in this study (1.5 nmol and 1.5 μmol/ mg C), β-$HgS(s)_{nano}$ with large hydrodynamic diameter formed (Fig. 10). TEM images of particles formed at a ratio of 1.5 nmol Hg^{II} /mg C in this study and at a ratio of 1 μmol Hg^{II} /mg C in our earlier studies confirm that particles ~ 5 nm (Fig. 11) formed at these ratios.[62] Large hydrodynamic diameters of Au and hematite particles have been detected under high DOM concentration or high ionic strength.[70,71] It has been suggested that under these conditions, inter and intramolecular forces of DOM are screened resulting in increased DOM adsorption.[70,72] To minimize repulsive forces between the adsorbed DOM molecules, the molecules adopt coiled structures that extend far in to solution.[70-72] Adsorption layers up to 55 nm have been witnessed for hematite nanoparticles stabilized with Aldrich humic acid.[71] The large hydrodynamic diameter of the particles (Fig. 10a) at the two lowest ratios of Hg^{II}:DOM used here are thus likely caused by conformational changes rather than by the aggregation of nanoparticles.

Using the linear relationship between size and Hg^{II}:DOM in Fig. 10b, we predict the average size of particles precipitating at a Hg^{II}:DOM ratio of 1.5 nmol/mg C to be 3.8 and those precipitating at 1.5 μmol/mg C to be 4.5 nm. This is similar to the diameter of the particles determined by TEM in this study

(Fig. 11) and in the earlier studies that we conducted.[62] Using the average diameters of the particles determined by our relation, we estimated that roughly 56 and 49 % of Hg^{II} atoms will be on the surface of the particles formed at a ratio of 1.5 nmol/mg C and 1.5 μmol/mg C, respectively. We used the density and molecular weight of β-HgS*(s)* to determine the volume of one Hg-S molecule (28.7 cm^3 mol^{-1}), and assumed a monolayer coverage of Hg-S monomers on the surface of the particle. As the particles, will have defects and vacancies which will affect the distribution of atoms, our calculations are simply rough estimates of surface atoms. In addition, our relation is based on the hydrodynamic diameter rather than the core diameter of the particles. We also assume that all the Hg atoms on the outermost layer of Hg-S monomers on the particle are accessible from the surface. The factors mentioned above, and which we don't take into account here, will affect the actual % of Hg atoms present on the surface. Nonetheless, our relation suggests that β-HgS*(s)* forming in the natural environment will have a size of ~ 5 nm with a substantial fraction of the atoms residing on the surface of the particles. The surface atoms on the nanoparticles are labile and maybe more prone to dissolution. It has also been suggested that the labile surface atoms could interact with ligands present on the cell wall of Hg methylating bacteria, and are thus more bioavailable for uptake by the bacteria relative to bigger micrometer sized particles.[34] The uptake mechanism of β-$HgS(s)_{nano}$ by Hg methylating bacteria has however, not been demonstrated.

Our results showing increase in size with decreasing concentration of organic matter are consistent with previous studies using fresh water and soil derived DOM.[26,42] For example, it was found that in the presence of Suwannee River Humic Acid (SRHA) at a ratio of 3 μmol Hg^{II}/mg C, the nanoparticles were ~ 50 nm, and increased with decreasing ratio to be >150 nm at a ratio of 12 μmol Hg^{II}/mg C.[42] Here we similarly show that high Hg^{II}:DOM ratios are required to induce aggregation and sedimentation. It is useful to consider the relative ratio of Hg^{II} to thiol ligands in the DOM under these conditions. Various investigators have estimated the number of thiol groups (RSH) in DOM and suggest that the mole ratio of RSH groups to DOC ranges from 0.0006 to 0.0009 mol RSH/mol C.[10,22] Using these ratios, we can estimate that at a Hg^{II}:DOM ratio of between 0.05 and 0.08 μmol Hg^{II}/mg C the mole ratio of Hg^{II} to RSH ligands starts to be >1. Considering that not all the Hg atoms are on the surface of the nanoparticles, especially as

they begin to increase in size, a higher ratio would be needed before aggregation and precipitation is induced.

As discussed above, size reflects the inability of the organic matter to effectively cap the surface and prevent aggregation, so this should start occurring in the range of concentrations where the ratio of surface Hg atoms to RSH is greater than 1. From Fig. 10 it appears that somewhat higher surface Hg^{II}:RSH mole ratios (~60) are required before substantial particle growth begins suggesting either that the estimate of thiol concentration above is too low, or that other ligands besides thiols, may be involved in the interaction with the nanoparticle surface. While previous studies have indicated that carboxylic acids are not effective in hindering the precipitation β-HgS*(s)* even at low Hg^{II}:DOM ratios (0.8 μmol Hg/mg C), it is possible that the amine groups and other strong binding sites within the DOM could also be involved in the passivation of the surface of β-HgS$(s)_{nano}$.[42] In calculating the mole ratios of surface Hg atoms to RSH in Fig. 10, we assumed 100% yield of β-HgS$(s)_{nano}$. The actual yield is however much less than 100%, but since the unreacted Hg^{II} likely exists as bound to two thiol groups on DOM molecules, the ratio of Hg atoms on the surface of the nanoparticles to unbound thiol groups will be higher than 60 further supporting the involvement of other functional groups in the passivation of the nanoparticle surface.

Under high ionic strength, the high salt concentration will undoubtedly shield repulsive forces induced by the adsorbed layer of DOM between particles and possibly lead to aggregation and sedimentation, even at low Hg^{II}: DOM ratios. We did not investigate the effect of ionic strength on the aggregation and growth of β-HgS$(s)_{nano}$. Previous studies on β-HgS$(s)_{nano}$ stabilized by humic acids indicate that the growth rate of particles increase at a higher ionic strength, though this was not reported to lead to bulk precipitation.[42] The presence of multivalent ions in solution is also likely to destabilize the nanoparticles by bridging DOM molecules, similar to the effect of the dithiols discussed earlier. Indeed, relatively small concentrations of Mg^{2+}, Ca^{2+}, and Al^{3+} induced the aggregation of CdTe quantum dots, yet they remained stable at high concentrations of KCl.[73] Even considering a well-passivated particle, high concentrations of mono and divalent ions in solution can induce aggregation and sedimentation. The settled particles, however, can be expected to remain loosely bound due to the intercalation of the DOM molecules

between the particles. Particles effectively passivated by DOM but aggregating under high salt concentration could be re-suspended with mechanical perturbation.

2.4.3. Persistence of β-HgS(s)$_{nano}$ in the Environment

Short and long term studies looking at the change in particle size reveal that the diameter of the β-HgS*(s)*$_{nano}$ formed in cysteine and marine DOM did not change appreciably with time (Fig. 3 and 4). This is similar to what previous studies have found for particles forming in Suwanee river humic and fulvic acid —a terrestrially derived DOM.[24,42] Pham *et al.*, using Small Angle X-ray Scattering (SAXS) suggests that contrary to the DLS results, particles are in fact aggregating in solution.[24] It was argued that the constant diameter by DLS is because the intensity weighted DLS measurements are biased towards bigger particles which in this case are not increasing in size. Other studies have shown that the Hg-S-DOM solution is in a state of dynamic equilibrium where the formation and dissolution of β-HgS*(s)*$_{nano}$ is happening continuously over time.[25] In our system, we monitored particles for over a month, and during this time the average growth rate was 0.6 and 4 nm/week for ELIS and SB DOM, respectively (Fig. 6). Also, no sedimentation was noticed during the entire period. Our results suggest that while it is possible that formation, aggregation, and dissolution of β-HgS*(s)*$_{nano}$ are all concurrently happening over time, the slight growth rate observed after 5 weeks indicates aggregation may be a more dominant process, albeit happening at a slow rate.

Rapid aggregation and growth happened when the solutions were purged with air and/or exposed to sunlight (Fig. 9). Irradiation is known to cause the photo-degradation of DOM by reactive oxygen species — produced from reactions involving an excited DOM molecule and a singlet $^1O_2$ molecule.[74,75] Photo-degradation degrades aromatic compounds, particularly those with phenolic structures.[74,76,77] The aromatic content, as determined from SUVA at 254 nm, of the DOM remaining in solution after particle precipitation was 2.4 L mg^{-1} m^{-1} for the light oxic vials and 2.9 L mg^{-1} m^{-1} for the dark anoxic vials. These values are both lower than the SUVA for ELIS DOM determined before the addition of Hg^{II} and HS^- (4.9 L mg^{-1}m^{-1}). For the dark anoxic vials, the precipitation of β-HgS*(s)*$_{nano}$ was induced by the addition of $CaCl_2$ to the reaction solutions while in the light oxic vials, particles precipitated naturally and $CaCl_2$ was added to keep

the conditions between the two experiments similar. While the lower SUVA value for the light oxic vials relative to the value for ELIS DOM before Hg^{II} and HS^- addition can be attributed to the degradation of the aromatic components of DOM; the lower SUVA for the DOM in the dark anoxic vials was likely because the DOM adsorbed on the β-HgS*(s)*$_{nano}$ also settled with the particles when precipitation was induced by adding $CaCl_2$. Thus, the supernatant solution from the dark anoxic vials was deficient in aromatic components of DOM. The photo-oxidation of DOM in the light oxic vials could have been enhanced by the presence of β-HgS*(s)*$_{nano}$ themselves. Because of the quantum confinement effect discussed earlier, the band gap of β-HgS*(s)*$_{nano}$ lies in the UV-Vis region. Absorption of light by the β-HgS*(s)*$_{nano}$ can result in the excitation of electrons from the valence band to the conduction band and if this electron is captured by a dissolved oxygen molecule, a superoxide radical can be produced. Indeed, the potential for photocatalytic degradation of aromatic pollutants by metal sulfide nanoparticles has been explored.[78,79] It is also possible that light and air induced other changes in the DOM molecules, such as the photoxidation of thiol groups or the formation of nanoparticles from DOM, which might have contributed to the growth and aggregation of β-HgS*(s)*$_{nano}$ when exposed to air and light.

Aside from photo-oxidizing the DOM, presence of dissolved oxygen in our systems might be suspected to cause the oxidative dissolution of the β-HgS*(s)*$_{nano}$. Oxidative/reductive dissolution is known to occur for minerals containing elements that are redox-sensitive.[64] Both Hg and S undergo redox reactions, but only the oxidation of S on HgS*(s)* has been shown to contribute to its dissolution.[64,80] The rate of dissolution of cinnabar (α-HgS*(s)*) was found to be similar to the weathering of stable minerals like quartz.[81] Though others have suggested that DOM can catalyze the oxidation of S, very little has been done to explore the role of DOM on the oxidative dissolution of HgS*(s)*.[64] In our experiments, dissolution could not have occurred appreciably as particle size increased rather than decreased with exposure to air and/or light (Fig.11). Additionally, sedimentation was noticed 2 weeks later in the light oxic vials and not in any of the other vials, suggesting that β-HgS*(s)*$_{nano}$ in light oxic conditions continued to aggregate and eventually precipitate out of solution. Overall, our results indicate that photo-induced changes in DOM affect the fate of β-HgS*(s)*$_{nano}$ forming in aquatic systems.

2.4.4. The Interaction of Hg^{II} with $CdS(s)_{nano}$

$CdS(s)_{nano}$ were formed from solutions containing 600 µM cysteine and 150 µM each of Cd^{II} and HS^-. The band gap energy of the $CdS(s)_{nano}$ synthesized here was 417 nm (Fig. 12) and the particle size calculated using equation 2 was 3.5 nm—comparable to the size determined from TEM images (Fig.13). When electrons in the valence band of the $CdS(s)_{nano}$ are excited to the conduction band, they can relax radiatively to give a band gap emission or a trap state emission. During a band gap emission, the excited electrons return straight from the conduction band back to the valence band and emit a photon of the same energy as the band gap of the particle. A trap state emission, on the other hand, arises from the presence of trap states in the lattice of $CdS(s)_{nano}$. During a trap state emission, the excited electrons first relax non-radiatively from the conduction band to a trap state; and then radiatively back to the valence band (Fig. 17). The trap state emission therefore occurs at a longer wavelength than the band gap emission. For the $CdS(s)_{nano}$ synthesized here, the emission of the particles was observed at 540 nm when particles were excited at 350 nm; thus, the emission lies lower in energy than the bag gap of the particles (417 nm). We can therefore conclude that the observed fluorescence of the $CdS(s)_{nano}$ in Fig. 14 is due to a trap state emission.

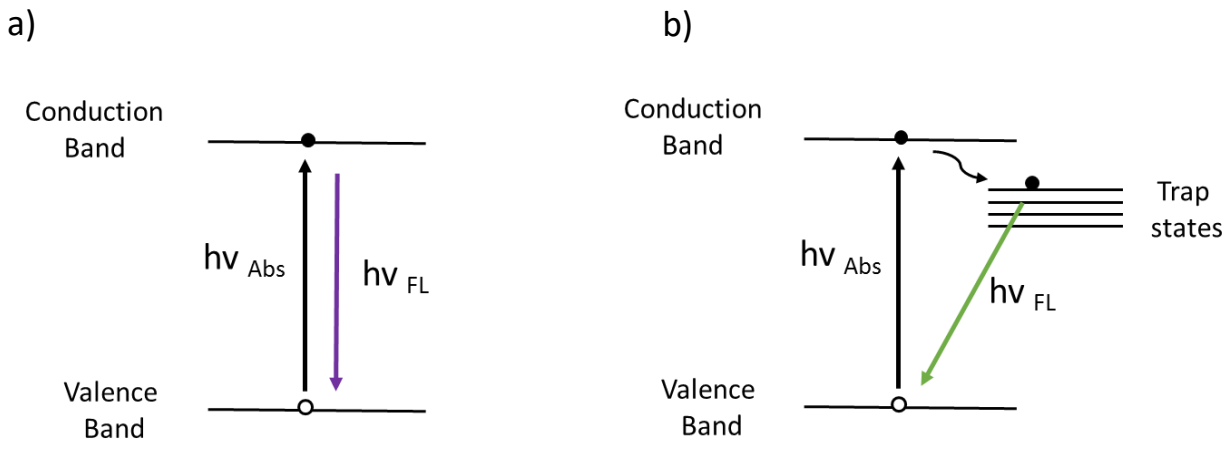

Fig. 17. Schematic diagram describing the bandgap (a); and trap state (b) emission of $CdS(s)_{nano}$.

Vaematahau *et al*. determined using photoluminescence spectroscopy and X-ray Photoelectron Spectroscopy (XPS), that the trap state emission in $CdS(s)_{nano}$ originates from the presence of unsaturated Cd atoms on the surface of the particles.[82] $CdS(s)_{nano}$ well passivated with thiol ligands or encapsulated with a layer of another material such as ZnS or $Cd(OH)_2$ showed no trap sate emission.[83-85] In our experiments, the $CdS(s)_{nano}$ were sulfide deficient as the concentration of HS^- in solution was half the concentration of Cd^{II}. The surface of the $CdS(s)_{nano}$ was thus Cd enriched and this may have contributed to the trap state emission observed. Though the concentration of cysteine was four times that of Cd^{II}, complete passivation of the surface trap states by the thiol ligands is difficult due to steric hindrance.[86]

The quenching of the fluorescence of $CdS(s)_{nano}$ observed in Fig. 14 on addition of different concentrations of Hg^{II} to the $CdS(s)_{nano}$ solutions, followed a linear trend described by the Stern-Volmer relationship (Eqn. 3). The quenching of the fluorescence can be due to static or dynamic quenching. While in static quenching, the quenching is due to the formation of a non-fluorescent complex, dynamic quenching occurs due to an increase in non-radiative decay processes caused by molecular collisions between the fluorophores and ions in solution. As dynamic quenching increases the non-radiative decay rate, it decreases the lifetime of the excited state of the material. Time-resolved fluorescence measurements of our $CdS(s)_{nano}$ solutions show that the lifetime of the excited state of $CdS(s)_{nano}$ did not change during the quenching process; suggesting that the quenching was static rather than dynamic. Using the Stern-Volmer relationship, we determined the stability constant for the reaction between Hg^{II} and $CdS(s)_{nano}$ (depicted in Eqn. 4) to be 10^{38}; a value similar to the constant for the formation of β-HgS*(s)*.

$$\underset{\textit{fluorescent}}{CdS(s)_{nano}} + Hg^{II} \longrightarrow \underset{\textit{non-fluorescent}}{Hg\text{–}CdS(s)_{nano}} \qquad (4)$$

The nature of the non-fluorescent complex formed in equation 4 could not be determined in this work. Efforts to map the elemental composition of the products using high resolution TEM (HRTEM) were unsuccessful as the images were blurred during mapping, likely because of the high concentration of cysteine present in our solutions. However, mixed complexes of Cd and Hg chalcogenide have been

synthesized before from the partial exchange of Cd^{II} in CdS or CdTe quantum dots by Hg^{II} added in solution, and is also possible here.[47,84,87]

2.5. Conclusions and Environmental Implications

Previous studies have reported higher Hg^{II} methylation rates in offshore marine environments relative to estuaries and coastal systems. For example, Hollweg *et al.* reported higher Hg^{II} methylation rates in the continental shelf and the slope of the mid-Atlantic continental margin relative to the Chesapeake Bay (an estuary).[11] Hammerschmidt *et al.*, reported higher MeHg production in Long Island Sound and continental shelf relative to the NY/NJ harbor.[8] Higher Hg^{II} methylation rates in certain systems over others has been mainly attributed to four things: i), low binding affinity of Hg^{II} to particulate organic matter in the sediment which increases the dissolved Hg^{II} concentrations in porewater and consequently its bioavailability to methylating bacteria; ii) fresh labile inputs of organic matter which stimulate bacterial methylating activity; iii) the formation of Hg-S neutral complexes which are more bioavailable than charged species; and iv) the formation of smaller β-HgS*(s)* particles which are more bioavailable than bigger particles.[8,11,14,88,89] While the first three reasons for higher MeHg production can be possible explanations for the high methylation rates recorded in offshore environments, the last cannot. Our results show that bigger and less stable NPs form in presence of SB DOM (extracted offshore) relative to ELIS DOM (extracted closer to shore). Thus, NPs forming in offshore environments, where the DOM is less humic, will be bigger and less available than those forming in coastal or estuarine environments.

In this work, we used equimolar concentrations of mercury and sulfur to precipitate the NPs. This is unlikely to be found in the environment, where the concentration of mercury is lower than that of sulfide. Typical concentrations of mercury and sulfur in uncontaminated systems range from 10–600 pM and 0.1–1000 µM, respectively.[10,15,90] In experiments where we varied the mole ratio of Hg:S from 1 to 10^{-5}, we were unable to get a consistent measurement from DLS as the solutions were highly variable and in most cases the measurement was aborted. Using speciation modeling, we determined that the saturation index of β-HgS*(s)* (Q/K) will be exceeded for environments containing nM concentrations of mercury and µM

concentrations of sulfide, close to what will be found in pristine systems. In contaminated environments, the concentration of mercury is in the nM range and the precipitation of β-HgS*(s)*$_{nano}$ capped with organic matter is very likely.[91,92] In both contaminated and pristine environments, the presence of various other metal ions in solution causes mixed metal sulfides to precipitate.[93] In systems containing iron, phosphate and arsenic, mixed co-precipitates with the composition Fe[$(OH)_3$, PO_4].nH_2O) and Fe[$(OH)_3$, AsO_4, PO_4].nH_2O are known to form at Fe/P ratios lower than predicted by the solubility of their respective bulk materials.[32,94] This suggests that mixed β-HgS*(s)*$_{nano}$ precipitates can also form in the environment at ratios lower than predicted from thermodynamic calculations.

Our results also show that β-HgS*(s)*$_{nano}$ forming in porewater should remain stable in dark anoxic conditions for more than a month. Additionally, as discussed in Chapter 3, there is evidence that Hg^{II} in the form of β-HgS*(s)*$_{nano}$ is more bioavailable to Hg methylating bacteria than micro-sized β-HgS*(s)*, although it is not as bioavailable as other Hg^{II} complexes. Therefore, the presence of nanoparticles in sediments could affect the rate at which inorganic Hg is converted into MeHg in sediments.

The transportation of β-HgS*(s)*$_{nano}$ from dark porewaters to surface waters can impact the stability of the particles as DOM adsorbed on the surface of the particles will photodegrade on exposure to sunlight. The *in situ* production or fresh inputs of unreacted DOM, however, can be expected to counteract its loss by photodegradation, and replace the degraded organic matter on the surface of the particles. Aggregation and sedimentation of the particles is also expected to happen when β-HgS*(s)*$_{nano}$ encounters solutions of high ionic strength; though this will likely result in the formation of loosely bound particles that can be easily re-suspended back into the water column with disturbances such as animal burrowing activities or during a storm event.

The interaction of Hg^{II} with CdS*(s)*$_{nano}$ shown here has major implications for the behavior of engineered nanoparticles and their exposure to marine organisms. Semiconductor nanoparticles commonly known as quantum dots, include CdS, CdSe, CdTe and ZnS. Their use in medical imaging, photovoltaic and solar cells, has increased over the years, which means their eventual release into the aquatic systems is inevitable.[95] Quantum dots entering the marine environment can be incorporated into marine snow and

taken up by filter-feeders such as bivalves, as has been shown for TiO_2 nanoparticles.[96] Marine snow is composed of organic and inorganic particles bound together by a polymeric material excreted by bacteria and phytoplankton.[97] As the capture efficiency of particles by bivalves increases with particles size, the incorporation of quantum dots into marine snow increases their bioavailability to marine organisms.[98] The incorporation of Hg^{II} in $CdS_{(s)nano}$, as shown in our experiments, will thus increase the bioavailability of Hg^{II} to bivalves and other filter feeders, who would otherwise not have taken up the mercury from the dissolved phase.

References

1. Compeau, G.C.; Bartha, R. Sulfate-reducing bacteria: Principal methylators of mercury in anoxic estuarine sediment. *Appl. Environ. Microbiol.* **1985,** *50* (2), 498-502.

2. Parks, J.M.; Johs, A.; Podar, M.; Bridou, R.; Hurt Jr., R.A.; Smith, S.D.; Tomanicek, S.J.; Qian, Y.; Brown, S.D.; Brandt, C.C.; Palumbo, A.V.; Smith, J.C.; Wall, J.D.; Elias, D.A.; Liang, L. The genetic basis for bacterial mercury methylation. *Science* **2013,** *339* (6125), 1332-1335; 10.1126/science.1230667.

3. Gilmour, C.C.; Podar, M.; Bullock, A.L.; Graham, A.M.; Brown, S.D.; Somenahally, A.C.; Johs, A.; Hurt, R.A.; Bailey, K.L.; Elias, D.A. Mercury methylation by novel microorganisms from new environments. *Environ. Sci. Technol.* **2013,** *47* (20), 11810-11820; 10.1021/es403075t.

4. Capone, D.G.; Kiene, R.P. Comparison of microbial dynamics in marine and freshwater sediments: Contrasts in anaerobic carbon catabolism. *Limnol. Oceanogr.* **1988,** *33* (4part2), 725-749; 10.4319/lo.1988.33.4part2.0725.

5. Mason, R.P.; Lawson, N.M.; Lawrence, A.L.; Leaner, J.J.; Lee, J.G.; Sheu, G.-. Mercury in the Chesapeake Bay. *Mar. Chem.* **1999,** *65* (1-2), 77-96.

6. King, J.K.; Kostka, J.E.; Frischer, M.E.; Saunders, F.M.; Jahnke, R.A. A quantitative relationship that demonstrates mercury methylation rates in marine sediments are based on the community composition and activity of sulfate-reducing bacteria. *Environ. Sci. Technol.* **2001,** *35* (12), 2491-2496; 10.1021/es001813q.

7. Balcom, P.H.; Fitzgerald, W.F.; Vandal, G.M.; Lamborg, C.H.; Rolfhus, K.R.; Langer, C.S.; Hammerschmidt, C.R. Mercury sources and cycling in the Connecticut River and Long Island Sound. *Mar. Chem.* **2004,** *90* (1-4 SPEC. ISS.), 53-74.

8. Hammerschmidt, C.R.; Fitzgerald, W.F.; Balcom, P.H.; Visscher, P.T. Organic matter and sulfide inhibit methylmercury production in sediments of New York/New Jersey Harbor. *Mar. Chem.* **2008,** *109* (1-2), 165-182.

9. Sunderland, E.M.; Gobas, F.A.P.C.; Branfireun, B.A.; Heyes, A. Environmental controls on the speciation and distribution of mercury in coastal sediments. *Mar. Chem.* **2006,** *102* (1-2), 111-123; 10.1016/j.marchem.2005.09.019.

10. Hollweg, T.A.; Gilmour, C.C.; Mason, R.P. Mercury and methylmercury cycling in sediments of the mid-Atlantic continental shelf and slope. *Limnol. Oceanogr.* **2010,** *55* (6), 2703-2722.

11. Hollweg, T.A.; Gilmour, C.C.; Mason, R.P. Methylmercury production in sediments of Chesapeake Bay and the mid-Atlantic continental margin. *Mar. Chem.* **2009,** *114* (3-4), 86-101; 10.1016/j.marchem.2009.04.004.

12. Mergler, D.; Anderson, H.A.; Chan, L.H.M.; Mahaffey, K.R.; Murray, M.; Sakamoto, M.; Stern, A.H. Methylmercury exposure and health effects in humans: A worldwide concern. *Ambio* **2007,** *36* (1), 3-11; 10.1579/0044-7447(2007)36[3:MEAHEI]2.0.CO;2.

13. Wood, J.M. Biological cycles for toxic elements in the environment. *Science* **1974,** *183* (4129), 1049-1052.

14. Benoit, J.M.; Gilmour, C.C.; Mason, R.P.; Heyes, A. Sulfide controls on mercury speciation and bioavailability to methylating bacteria in sediment pore waters. *Environ. Sci. Technol.* **1999,** *33* (6), 951-957; 10.1021/es9808200.

15. Schartup, A.T.; Mason, R.P.; Balcom, P.H.; Hollweg, T.A.; Chen, C.Y. Methylmercury production in estuarine sediments: Role of organic matter. *Environmental Science and Technology* **2013,** *47* (2), 695-700.

16. Schartup, A.T.; Balcom, P.H.; Mason, R.P. Sediment-porewater partitioning, total sulfur, and methylmercury production in estuaries. *Environ. Sci. Technol.* **2014,** *48* (2), 954-960; 10.1021/es403030d; 10.1021/es403030d.

17. Liu, B.; Schaider, L.A.; Mason, R.P.; Shine, J.P.; Rabalais, N.N.; Senn, D.B. Controls on methylmercury accumulation in northern Gulf of Mexico sediments. *Estuar. Coast. Shelf Sci.* **2015,** *159*, 50-59; 10.1016/j.ecss.2015.03.030.

18. Jonsson, S.; Skyllberg, U.; Nilsson, M.B.; Westlund, P.-.; Shchukarev, A.; Lundberg, E.; Björn, E. Mercury methylation rates for geochemically relevant HgII species in sediments. *Environmental Science and Technology* **2012,** *46* (21), 11653-11659.

19. Schaefer, J.K.; Morel, F.M.M. High methylation rates of mercury bound to cysteine by Geobacter sulfurreducens. *Nat. Geosci.* **2009,** *2* (2), 123-126; 10.1038/ngeo412.

20. Schaefer, J.K.; Szczuka, A.; Morel, F.M.M. Effect of divalent metals on Hg(II) uptake and methylation by bacteria. *Environ. Sci. Technol.* **2014,** *48* (5), 3007-3013; 10.1021/es405215v.

21. Tossell, J.A. Calculation of the structures, stabilities, and properties of mercury sulfide species in aqueous solution. *Journal of Physical Chemistry A* **2001,** *105* (5), 935-941.

22. Skyllberg, U. Competition among thiols and inorganic sulfides and polysulfides for Hg and MeHg in wetland soils and sediments under suboxic conditions: Illumination of controversies and implications for MeHg net production. *Journal of Geophysical Research: Biogeosciences* **2008,** *113* (G2), - G00C03; 10.1029/2008JG000745.

23. Hsu-Kim, H.; Kucharzyk, K.H.; Zhang, T.; Deshusses, M.A. Mechanisms regulating mercury bioavailability for methylating microorganisms in the aquatic environment: A critical review. *Environ. Sci. Technol.* **2013,** *47* (6), 2441-2456; 10.1021/es304370g.

24. Pham, A.L.T.; Morris, A.; Zhang, T.; Ticknor, J.; Levard, C.; Hsu-Kim, H. Precipitation of nanoscale mercuric sulfides in the presence of natural organic matter: Structural properties, aggregation, and biotransformation. *Geochim. Cosmochim. Acta* **2014,** *133*, 204-215; 10.1016/j.gca.2014.02.027.

25. Slowey, A.J. Rate of formation and dissolution of mercury sulfide nanoparticles: The dual role of natural organic matter. *Geochim. Cosmochim. Acta* **2010,** *74* (16), 4693-4708.

26. Gerbig, C.A.; Kim, C.S.; Stegemeier, J.P.; Ryan, J.N.; Aiken, G.R. Formation of nanocolloidal metacinnabar in mercury-DOM-sulfide systems. *Environ. Sci. Technol.* **2011,** *45* (21), 9180-9187; 10.1021/es201837h.

27. Barnett, M.O.; Harris, L.A.; Turner, R.R.; Stevenson, R.J.; Henson, T.J.; Melton, R.C.; Hoffman, D.P. Formation of mercuric sulfide in soil. *Environ. Sci. Technol.* **1998,** *31* (11), 3037-3043; 10.1021/es960389j.

28. Labrenz, M.; Druschel, G.K.; Thomsen-Ebert, T.; Gilbert, B.; Welch, S.A.; Kemner, K.M.; Logan, G.A.; Summons, R.E.; De Stasio, G.; Bond, P.L.; Lai, B.; Kelly, S.D.; Banfield, J.F. Formation of sphalerite (ZnS) deposits in natural biofilms of sulfate-reducing bacteria. *Science* **2000,** *290* (5497), 1744-1747.

29. Hochella Jr., M.F.; Moore, J.N.; Putnis, C.V.; Putnis, A.; Kasama, T.; Eberl, D.D. Direct observation of heavy metal-mineral association from the Clark Fork River Superfund Complex: Implications for metal transport and bioavailability. *Geochim. Cosmochim. Acta* **2005,** *69* (7), 1651-1663.

30. Weber, F.-.; Voegelin, A.; Kaegi, R.; Kretzschmar, R. Contaminant mobilization by metallic copper and metal sulphide colloids in flooded soil. *Nature Geoscience* **2009,** *2* (4), 267-271.

31. Lowry, G.V.; Shaw, S.; Kim, C.S.; Rytuba, J.J.; Brown Jr., G.E. Macroscopic and microscopic observations of particle-facilitated mercury transport from New Idria and Sulphur Bank mercury mine tailings. *Environ. Sci. Technol.* **2004,** *38* (19), 5101-5111; 10.1021/es034636c.

32. Hochella, M.F.,Jr; Lower, S.K.; Maurice, P.A.; Penn, R.L.; Sahai, N.; Sparks, D.L.; Twining, B.S. Nanominerals, mineral nanoparticles, and Earth systems. *Science* **2008,** *319* (5870), 1631-1635; 10.1126/science.1141134; 10.1126/science.1141134.

33. Auffan, M.; Rose, J.; Bottero, J.Y.; Lowry, G.V.; Jolivet, J.P.; Wiesner, M.R. Towards a definition of inorganic nanoparticles from an environmental, health and safety perspective. *Nat. Nanotechnol* **2009,** *4* (10), 634-641; 10.1038/nnano.2009.242; 10.1038/nnano.2009.242.

34. Zhang, T.; Kim, B.; Levard, C.; Reinsch, B.C.; Lowry, G.V.; Deshusses, M.A.; Hsu-Kim, H. Methylation of mercury by bacteria exposed to dissolved, nanoparticulate, and microparticulate mercuric sulfides. *Environmental Science and Technology* **2012,** *46* (13), 6950-6958.

35. Zhang, T.; Kucharzyk, K.H.; Kim, B.; Deshusses, M.A.; Hsu-Kim, H. Net methylation of mercury in estuarine sediment microcosms amended with dissolved, nanoparticulate, and microparticulate mercuric sulfides. *Environ. Sci. Technol.* **2014,** *48* (16), 9133-9141; 10.1021/es500336j.

36. Polte, J. Fundamental growth principles of colloidal metal nanoparticles - a new perspective. *Crystengcomm* **2015,** *17* (36), 6809-6830; 10.1039/c5ce01014d.

37. Mullaugh, K.M.; Luther III, G.W. Growth kinetics and long-term stability of CdS nanoparticles in aqueous solution under ambient conditions. *Journal of Nanoparticle Research* **2011,** *13* (1), 393-404.

38. Philippe, A.; Schaumann, G.E. Interactions of dissolved organic matter with natural and engineered inorganic colloids: A review. *Environ. Sci. Technol.* **2014,** *48* (16), 8946-8962; 10.1021/es502342r.

39. Yin, Y.; Alivisatos, A.P. Colloidal nanocrystal synthesis and the organic-inorganic interface. *Nature* **2005,** *437* (7059), 664-670; 10.1038/nature04165.

40. Boles, M.A.; Ling, D.; Hyeon, T.; Talapin, D.V. The surface science of nanocrystals. *Nat. Mater.* **2016,** *15* (2), 141-153; 10.1038/nmat4526.

41. Qin, D.Z.; Ma, X.M.; Yang, L.; Zhang, L.; Ma, Z.J.; Zhang, J. Biomimetic synthesis of HgS nanoparticles in the bovine serum albumin solution. *J. Nanopart. Res.* **2008,** *10* (4), 559-566; 10.1007/s11051-007-9284-9.

42. Deonarine, A.; Hsu-Kim, H. Precipitation of mercuric sulfide nanoparticles in NOM-containing water: Implications for the natural environment. *Environmental Science and Technology* **2009,** *43* (7), 2368-2373.

43. Ravichandran, M.; Aiken, G.R.; Ryan, J.N.; Reddy, M.M. Inhibition of precipitation and aggregation of metacinnabar (mercuric sulfide) by dissolved organic matter isolated from the Florida Everglades. *Environ. Sci. Technol.* **1999,** *33* (9), 1418-1423; 10.1021/es9811187.

44. Deonarine, A.; Lau, B.L.; Aiken, G.R.; Ryan, J.N.; Hsu-Kim, H. Effects of humic substances on precipitation and aggregation of zinc sulfide nanoparticles. *Environ. Sci. Technol.* **2011,** *45* (8), 3217-3223; 10.1021/es1029798; 10.1021/es1029798.

45. Lau, B.L.T.; Hsu-Kim, H. Precipitation and growth of zinc sulfide nanoparticles in the presence of thiol-containing natural organic ligands. *Environ. Sci. Technol.* **2008,** *42* (19), 7236-7241; 10.1021/es801360b.

46. Aiken, G.R.; Hsu-Kim, H.; Ryan, J.N. Influence of dissolved organic matter on the environmental fate of metals, nanoparticles, and colloids. *Environ. Sci. Technol.* **2011,** *45* (8), 3196-3201; 10.1021/es103992s; 10.1021/es103992s.

47. Smith, A.M.; Nie, S. Bright and compact alloyed quantum dots with broadly tunable near-infrared absorption and fluorescence spectra through mercury cation exchange. *J. Am. Chem. Soc.* **2011,** *133* (1), 24-26; 10.1021/ja108482a.

48. Jaiswal, A.; Ghsoh, S.S.; Chattopadhyay, A. Quantum dot impregnated-chitosan film for heavy metal ion sensing and removal. *Langmuir* **2012,** *28* (44), 15687-15696; 10.1021/la3027573.

49. Beberwyck, B.J.; Surendranath, Y.; Alivisatos, A.P. Cation exchange: A versatile tool for nanomaterials synthesis. *J. Phys. Chem. C* **2013,** *117* (39), 19759-19770; 10.1021/jp405989z.

50. Haitzer, M.; Aiken, G.R.; Ryan, J.N. Binding of mercury(II) to dissolved organic matter: The role of the mercury-to-DOM concentration ratio. *Environ. Sci. Technol.* **2002,** *36* (16), 3564-3570; 10.1021/es025699i.

51. Dittmar, T.; Koch, B.; Hertkorn, N.; Kattner, G. A simple and efficient method for the solid-phase extraction of dissolved organic matter (SPE-DOM) from seawater. *Limnol. Oceanogr. Methods* **2008,** *6* (JUN), 230-235.

52. Brouwer, H.; Murphy, T.P. Diffusion method for the determination of acid-volatile sulfides (AVS) in sediment. *Environ. Toxicol. Chem.* **1994,** *13* (8), 1273-1275.

53. Skyllberg, U. Chemical speciation of mercury in soil and sediment, In *Environmental Chemistry and Toxicology of Mercury*, Anonymous ;2011; pp. 219-258.

54. Lamborg, C.H.; Tseng, C.-.; Fitzgerald, W.F.; Balcom, P.H.; Hammerschmidt, C.R. Determination of the mercury complexation characteristics of dissolved organic matter in natural waters with "reducible Hg" titrations. *Environ. Sci. Technol.* **2003,** *37* (15), 3316-3322; 10.1021/es0264394.

55. Miller, C.L.; Southworth, G.; Brooks, S.; Liang, L.; Gu, B. Kinetic controls on the complexation between mercury and dissolved organic matter in a contaminated environment. *Environ. Sci. Technol.* **2009,** *43* (22), 8548-8553; 10.1021/es901891t.

56. Gasper, J.D.; Aiken, G.R.; Ryan, J.N. A critical review of three methods used for the measurement of mercury (Hg2+)-dissolved organic matter stability constants. *Appl. Geochem.* **2007,** *22* (8 SPEC. ISS.), 1583-1597; 10.1016/j.apgeochem.2007.03.018.

57. Jiang, T.; Skyllberg, U.; Wei, S.; Wang, D.; Lu, S.; Jiang, Z.; Flanagan, D.C. Modeling of the structure-specific kinetics of abiotic, dark reduction of Hg(II) complexed by O/N and S functional groups in humic acids while accounting for time-dependent structural rearrangement. *Geochim. Cosmochim. Acta* **2015,** *154*, 151-167; 10.1016/j.gca.2015.01.011.

58. Burdige, D.J.; Kline, S.W.; Chen, W. Fluorescent dissolved organic matter in marine sediment pore waters. *Mar. Chem.* **2004,** *89* (1-4), 289-311; 10.1016/j.marchem.2004.02.015.

59. Lawaetz, A.J.; Stedmon, C.A. Fluorescence intensity calibration using the Raman scatter peak of water. *Appl. Spectrosc.* **2009,** *63* (8), 936-940; 10.1366/000370209788964548.

60. Green, N.W.; Perdue, E.M.; Aiken, G.R.; Butler, K.D.; Chen, H.; Dittmar, T.; Niggemann, J.; Stubbins, A. An intercomparison of three methods for the large-scale isolation of oceanic dissolved organic matter. *Mar. Chem.* **2014,** *161*, 14-19; 10.1016/j.marchem.2014.01.012.

61. Wang, Y.; Herron, N. Nanometer-sized semiconductor clusters: Materials synthesis, quantum size effects, and photophysical properties. *J. Phys. Chem.* **1991,** *95* (2), 525-532.

62. Mazrui, N.M.; Jonsson, S.; Thota, S.; Zhao, J.; Mason, R.P. Enhanced availability of mercury bound to dissolved organic matter for methylation in marine sediments. *Geochim. Cosmochim. Acta* **2016,** *194*, 153-162; 10.1016/j.gca.2016.08.019.

63. Mullaugh, K.M.; Luther III, G.W. Spectroscopic determination of the size of cadmium sulfide nanoparticles formed under environmentally relevant conditions. *Journal of Environmental Monitoring* **2010,** *12* (4), 890-897.

64. Ravichandran, M.; Aiken, G.R.; Reddy, M.M.; Ryan, J.N. Enhanced dissolution of cinnabar (mercuric sulfide) by dissolved organic matter isolated from the Florida Everglades. *Environ. Sci. Technol.* **1998,** *32* (21), 3305-3311; 10.1021/es9804058.

65. McPhail, M.R.; Campbell, G.P.; Bedzyk, M.J.; Weiss, E.A. Structural Features of PbS Nanocube Monolayers upon Treatment with Mono- and Dicarboxylic Acids and Thiols at a Liquid-Air Interface. *Langmuir* **2016,** *32* (26), 6666-6673; 10.1021/acs.langmuir.6b01444.

66. Jupally, V.R.; Kota, R.; Dornshuld, E.V.; Mattern, D.L.; Tschumper, G.S.; Jiang, D.-.; Dass, A. Interstaple dithiol cross-linking in Au 25(SR) 18 nanomolecules: A combined mass spectrometric and computational study. *J. Am. Chem. Soc.* **2011,** *133* (50), 20258-20266; 10.1021/ja206436x.

67. Koole, R.; Luigjes, B.; Tachiya, M.; Pool, R.; Vlugt, T.J.H.; De Mello Donegá, C.; Meijerink, A.; Vanmaekelbergh, D. Differences in cross-link chemistry between rigid and flexible dithiol molecules revealed by optical studies of CdTe quantum dots. *J. Phys. Chem. C* **2007,** *111* (30), 11208-11215; 10.1021/jp072407x.

68. Penn, R.L. Kinetics of oriented aggregation. *J Phys Chem B* **2004,** *108* (34), 12707-12712; 10.1021/jp036490.

69. Peng, X.; Manna, L.; Yang, W.; Wickham, J.; Scher, E.; Kadavanich, A.; Alivisatos, A.P. Shape control of CdSe nanocrystals. *Nature* **2000,** *404* (6773), 59-61; 10.1038/35003535.

70. Nason, J.A.; McDowell, S.A.; Callahan, T.W. Effects of natural organic matter type and concentration on the aggregation of citrate-stabilized gold nanoparticles. *Journal of Environmental Monitoring* **2012,** *14* (7), 1885-1892.

71. Vermeer, A.W.P.; Van Riemsdijk, W.H.; Koopal, L.K. Adsorption of humic acid to mineral particles. 1. Specific and electrostatic interactions. *Langmuir* **1998,** *14* (10), 2810-2815.

72. Au, K.-.; Penisson, A.C.; Yang, S.; O'Melia, C.R. Natural organic matter at oxide/water interfaces: Complexation and conformation. *Geochim. Cosmochim. Acta* **1999,** *63* (19-20), 2903-2917; 10.1016/S0016-7037(99)00268-9.

73. Zhang, Y.; Chen, Y.; Westerhoff, P.; Crittenden, J.C. Stability and removal of water soluble CdTe quantum dots in water. *Environ. Sci. Technol.* **2008,** *42* (1), 321-325; 10.1021/es0714991.

74. Sharpless, C.M.; Aeschbacher, M.; Page, S.E.; Wenk, J.; Sander, M.; McNeill, K. Photooxidation-induced changes in optical, electrochemical, and photochemical properties of humic substances. *Environ. Sci. Technol.* **2014,** *48* (5), 2688-2696; 10.1021/es403925g.

75. Sharpless, C.M.; Blough, N.V. The importance of charge-transfer interactions in determining chromophoric dissolved organic matter (CDOM) optical and photochemical properties. *Environ. Sci. Process. Impacts* **2014,** *16* (4), 654-671; 10.1039/c3em00573a.

76. Spencer, R.G.M.; Hernes, P.J.; Ruf, R.; Baker, A.; Dyda, R.Y.; Stubbins, A.; Six, J. Temporal controls on dissolved organic matter and lignin biogeochemistry in a pristine tropical river, Democratic Republic of Congo. *J. Geophys. Res. G Biogeosci.* **2010,** *115* (3); 10.1029/2009JG001180.

77. Sulzberger, B.; Durisch-Kaiser, E. Chemical characterization of dissolved organic matter (DOM): A prerequisite for understanding UV-induced changes of DOM absorption properties and bioavailability. *Aquatic Sci.* **2009,** *71* (2), 104-126; 10.1007/s00027-008-8082-5.

78. Praus, P.; Matys, J.; Kozák, O. Photocatalytic decomposition of phenol by nanocomposite of ZnS nanoparticles and montmorillonite. *J. Braz. Chem. Soc.* **2012,** *23* (10), 1900-1906; 10.1590/S0103-50532012005000063.

79. Kumar, N.; Komarala, V.K.; Dutta, V. In-situ synthesis of Au-CdS plasmonic photocatalyst by continuous spray pyrolysis and its visible light photocatalysis. *Chem. Eng. J.* **2014,** *236*, 66-74; 10.1016/j.cej.2013.09.052.

80. Holley, E.A.; James McQuillan, A.; Craw, D.; Kim, J.P.; Sander, S.G. Mercury mobilization by oxidative dissolution of cinnabar (a-HgS) and metacinnabar (ß-HgS). *Chem. Geol.* **2007,** *240* (3-4), 313-325; 10.1016/j.chemgeo.2007.03.001.

81. Barnett, M.O.; Turner, R.R.; Singer, P.C. Oxidative dissolution of metacinnabar (ß-HgS) by dissolved oxygen. *Appl. Geochem.* **2001,** *16* (13), 1499-1512; 10.1016/S0883-2927(01)00026-9.

82. Veamatahau, A.; Jiang, B.; Seifert, T.; Makuta, S.; Latham, K.; Kanehara, M.; Teranishi, T.; Tachibana, Y. Origin of surface trap states in CdS quantum dots: Relationship between size dependent photoluminescence and sulfur vacancy trap states. *Phys. Chem. Chem. Phys.* **2015,** *17* (4), 2850-2858; 10.1039/c4cp04761c.

83. Spanhel, L.; Haase, M.; Weller, H.; Henglein, A. Photochemistry of colloidal semiconductors. 20. Surface modification and stability of strong luminescing CdS particles. *J. Am. Chem. Soc.* **1987,** *109* (19), 5649-5655.

84. Mews, A.; Eychmueller, A.; Giersig, M.; Schooss, D.; Weller, H. Preparation, characterization, and photophysics of the quantum dot quantum well system CdS/HgS/CdS. *J. Phys. Chem.* **1994,** *98* (3), 934-941.

85. Huang, L.; Wang, X.; Yang, J.; Liu, G.; Han, J.; Li, C. Dual cocatalysts loaded type i CdS/ZnS core/shell nanocrystals as effective and stable photocatalysts for H2 evolution. *J. Phys. Chem. C* **2013,** *117* (22), 11584-11591; 10.1021/jp400010z.

86. Rabouw, F.T.; de Mello Donega, C. Excited-State Dynamics in Colloidal Semiconductor Nanocrystals. *Top. Curr. Chem.* **2016,** *374* (5); 10.1007/s41061-016-0060-0.

87. Taniguchi, S.; Green, M.; Lim, T. The room-temperature synthesis of anisotropic CdHgTe quantum dot alloys: A "molecular welding" effect. *J. Am. Chem. Soc.* **2011,** *133* (10), 3328-3331; 10.1021/ja200132d.

88. Graham, A.M.; Aiken, G.R.; Gilmour, C.C. Dissolved organic matter enhances microbial mercury methylation under sulfidic conditions. *Environ. Sci. Technol.* **2012,** *46* (5), 2715-2723; 10.1021/es203658f; 10.1021/es203658f.

89. Kim, M.; Han, S.; Gieskes, J.; Deheyn, D.D. Importance of organic matter lability for monomethylmercury production in sulfate-rich marine sediments. *Sci. Total Environ.* **2011,** *409* (4), 778-784; 10.1016/j.scitotenv.2010.10.050.

90. Balcom, P.H.; Schartup, A.T.; Mason, R.P.; Chen, C.Y. Sources of water column methylmercury across multiple estuaries in the Northeast U.S. *Mar. Chem.* **2015,** *177*, 721-730; 10.1016/j.marchem.2015.10.012.

91. Tao, W.; Chen, G.; Zeng, G.; Yan, M.; Chen, A.; Guo, Z.; Huang, Z.; He, K.; Hu, L.; Wang, L. Influence of silver nanoparticles on heavy metals of pore water in contaminated river sediments. *Chemosphere* **2016,** *162*, 117-124; 10.1016/j.chemosphere.2016.07.043.

92. *Distribution and biogeochmical controls on net methyl mercury production in Penobscot River marshes and sediments 2009-2012*.

93. Morse, J.W.; Luther III, G.W. Chemical influences on trace metal-sulfide interactions in anoxic sediments. *Geochim. Cosmochim. Acta* **1999,** *63* (19-20), 3373-3378.

94. Sahai, N.; Lee, Y.J.; Xu, H.; Ciardelli, M.; Gaillard, J.-. Role of Fe(II) and phosphate in arsenic uptake by coprecipitation. *Geochim. Cosmochim. Acta* **2007,** *71* (13), 3193-3210; 10.1016/j.gca.2007.04.008.

95. Klaine, S.J.; Alvarez, P.J.J.; Batley, G.E.; Fernandes, T.F.; Handy, R.D.; Lyon, D.Y.; Mahendra, S.; McLaughlin, M.J.; Lead, J.R. Nanomaterials in the environment: Behavior, fate, bioavailability, and effects. *Environ. Toxicol. Chem.* **2008,** *27* (9), 1825-1851; 10.1897/08-090.1.

96. Doyle, J.J.; Ward, J.E.; Mason, R. An examination of the ingestion, bioaccumulation, and depuration of titanium dioxide nanoparticles by the blue mussel (Mytilus edulis) and the eastern oyster (Crassostrea virginica). *Mar. Environ. Res.* **2015,** *110*, 45-52; 10.1016/j.marenvres.2015.07.020.

97. Alldredge, A.L.; Silver, M.W. Characteristics, dynamics and significance of marine snow. *Prog. Oceanogr.* **1988,** *20* (1), 41-82; 10.1016/0079-6611(88)90053-5.

98. Doyle, J.J.; Palumbo, V.; Huey, B.D.; Ward, J.E. Behavior of titanium dioxide nanoparticles in three aqueous media samples: Agglomeration and implications for benthic deposition. *Water Air Soil Pollut.* **2014,** *225* (9); 10.1007/s11270-014-2106-7.

3. Enhanced Availability of Mercury Bound to Dissolved Organic Matter for Methylation in Marine Sediments

The paper has been published in *Geochimica et Cosmochimica Acta* on 08/28/2016. A modified word copy of the article is presented here with permission from Elsevier.

Mazrui, N.M.; Jonsson, S.; Thota, S.; Zhao, J.; Mason, R.P. Enhanced availability of mercury bound to dissolved organic matter for methylation in marine sediments. *Geochim. Cosmochim. Acta* **2016,** *194*, 153-162; 10.1016/j.gca.2016.08.019

3.1 Abstract

The forms of inorganic mercury (Hg^{II}) taken up and methylated by bacteria in sediments still remain largely unknown. From pure cultures studies, it has been suggested that dissolved organic matter (DOM) may facilitate the uptake either by acting as a shuttle molecule, transporting the Hg^{II} atom to divalent metal transporters, or by binding Hg^{II} and then being transported into the cell as a carbon source. Enhanced availability of Hg^{II} complexed to DOM has however not yet been demonstrated in natural systems. Here, we show that Hg^{II} complexed with DOM of marine origin was up to 2.7 times more available for methylation in sediments than Hg^{II} added as a dissolved inorganic complex (Hg^{II}*(aq)*). We argue that the DOM used to complex Hg^{II} directly facilitated the bacterial uptake of Hg^{II} whereas the inorganic dissolved Hg^{II}-complex adsorbed to the sediment matrix before forming bioavailable dissolved Hg^{II} complexes. We further demonstrate that differences in net methylation in sediments with high and low organic carbon content may be explained by differences in the availability of carbon to stimulate the activity of Hg methylating bacteria rather than, as previously proposed, be due to differences in Hg^{II} binding capacities between sediments.

3.2. Introduction

Methylmercury (MeHg) is a neurotoxic form of Mercury (Hg) that is produced under anoxic conditions in sediments, soils and aquatic waters from inorganic divalent mercury (Hg^{II}) mainly by sulfur and iron reducing bacteria (Compeau and Bartha, 1985; Benoit, et al., 2003). A fraction of the MeHg formed bioaccumulates in aquatic food webs to concentrations of concern for human and wildlife health (Mergler, et al., 2007). Though anthropogenic emissions of Hg have decreased substantially in the US, predicting future concentrations of MeHg amidst changes in global Hg emissions remains a challenge (Mason, et al., 2012; Driscoll, et al., 2013). To address this challenge, a better understanding of the factors that control net methylation in aquatic systems is warranted (Benoit, et al., 1999). While the ability to methylate Hg^{II} is restricted to specific strains of bacteria carrying the *hgcA* and *hgcB* genes, methylation is known to depend both on the activity and composition of the bacterial community as well as the pool of Hg^{II} available to Hg^{II} methylating bacteria (Jonsson, et al., 2012; King, et al., 2000; Parks, et al., 2013).

The Hg^{II} methylation potential has been widely studied across systems, using isotopically enriched Hg^{II} tracers in intact sediment cores or sediment slurries (Hammerschmidt, et al., 2008; Jonsson, et al., 2012; Benoit, et al., 1999; Hollweg, et al., 2010). The Hg^{II} methylated is assumed to be taken up from the dissolved pool which, in comparison to the amount of Hg^{II} methylated within a day at typically reported potential methylation rate constants (k_m) (0.01-0.12 d^{-1}) (Hammerschmidt, et al., 2008; Hollweg, et al., 2010; Schartup, et al., 2013; Jonsson, et al., 2012), is at least ten times smaller (a typical distribution coefficient between the solid and aqueous phase, K_D, of 10^3-10^5) (Schartup, et al., 2013; Hollweg, et al., 2010; Hammerschmidt, et al., 2008). Therefore, desorption and dissolution of Hg^{II} from the much more abundant pool of Hg^{II} present in the sediment occurs to sustain the typically observed methylation rates (Jonsson, et al., 2012). Hence, the speciation of Hg^{II} in both the dissolved and solid phase will influence the pool of Hg^{II} available to methylating bacteria. Previous work has shown that the availability for methylation of the adsorbed and solid forms of Hg^{II} found in sediments, differs up to two orders of magnitude, and that the rate of methylation was controlled by both the thermodynamic stability of the solid phase as well as the

kinetics of Hg^{II} desorption/dissolution (Jonsson, et al., 2012). Here, we present an examination of the methylation rates of isotopically enriched Hg^{II} tracers added as different solid, adsorbed and dissolved forms to four different sediments. Although the availability of both the adsorbed and solid forms will be discussed in this paper, the focus is primarily on the availability of dissolved Hg^{II} added to the sediment as Hg^{II} complexed with dissolved organic matter (DOM) extracted from coastal waters, or with inorganic ligands.

The dissolved forms of Hg^{II} complexes first proposed to be available for methylation included neutrally charged sulfide complexes, which have been assumed to passively diffuse into the cell of the bacteria (Benoit, et al., 1999). This hypothesis was based on field data and pure culture experiments where the concentration of MeHg was related to the modelled concentration of neutrally charged Hg^{II}-S species (Benoit, et al., 1999; Hollweg, et al., 2010; Hammerschmidt and Fitzgerald, 2004). It should be noted that the stability constants used in the speciation models are highly uncertain (Skyllberg, 2011). More recent work done in pure bacterial cultures (Schaefer and Morel, 2009; Schaefer, et al., 2014) has suggested that low-molecular weight thiol complexes facilitate the uptake of Hg^{II} by methylating bacteria, by serving as a transporting shuttle for Hg^{II} to the cell wall, where Hg^{II} is then taken up by a divalent metal ion transporter in place of Zn^{II} (an essential element) (Schaefer, et al., 2014). The methylation rate was found to differ between different Hg-thiol complexes with the highest rate observed for Hg bound to cysteine (Schaefer, et al., 2014). It has also been suggested that Hg^{II}-DOM complexes are more available because the DOM is taken up as a source of energy by the bacteria, resulting in the unintentional uptake of Hg^{II} (Chiasson-Gould, et al., 2014; Schaefer, et al., 2014) or alternatively that DOM may indirectly enhance the availability of Hg^{II} under sulfidic conditions by hindering the formation of β-HgS*(s)* particles large enough to reduce Hg^{II} availability (Graham, et al., 2012; Graham, et al., 2013). Although the different theories have been argued for in various pure culture studies, direct experimental support, except for DOM acting as a shuttle molecule for Hg^{II} to the divalent metal ion transporters, is missing (Schaefer, et al., 2014).

One of the major challenges in studying bioavailable forms of Hg^{II} in natural samples comes from the multiple effects complexing agents (sulfide, thiols etc.) may have on Hg^{II} speciation and availability for

methylation as well as their effects on bacterial activity. Here, we have compared the methylation rate constant (k_m, d^{-1}) determined from Hg^{II} added as chloride complexes, hereon referred to as Hg^{II} *(aq)* and Hg^{II} complexed to DOM (Hg^{II}-DOM) in four different estuarine sediments. To distinguish the effect that the added DOM may have on Hg^{II} availability and bacterial activity, we also examined the k_m of Hg^{II} *(aq)* in presence of an equal amount of simultaneously added DOM (as used to produce the Hg^{II}-DOM tracer). We also determined the k_m of Hg^{II} adsorbed onto particulate organic matter of marine origin (Hg^{II}-POM), and Hg^{II} precipitated with sulfide as micro or nanoparticles of metacinnabar (respectively, β-HgS*(s)*$_{micro}$ and β-HgS*(s)*$_{nano}$), as well as Hg^{II} equilibrated with two previously collected sediments.

3.3. Material and Methods

3.3.1. Preparation of Hg tracers

Methylation assay sets were used containing a ^{200}Hg and a ^{199}Hg enriched species specific Hg^{II} tracer, individually frozen in 15 ml falcon tubes. The isotopically enriched Hg^{II} tracers were prepared from $^{200}HgCl_2$ and $^{199}HgCl_2$ (Oak Ridge National Laboratory, TN, USA) dissolved in 0.1 M HCl (diluted and pH neutralized before use). Hg^{II} tracers complexed to dissolved or particulate organic matter (DOM and POM) were prepared by pre-equilibrating $^{200}Hg^{II}$ with DOM or POM for 24 h. The organic matter was extracted from water sampled at Eastern Long Island Sound (ELIS) using Bond Elute PPL cartridges for DOM (as described in the Supporting Information), and by filtering the water through a 1.0 µm plankton net, after which the collected particles were rinsed, freeze-dried and re-suspended in purified water for POM. Our experiments aimed at studying differences in the availability between different dissolved, adsorbed and solid Hg^{II} tracers for methylation. To complex Hg^{II}, it was thus desired to have a Hg^{II}:ligand ratio low enough to ensure that the binding sites to which Hg^{II} would complex under natural concentrations, are not saturated. At the same time, higher amounts of DOM and POM could alter the activity of Hg methylating bacteria and were thus avoided. For DOM, we used a Hg^{II}:ligand ratio of 1 µg Hg^{II} mg^{-1} DOC. A high and constant binding coefficient of Hg^{II} to DOM has been previously demonstrated at ratios equal to or less

than the ratio we used (Haitzer, et al., 2002). For POM, we used a concentration ratio of 2.4 μmol Hg^{II} g^{-1} POM. This is comparable to the Hg^{II}:POM ratio used in previous work by Jonsson et al. (2012). For all sets containing DOM and POM, controls (n=2) were prepared where a $^{200}Hg^{II}$*(aq)* tracer and a DOM or POM slurry were individually frozen in the assay tubes. These controls were used to test if added amounts of DOM or POM increased Hg^{II} methylation when not complexed to added Hg^{II} tracer by e.g. altering the activity of Hg^{II} methylating bacteria.

Synthesis of β-^{200}HgS*(s)*$_{micro}$ and β-^{199}HgS*(s)*$_{nano}$ tracers was done under low O_2 conditions (using a N_2 flushed glove bag) by adding 1.3 μmoles of dissolved sulfide to equimolar concentrations of $^{200}Hg^{II}$ and $^{199}Hg^{II}$ dissolved in purified water or in purified water with 1.3 mg of DOC extracted from ELIS, respectively. All solutions were prepared in purified water degassed by boiling while purging with N_2 for 20 minutes. The Na_2S stock solution was prepared by dissolving 10 g of washed and dried sodium sulfide crystals in 5 ml of degassed water and standardized using an ion-selective electrode (Orion) and titrating with 0.1M $Pb(NO_3)_2$. The particles were aged for 3 days before the slurries were diluted and individually frozen in the assay tubes. Controls for β-^{199}HgS*(s)*$_{nano}$ assays were prepared containing the β-^{199}HgS*(s)*$_{nano}$ and the $^{200}Hg^{II}$*(aq)* tracers, also individually frozen. Formation of nanoparticles was confirmed by transmission electron microscopy (TEM, Fig. S1). Details for the preparation and analysis of TEM samples are given in the Supporting Information.

Additional sets of tracers, (Hg^{II}-$LOC_{sediment}$ and Hg^{II}-$HOC_{sediment}$), were prepared where $^{200}Hg^{II}$ was pre-equilibrated in the dark for 24 h with freeze-dried sediments, of low and high organic carbon content, previously collected from two of the sites (Barn Island LOC and HOC) in 2013. The characteristics of the freeze-dried sediments are presented in Table S1. The ratio of Hg^{II} to sediment in all the tracers was 7 and 35 nmol Hg^{II} g^{-1} d.w Barn Island LOC and HOC sediment, respectively. All the tracers were frozen individually. A conceptual diagram with the study design is presented in Fig. 1.

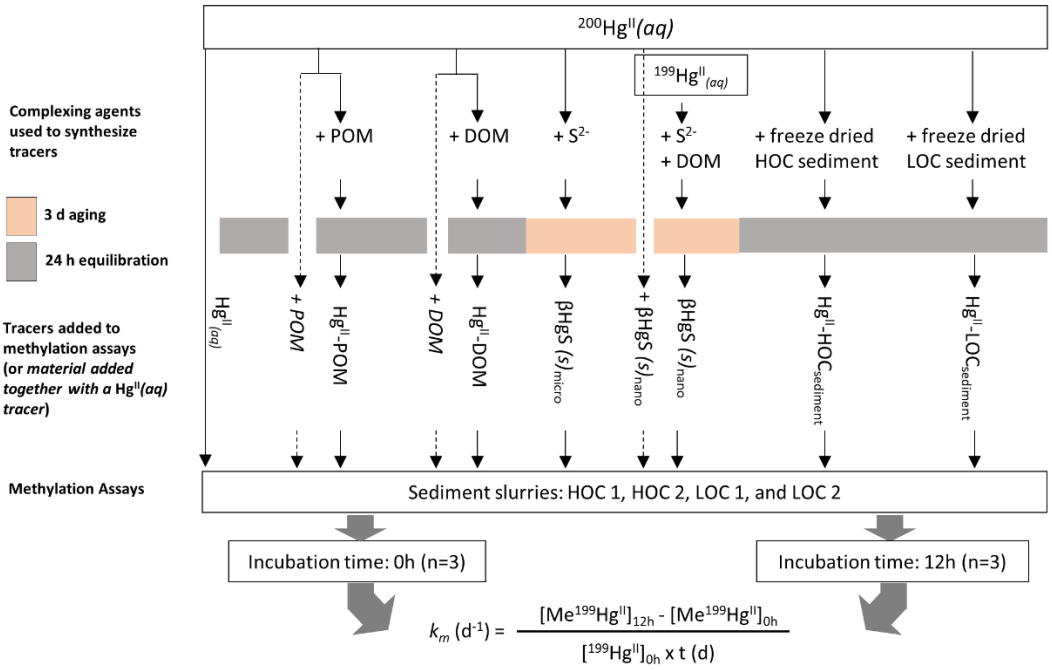

Fig. 1. Illustration of the experimental design. Starting from the top, the illustration shows the complexing agents used to synthesize the different Hg^{II} tracers utilized in this study. To prepare Hg^{II}-POM, Hg^{II}-DOM, Hg^{II}-$HOC_{sediment}$ and Hg^{II}-$LOC_{sediment}$, the isotopically enriched Hg^{II}*(aq)* tracer was equilibrated for 24 h (gray field) with the complexing agent. For the case of HgS*(s)* particles, β-HgS$(s)_{micro}$ was formed when S^{2-} was added to the Hg^{II}*(aq)* tracer while β-HgS$(s)_{nano}$ was formed when DOM followed by S^{2-} were added to the Hg^{II} *(aq)* tracer. Both particles were aged for 3 days (pink field). The synthesized tracers were then added to four different sediment slurries and incubated for 0 h and 12 h. Finally, the methylation rate constant (k_m) was calculated using the formula shown in the bottom of the illustration. Dashed lines represent control experiments where k_m of Hg^{II}*(aq)* was quantified in presence of POM, DOM or β-HgS$(s)_{nano}$ (by the simultaneous addition of Hg^{II}*(aq)* with POM, DOM or β-HgS$(s)_{nano}$ to sediment slurries). If methylation was not different from the k_m of Hg^{II}*(aq)* when added without DOM, POM or β-HgS$(s)_{nano}$, we conclude that the complexing agent did not impact the rate of methylation by e.g. altering the activity of Hg^{II} methylating bacteria.

3.3.2. Sediment Sampling and Methylation Assays

Sediments from Barn Island (site 1) and Goshen Cove (site 2), Connecticut, USA, were manually collected using acid cleaned polycarbonate core samplers, (diameter of 4.8 cm) from two subsites at each location during low tide in August 2015 (Fig. S2). The top 4 cm of multiple sediment cores was pooled and manually homogenized under low oxygen conditions using a N_2 flushed glove bag. Tubes with prepared Hg^{II} tracers (n=3 per set) were brought to room temperature and while thawing, ~10 g of sediment slurry was added and mixed with the tracer using a vortex. The concentration of Hg^{II} added to the sediment with the

tracer, and the tracer to ambient Hg ratio is given in Table S2. Samples were incubated for 0 and 12 h (t=0 and t=12, respectively) in a water bath at ambient temperature (±2°C) before the incubation was terminated by flash freezing on dry ice. To verify that steady state in methylation and demethylation was not reached during the course of the 12 h incubations, a subset of experiments with the Hg^{II}*(aq)* tracer were also incubated for 4 h and 24 h. All methylation assays were conducted on the day of sampling. The ambient temperature of the overlying water at the time of sampling is presented in the Supporting Information, Table S3. All samples were then stored frozen before being freeze-dried. $Me^{201}Hg$*(aq)* was added as an internal standard to 0.5-2 g of the sediment and equilibrated for 1 h (in dark) before MeHg was double extracted into purified water using $CuSO_4/KBr/H_2SO_4$ followed by CH_2Cl_2 (Lambertsson, et al., 2001). The isotopic composition of extracted MeHg was analyzed by direct ethylation with $NaB(C_2H_5)_4$, purged and trapped on Carbotrap columns followed by thermal desorption and gas chromatograpy inductively coupled plasma mass spectrometry (GC-ICPMS) as described elsewhere (Hollweg, et al., 2009). Signal deconvolution was performed on mass bias corrected signals (Hintelmann, et al., 2000; Heyes, et al., 2006) and the methylation rate constant (k_m, d^{-1},) was calculated in t=12 h samples after correcting for the MeHg concentration detected in t=0 h samples ($k_m\,(d^{-1}) = \Delta[MeHg] \cdot ([Hg^{II}]_{t0} \cdot t(d))^{-1}$). The concentration of $^{200}Hg^{II}$*(aq)* and $^{199}Hg^{II}$*(aq)* stock solutions used to prepare the different tracers as well as the $Me^{201}Hg$*(aq)* used as an internal standard, were determined by reversed isotope dilution using solutions of ambient Hg^{II}*(aq)* and MeHg*(aq)* with known concentrations (diluted from 1000 ppm stock solutions, Alfa Aeser). Methodology for calculating the limit of detection (LOD, Table S4) is described in the Supporting Information. Statistical data treatment was conducted on log transformed k_m values using SPSS software (IBM® SPSS). Differences in k_m values was tested using two-way ANOVA and if the null-hypothesis was rejected ($p<0.05$) groups statistically differing were identified using Tukey's *post hoc* analysis. Normal distribution of the data was verified using the Shapiro-Wilk test.

Ancillary parameters (concentration of total Hg and loss on ignition in sediments collected, and the concentration of total Hg, MeHg, sulfide and organic carbon (DOC) and fluorescence excitation and emission matrices in sediment pore water) were determined as described in the Supporting Information.

The chemical speciation of Hg^{II} in the pore water was also calculated as described in the Supporting Information.

3.4. Results

The concentrations of total Hg (HgT) and MeHg in sediment and sediment pore water (Table 1, Table S5) collected in the four estuarine locations are within the range typically reported from sites without local point source Hg pollution (Balcom, et al., 2015). Loss on ignition (LOI, Table 1), here used as a proxy for organic matter content (Schartup, et al., 2013), was 15-17 % for two of the sediments ("HOC 1" and "HOC 2") and ~2% for the two more sandy sediments ("LOC 1" and "LOC 2").

The potential methylation rate constant, k_m, was calculated assuming pseudo-first-order reaction kinetics (Hintelmann, et al., 2000). To correctly determine k_m, a linear increase in the amount of MeHg formed from the added Hg^{II} tracer is required during the incubation period. Incubation experiments conducted for up to 24 h showed this was true within the first 12 h of the incubations for all sediments, except for HOC 2 (Fig. S3). Though the lack of linearity suggests that the system was approaching steady state, the k_m and the fraction methylated after steady state has been reached (i.e. stable $MeHg/Hg^{II}$) have both been shown useful for comparing differences in availability of Hg^{II}*(aq)* and solid or adsorbed Hg^{II} tracers (Jonsson, et al., 2012). In this paper, we use k_m calculated from 12 h long incubation experiments, even if we recognize that the calculated value may slightly underestimate the true k_m of added Hg^{II} tracers in HOC 2 sediment.

The k_m of Hg^{II} pre-equilibrated for 24 h with POM of marine origin (Hg^{II}-POM) was not different than the k_m of the Hg^{II}*(aq)* tracer in all sediments (Fig. 2a and b, ANOVA, $p>0.05$). Methylation of Hg^{II}*(aq)* tracer with an equal amount of POM added, as used to synthesize the Hg^{II}-POM tracer, (Hg^{II} *(aq)* + POM), was also not different from the k_m of Hg^{II}*(aq)* tracer in samples with no additional POM added (ANOVA, $p>0.05$).

Metacinnabar (β-HgS*(s)*) tracers were synthesized by precipitation of equimolar amounts of isotopically labelled Hg^{II} and S^{2-} with and without the presence of DOM. In the absence of DOM, β-HgS*(s)* precipitated instantly and was assumed, based on previous studies (Jonsson, et al., 2012), to consist of smaller particles (ca 100-200 nm in diameter) aggregated into micrometer sized clusters (β-HgS*(s)*$_{micro}$). In the presence of DOM, monodispersed β-HgS*(s)* particles with a diameter of 4.9 ± 1.2 nm were formed (β-HgS*(s)*$_{nano}$) (Fig. S1). The methylation of Hg^{II} tracer added as β-HgS*(s)*$_{micro}$ was below the LOD in all the sediments tested and lower than the k_m of all other tracers tested (ANOVA following Tukey's *post hoc* analysis, $p<0.05$), and at least 5-23 times lower than the methylation of Hg^{II} added as β-HgS*(s)*$_{nano}$.

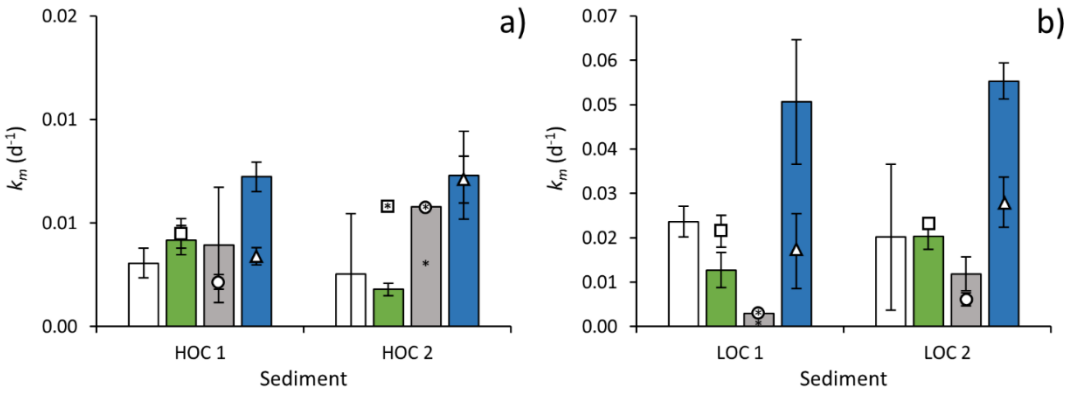

Fig 2. Methylation rate constant determined using different Hg^{II} tracers in sediments with a) high organic carbon content (HOC 1 and HOC 2) and b) low organic carbon content (LOC 1 and LOC 2). The methylation rate constant (k_m, d^{-1}; ±SD, n=3) was determined by adding Hg^{II} to sediment slurries as an inorganic aqueous tracer (Hg^{II}*(aq)*, white bars), as Hg^{II} bound to particulate organic matter (Hg^{II}-POM, green bars), as β-HgS*(s)* nanoparticles (β-HgS*(s)*$_{nano}$, gray bars), and as Hg^{II} bound to dissolved organic matter (Hg^{II}-DOM, blue bars). To test how POM and DOM added with the Hg^{II}-POM, β-HgS*(s)*$_{nano}$, and Hg^{II}-DOM tracers affected Hg^{II} methylation rates when not complexed to the Hg^{II} substrate (by e.g. altering the activity of Hg^{II} methylating bacteria), control experiments were conducted. In these control experiments, the Hg^{II}*(aq)* tracer was added to the sediment slurries simultaneously with POM (squares), β-HgS*(s)*$_{nano}$ (circles) or DOM (triangles). For the controls, error bars show ±SD calculated from n=2. An * associated with any bar or symbol indicates the data < Limit of Detection (LOD) and this value is shown.

The k_m of all tracers added was 2-8 times higher in the LOC sediments than in HOC sediments (Figs. 2 & 3, ANOVA $p<0.05$). This is consistent with the higher net methylation observed for ambient Hg^{II} in the LOC sediment as evident from the higher fraction (%) of Hg occurring as MeHg (Table 1). To

examine how binding of Hg^{II} to sediments of different organic carbon content affects the availability for methylation, we prepared two tracers, (Hg^{II}-$LOC_{sediment}$ and Hg^{II}-$HOC_{sediment}$), by pre-equilibrating Hg^{II}*(aq)* for 24 h with two freeze-dried sediments of low and high organic carbon content previously collected from the same sites as LOC 1 and HOC 1, respectively. No significant methylation of the tracer was observed during the pre-equilibration time. After incubation with fresh sediment we observed similar k_m values (ANOVA, $p>0.05$) for the Hg^{II}-$LOC_{sediment}$ and Hg^{II}-$HOC_{sediment}$ (Fig. 3).

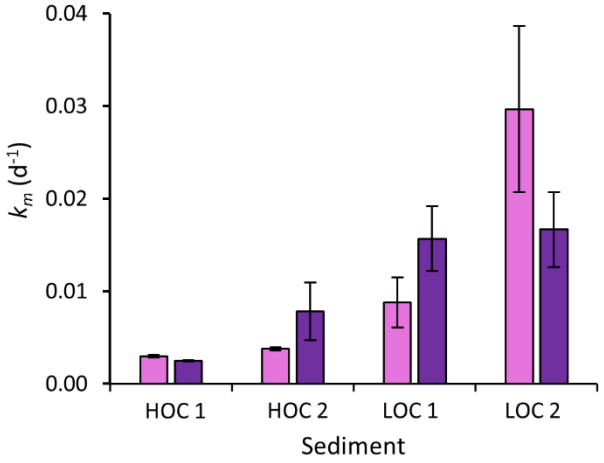

Fig 3. Methylation rate constant determined using Hg^{II} tracers added to sediment slurries (HOC 1, HOC 2, LOC 1 and LOC 2) as Hg^{II} bound to freeze dried sediments. The methylation rate constant (k_m, d^{-1}; ±SD, n=3) of Hg^{II} pre-equilibrated with freeze dried sediment with low organic carbon content (Hg^{II}-$LOC_{sediment}$) is shown in light purple bars and that of Hg^{II} pre-equilibrated with freeze dried sediment with high organic carbon content (Hg^{II}-$HOC_{sediment}$) is shown in dark purple bars.

The k_m of Hg^{II} pre-equilibrated for 24 h with DOM of marine origin (Hg^{II}-DOM) was 2.1 times and 2.7 times higher (ANOVA following Tukey's post hoc test, $p<0.05$) than the average k_m of Hg^{II}*(aq)* in LOC 1 and LOC 2 sediments, respectively (Fig. 2b). The average methylation of Hg^{II}-DOM tracer was also higher than that of Hg^{II}*(aq)* in HOC sediments, however, the differences were not statistically significant. In the LOC sediments, the methylation rate of Hg^{II}*(aq)* added to the sediment with the same amount of DOM as used to complex the Hg^{II}-DOM tracer, (Hg^{II} *(aq)* + DOM) was similar to observed k_m of Hg^{II}*(aq)* when no DOM was added (ANOVA following Tukey's *post hoc* test, $p>0.05$).

3.5. Discussion

3.5.1. Methylation of Hg from the Solid/Adsorbed Hg pool

The similar k_m values observed for Hg^{II}-POM and Hg^{II}*(aq)* suggests similar availability for methylation of Hg^{II} added as complexed to marine POM or as dissolved chloride complexes (Fig. 2a and b). The latter tracer can be assumed to rapidly bind (within seconds) (Hintelmann and Harris, 2004; Jiang, et al., 2015) to easily available adsorption sites (O and N) in the sediment POM matrix, which are much more abundant than any pore water DOM ligands, and with time migrate to less available, but more thermodynamically stable, POM binding sites (reduced sulfur sites) (Jiang, et al., 2015). In contrast to our results, adsorption of Hg^{II} complexed to organic matter (OM) derived from a peat soil has previously been demonstrated to reduce the availability of Hg^{II} for methylation in a brackish water sediment (Jonsson, et al., 2012). For the POM used by Jonsson et al. (2012), Hg^{II} was shown to bind to the OM via a linear coordination to two thiol groups (Skyllberg, et al., 2006). We have no such information available for the specific binding of Hg^{II} to the marine POM used in this study, however a growing number of studies suggest that Hg^{II} bound to OM of marine origin is more labile than Hg^{II} bound to terrestrial OM (Hammerschmidt, et al., 2008). That we, in contrast to Jonsson et al. (2012), did not observe a lower methylation of Hg^{II} when added to the sediment as Hg^{II} adsorbed onto POM despite using a similar Hg to POM ratio (mol $mass^{-1}$), may be explained by the differences in the bioavailability (i.e. desorption kinetics) between Hg^{II} bound to terrestrial and marine POM. This demonstrates that the type of OM present will determine if, and to what degree, adsorption of Hg^{II} to OM affects its availability for methylation.

The lower availability of Hg^{II} for methylation when added to the sediment as β-HgS*(s)*$_{micro}$ has previously been shown (Jonsson, et al., 2012; Zhang, et al., 2014) and is expected due to the higher thermodynamic stability of β-HgS*(s)* in comparison to e.g. Hg^{II} bound to POM or other complexes. The similar availability of β-HgS*(s)*$_{nano}$ and Hg^{II}*(aq)* tracers (ANOVA, $p>0.05$) in three of the four sediments (Fig. 2a and b) is in agreement with previous studies (Zhang, et al., 2014). As the nanoparticles are challenging to separate from the surrounding media, it is difficult to evaluate if all Hg^{II} has been precipitated

and it is possible that the nanoparticle slurry still contained dissolved or clusters of Hg^{II} and sulfide. For HgS*(s)* precipitated in the absence of DOM, previous experiments have confirmed that the Hg^{II} methylated originated from the particles themselves and not from Hg^{II} remaining in solution (Jonsson, et al., 2012). The higher availability of β-HgS*(s)*$_{nano}$ relative to β-HgS*(s)*$_{micro}$ may also be caused by a higher surface area of the nanoparticles which would increase the rate at which the particles dissolve to establish equilibrium, or by a lower presumed thermodynamic stability caused by the DOM preventing aggregation and continuous growth of the particles (Deonarine and Hsu-Kim, 2009). Though the thermodynamic stability of lab synthesized β-HgS*(s)* nanoparticles and the stability of them in sediment systems has not been well studied, recent work has shown that β-HgS*(s)* particles forming in presence of terrestrial DOM (Suwanee River and Pony Lake fulvic acid) are more structurally disordered than metacinnabar (Slowey, 2010). It also remains to be demonstrated if β-HgS*(s)* nanoparticles in sediments constitute a quantitatively important pool of the Hg^{II} from which MeHg is formed. Our results and previous work are however of interest since they demonstrate that β-HgS*(s)*, depending on the particle size and stability, differs in its availability for methylation. It is reasonable to assume that the stability of β-HgS*(s)* precipitated under natural conditions in sediment pore water may be reduced due to the presence of a higher degree of impurities either incorporated or adsorbed onto the solid surface in comparison to β-HgS*(s)* precipitated in purified water.

3.5.2. Methylation of Tracer and Ambient Hg in LOC vs. HOC Sediments

Past studies have demonstrated a negative correlation between the k_m (or fraction of Hg occurring as MeHg) and the content of OM present across different estuarine sediments, and it was suggested that binding to sediment lowers the availability of Hg^{II} for methylation (Hammerschmidt and Fitzgerald, 2004; Hollweg, et al., 2010). A negative correlation between k_m (or % MeHg) and K_D was also found in our sediment systems (Fig. S4). However, the activity of Hg^{II} methylating bacteria has also been coupled to the type of organic carbon present, where autochthonous carbon has been suggested to be a strong driver for Hg^{II} methylation than allochthonous carbon (Kim, et al., 2011). The similar availability of the two tracers, Hg^{II}-$LOC_{sediment}$ and Hg^{II}-$HOC_{sediment}$, for methylation (Fig. 3, no significant difference between observed

k_m values, ANOVA, $p>0.05$) in each of the sediment slurries suggest that the binding of Hg to LOC relative to HOC sediment does not limit its availability for methylation. Thus, the higher methylation of Hg^{II} in LOC 1 & LOC 2 relative to HOC 1 & HOC 2 (as seen from the added tracers and the higher % MeHg of ambient Hg^{II}), is explained by the type of organic matter present for fueling the activity of Hg^{II} methylating bacteria (Fig. S5), rather than by differences in the binding strength of the sediments. The two HOC sediment samples were collected more inland (Fig. S2), and as seen from the fluorescence excitation and emission matrices of pore water collected from these sediments (Fig. S5), LOC sediments show a more intense proteinaceous fluorescence (maximum emission at a lower wavelength) and a lower humic-like emission (maximum emission at a higher wavelength) in comparison to the HOC sediments. Previous fluorescence studies in the marine environment have shown that regions of high biological activity have high protein concentrations and that protein-like fluorescence is a proxy for labile DOM (Yamashita and Tanoue, 2003; Mayer, et al., 1999; Para, et al., 2010; Mopper and Schultz, 1993).

3.5.3. Methylation of Hg Complexed to DOM

In the two LOC sediments, the average k_m of Hg^{II}-DOM was 2.1-2.7 times higher in comparison to the average k_m of the Hg^{II}*(aq)* tracer (Fig. 2b). The methylation rate of Hg^{II}*(aq)* added to the sediment with the same amount of DOM as used to complex the Hg^{II}-DOM tracer, (Hg^{II} *(aq)* + DOM) was however not higher, showing that the increased DOC concentration of 8-15% from the added tracer in these sediments (Fig. S6) did not have an apparent effect on Hg^{II} methylation (by e.g. altering the activity of Hg^{II} methylating bacteria). This is further supported by the lack of proteinaceous fluorescence, suggested to be a proxy for labile DOM (Yamashita and Tanoue, 2003; Mopper and Schultz, 1993; Para, et al., 2010), as seen in the EEM recorded for the extracted DOM used in our experiments (Fig. S7). The similar methylation rates observed for the Hg^{II}*(aq)* tracer when added to the sediment with and without the simultaneous addition of DOM, also demonstrates that the DOM added did not increase the availability of Hg^{II} by increasing the fraction of Hg^{II} occurring in the dissolved phase (Waples, et al., 2005; Miller, et al., 2007; Slowey, 2010; Deonarine and Hsu-Kim, 2009). The higher observed k_m of Hg^{II}-DOM in comparison to Hg^{II}*(aq)*, thus

indicates a higher availability of added Hg^{II}-DOM complexes for methylation. This enhanced availability is not apparent in HOC 1 and HOC 2 possibly because here, mercury methylation is limited by bacterial uptake rather than the bioavailability of Hg complexes. Since the HOC sediment slurries have lower bacterial activity as implied by the lower fraction of autochthonous organic matter present in pore water samples (Fig. S5), mercury uptake by methylating bacteria likely occurs much slower than the combined process of Hg desorption from the solid phase and conversion to a bioavailable complex, (as described in Fig. 4). As such, we find no statistical difference between the availability of Hg^{II}*(aq)* and Hg^{II}-DOM in the HOC sediment slurries. Zhang and coworkers observed a similar phenomenon for tracers added to sediments with high and low bacterial activity (Zhang, et al., 2014). Although the higher methylation rate of Hg^{II} complexed to low molecular weight thiols and natural DOM has been previously demonstrated in pure bacteria cultures, our study is the first demonstrating this in natural samples.

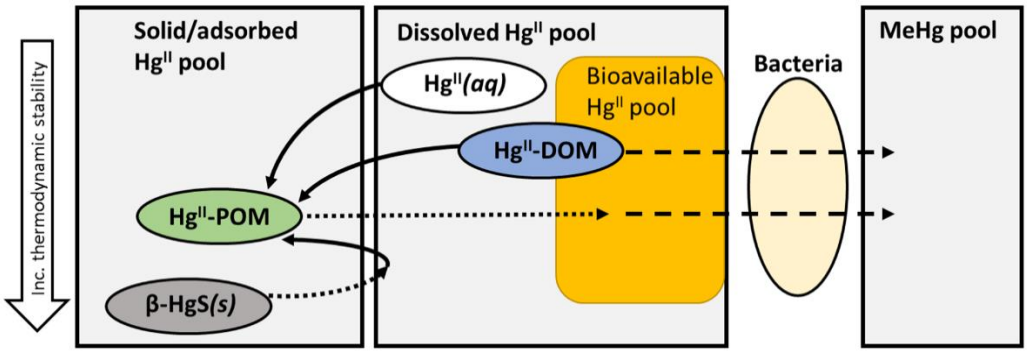

Fig. 4. **Conceptual model of the availability of added tracers (Hg^{II}*(aq)*, Hg^{II}-DOM, Hg^{II}-POM, β-HgS*(s)*) in marine sediments**. The arrows represent; adsorption (solid lines), dissolution/desorption and formation of bioavailable Hg^{II} complexes (dotted lines) and uptake and methylation of Hg^{II} (dashed lines).

Below we discuss the enhanced availability of our Hg^{II}-DOM tracer based on the assumption that the adsorption of Hg^{II}*(aq)* to the sediment occurs faster than the formation and uptake of bioavailable complexes (presumably dissolved) into Hg^{II} methylating bacteria. In more traditional methylation assays, where Hg^{II}*(aq)* is used as the methylation tracer, the Hg^{II}*(aq)* added is assumed to quickly partition to easily

available binding sites in the sediment (Hintelmann, et al., 2000; Hintelmann and Harris, 2004; Jiang, et al., 2015) and with time migrate to less available and more stable binding sites thereby adopting an overall binding strength resembling that of ambient Hg (Hintelmann, et al., 2000; Jonsson, et al., 2012). If our assumption was incorrect, a rapid increase in the concentration of MeHg formed from the Hg^{II}*(aq)* tracer would be expected within the first minutes of such incubation experiments. However, the concentration of the methylated tracer in "t=0" samples (which, in reality represents a time of incubation of up to a few minutes, depending on the method of termination used), is typically very low when compared to the concentration of MeHg formed in samples incubated for hours (Jonsson, et al., 2012). This was also true in our LOC sediments (Fig. S3), thus justifying our assumption that the adsorption of Hg^{II}*(aq)* to binding sites in the sediment (predominantly surface sites on the POM present) is faster than the formation and uptake of bioavailable Hg^{II} complexes. We thus argue that the binding sites to which Hg^{II}*(aq)* first adsorbs to, will also rapidly bind any Hg^{II} released by another tracer (e.g. Hg^{II}-DOM), before the released Hg^{II} is transformed to a bioavailable form and taken up by the bacteria. The readily available and abundant binding sites on POM in the sediment thus act as a buffer, regulating the dissolved concentration of Hg^{II} that can be transformed to a bioavailable form.

To explain the observed enhanced availability of Hg^{II} complexed with DOM for bacterial uptake and Hg^{II} methylation, we consider two main theories that have been suggested from experiments done in pure bacteria cultures: i) the complexation of Hg^{II} to DOM favors the formation of smaller β-HgS*(s)* particles whereas Hg*(aq)* precipitates as larger, and less available β-HgS*(s)* particles and ii) Hg^{II}-DOM complexes are directly available for uptake by Hg^{II} methylating bacteria. We argue that the latter is the more likely explanation of the enhanced availability of added Hg^{II}-DOM tracer in our sediment systems.

The formation of smaller, less stable, β-HgS*(s)* particles from Hg^{II} complexed to DOM has previously been used to explain the enhanced methylation of Hg^{II}*(aq)* in pure bacterial cultures under low sulfide conditions (≤ 30 μM) in the presence of various DOM isolates obtained from fresh water and marine environments (Graham, et al., 2012; Graham, et al., 2013). Indeed, we observed a higher availability for methylation of the nano-sized β-HgS*(s)* particles (β-HgS$(s)_{nano}$) compared to the larger ones (β-HgS$(s)_{micro}$)

(Table S6, ANOVA following Tukey's *post hoc* test, $p<0.05$). However, as binding to POM would also be expected to partly prevent the precipitation of β-HgS*(s)*, it can be argued that the k_m obtained for added Hg^{II}*(aq)* should have been lower than the k_m of β-HgS$(s)_{nano}$ and Hg^{II}-POM. As previously discussed, this was not the case in our experiments. Additionally, our speciation calculations, described in the Supporting Information, do not predict the precipitation of β-HgS*(s)* at the sulfide, DOM and Hg^{II} levels present in our sediment pore waters. We thus argue that the enhanced availability of Hg^{II}-DOM was not due to formation of smaller sized and less stable β-HgS*(s)* particles.

Instead, we posit that a fraction of the Hg^{II} added as Hg^{II}-DOM complexes, was directly available for uptake by Hg^{II} methylating bacteria (Fig. 4). The DOM could either be acting as a shuttle for the Hg^{II} to divalent metal ion transporters within the cell wall of the bacteria, or be taken up into the cell as a Hg^{II}-DOM complex. Both these processes have previously been suggested from studies done in pure bacterial cultures (Schaefer, et al., 2014; Chiasson-Gould, et al., 2014). Chiasson-Gould *et al*. (2014) further found that the equilibration time of Hg^{II} with riverine humic and fulvic acid isolates changed the availability of Hg^{II} for uptake into an *E. coli* strain. The difference observed was suggested to be from the transfer of Hg^{II} during equilibration, from labile, bio accessible and/or weaker sites on the DOM to stronger sites on refractory and inaccessible macromolecules. In a similar way, Schartup *et al*. (2015) found enhanced availability of Hg^{II} complexed to marine DOM (extracted from New England shelf waters and similar to the ELIS DOM used in our experiments) in comparison to Hg^{II} complexed to, presumably less bioavailable, riverine DOM. The mechanism involving DOM as a shuttle molecule, has been proposed by Schaefer *et al*. (2014) who found that the methylation of Hg^{II} by *Geobacter sulfurreducens* was fifty times higher in the presence of cysteine, or when sulfide was added with/without cysteine (Schaefer and Morel, 2009). The molecular configuration of the $Hg(Cysteine)_2$ complex was proposed to allow for ligand exchange with metal transporting sites on the cell wall of the bacteria (Schaefer and Morel, 2009; Schaefer, et al., 2014). This mechanism was supported by the addition of Zn^{II} and Cd^{II} inhibiting uptake and methylation of Hg^{II} (Schaefer, et al., 2014). Though the concentration of cysteine was not determined in our DOM samples, nM levels of low molecular weight thiols have been detected in Long Island Sound waters and other coastal

systems (Hu, et al., 2006; Ndu, 2011). Whether the Hg^{II}-DOM complexes were taken up by the bacteria or DOM acted as a transporter for Hg^{II} to the cell wall of the bacteria cannot be elucidated from this study. It is possible that these two processes are occurring simultaneously.

3.6. Conclusions and Environmental Implications

Although several forms of Hg^{II} have been suggested to be available to Hg^{II} methylating bacteria, based primarily on pure bacterial culture studies, the form of Hg^{II} taken up (i.e. either as the free ion or a complex) and methylated in natural systems remains unknown. Such information is needed in order to fully evaluate the biogeochemical cycle of Hg in sediments and to identify factors limiting the net methylation of Hg^{II}. Our results, showing enhanced availability of Hg^{II} added as complexed to DOM of marine origin, suggest some Hg^{II}-DOM complexes are part of the dissolved Hg^{II} pool taken up and methylated by bacteria in sediments. As previously demonstrated (Jonsson, et al., 2012) and as shown here, the speciation of Hg^{II} in the solid phase is also an important factor controlling the net methylation of Hg^{II} present. Indeed, the fraction of Hg^{II}*(aq)* methylated in our sediments was 60-100 times higher than the pool of added tracer expected to be present in the sediment pore water at equilibrium (based on the measured partition coefficients), demonstrating that the dissolved bioavailable pool of Hg^{II} was readily resupplied from the adsorbed/solid phase during the course of the 12 h experiments. This may also suggest that the pool of ligands available to form bioavailable Hg^{II} complexes exceeds the dissolved pool of Hg^{II} in the pore water, assuming the ligands are also taken up by the bacteria. Whether the size of the pool of these ligands could be a potential factor limiting net methylation of Hg^{II} remains unclear as the specific forms bioavailable are still largely unknown. The relatively low concentration of individual Hg^{II}-DOM complexes makes them analytically challenging to determine, however emerging analytical techniques (Liem-Nguyen, et al., 2015), and a better understanding of the DOM pools available and Hg^{II}-DOM complexes being formed in natural environments could provide further insights in the near future. Our study emphasizes the power of using species/chemical specific forms of isotopically enriched Hg^{II} tracers to study which DOM complexes of Hg^{II}, are directly bioavailable to Hg^{II} methylating bacteria in natural systems.

In our work, we show that Hg^{II} added to sediment slurries as Hg^{II} equilibrated with freeze-dried sediments of different organic matter content, total sulfur and % autochthonous carbon (Hg^{II}-$LOC_{sediment}$ and Hg^{II}-$HOC_{sediment}$) were similar in their availability to the methylating bacteria in each of our four systems. Our results question the hypothesis that OM controls the methylation by controlling the amount of Hg^{II} in the dissolved phase. As allochthonous carbon is both suggested to bind Hg^{II} more strongly and be less available as a carbon source to Hg^{II} methylating bacteria, the K_D and bacterial activity can be expected to co-vary, and thus differences in bacterial activity could possibly also explain differences in methylation rates observed among sites where a correlation has been found between K_D and k_m. In line with the earlier proposed hypothesis, that organic matter would control k_m by controlling the dissolved pool, eutrophication in estuaries has been suggested to limit the net production of MeHg. The opposite would however be expected if a surge in nutrient loading to estuaries would increase the bacterial activity via an increase in deposits of autochthonous carbon to the sediment (following a rise in primary production). It is evident from our study, as well as previous work (Jonsson, et al., 2012; Zhang, et al., 2014; King, et al., 2000), that both bacterial activity and speciation of Hg^{II} in the adsorbed/solid phase influences the net methylation of Hg in sediments. It has been suggested that there may be a threshold of bacterial activity, beyond which Hg^{II} methylation is controlled mostly by the bioavailability of the Hg^{II} species (Kucharzyk, et al., 2015). Our work indicates that Hg^{II} bound to OM would not result in conditions where the methylation is entirely controlled by the speciation. Our results also suggest that the higher methylation rates recoded in off shore sediments relative to estuarine sediments (Hollweg, et al., 2010) may be due to a higher proportion of in situ derived organic matter load to the sediment in these locations. It is clear from this research that predicting future changes in MeHg concentrations across estuaries with climate change and changing system eutrophication, requires a holistic approach aimed at examining the factors that affect both Hg^{II} bioavailability to methylating bacteria and the bacterial methylating activity.

Acknowledgments

This research was supported by the Swedish Research Council (International Postdoc grant 637-2014-54) to S.J, partial support for N.M.M and R.P.M came from the National Institutes of Health, through collaboration with investigators at Dartmouth College (NIH Grant Number P42 ES007373) and partial supported for S.T was through the FEI Graduate Fellowship award. The TEM studies were performed using the facilities in the UConn/FEI Center for Advanced Microscopy and Materials Analysis (CAMMA). Staff and students from the labs of Robert P. Mason (University of Connecticut) and Celia Chen (Dartmouth College) are acknowledged for their help during field sampling.

References

Balcom P. H., Schartup A. T., Mason R. P. and Chen C. Y. (2015) Sources of water column methylmercury across multiple estuaries in the Northeast U.S. *Mar. Chem.* **177,** 721-730.

Benoit J. M., Gilmour C. C., Heyes A., Mason R. P. and Miller C. L. (2003) Geochemical and Biological Controls over Methylmercury Production and Degradation in Aquatic Ecosystems. In *Biogeochemistry of Environmentally Important Trace Elements* (eds. Y. Cai and O. C. Braids). American Chemical Society, pp. 262-297.

Benoit J. M., Gilmour C. C., Mason R. P. and Heyes A. (1999) Sulfide controls on mercury speciation and bioavailability to methylating bacteria in sediment pore waters. *Environ. Sci. Technol.* **33,** 951-957.

Chiasson-Gould S. A., Blais J. M. and Poulain A. J. (2014) Dissolved organic matter kinetically controls mercury bioavailability to bacteria. *Environ. Sci. Technol.* **48,** 3153-3161.

Compeau G. C. and Bartha R. (1985) Sulfate-reducing bacteria: Principal methylators of mercury in anoxic estuarine sediment. *Appl. Environ. Microbiol.* **50,** 498-502.

Deonarine A. and Hsu-Kim H. (2009) Precipitation of mercuric sulfide nanoparticles in NOM-containing water: Implications for the natural environment. *Environmental Science and Technology* **43,** 2368-2373.

Driscoll C. T., Mason R. P., Chan H. M., Jacob D. J. and Pirrone N. (2013) Mercury as a global pollutant: Sources, pathways, and effects. *Environmental Science and Technology* **47,** 4967-4983.

Graham A. M., Aiken G. R. and Gilmour C. C. (2013) Effect of dissolved organic matter source and character on microbial Hg methylation in Hg-S-DOM solutions. *Environ. Sci. Technol.* **47,** 5746-5754.

Graham A. M., Aiken G. R. and Gilmour C. C. (2012) Dissolved organic matter enhances microbial mercury methylation under sulfidic conditions. *Environ. Sci. Technol.* **46,** 2715-2723.

Haitzer M., Aiken G. R. and Ryan J. N. (2002) Binding of mercury(II) to dissolved organic matter: The role of the mercury-to-DOM concentration ratio. *Environ. Sci. Technol.* **36,** 3564-3570.

Hammerschmidt C. R. and Fitzgerald W. F. (2004) Geochemical Controls on the Production and Distribution of Methylmercury in Near-Shore Marine Sediments. *Environmental Science and Technology* **38,** 1487-1495.

Hammerschmidt C. R., Fitzgerald W. F., Balcom P. H. and Visscher P. T. (2008) Organic matter and sulfide inhibit methylmercury production in sediments of New York/New Jersey Harbor. *Mar. Chem.* **109,** 165-182.

Heyes A., Mason R. P., Kim E. -. and Sunderland E. (2006) Mercury methylation in estuaries: Insights from using measuring rates using stable mercury isotopes. *Mar. Chem.* **102,** 134-147.

Hintelmann H. and Harris R. (2004) Application of multiple stable mercury isotopes to determine the adsorption and desorption dynamics of Hg(II) and MeHg to sediments. *Mar. Chem.* **90,** 165-173.

Hintelmann H., Keppel-Jones K. and Evans R. D. (2000) Constants of mercury methylation and demethylation rates in sediments and comparison of tracer and ambient mercury availability. *Environ. Toxicol. Chem.* **19,** 2204-2211.

Hollweg T. A., Gilmour C. C. and Mason R. P. (2010) Mercury and methylmercury cycling in sediments of the mid-Atlantic continental shelf and slope. *Limnol. Oceanogr.* **55,** 2703-2722.

Hollweg T. A., Gilmour C. C. and Mason R. P. (2009) Methylmercury production in sediments of Chesapeake Bay and the mid-Atlantic continental margin. *Mar. Chem.* **114,** 86-101.

Hu H., Mylon S. E. and Benoit G. (2006) Distribution of the thiols glutathione and 3-mercaptopropionic acid in Connecticut lakes. *Limnol. Oceanogr.* **51,** 2763-2774.

Jiang T., Skyllberg U., Wei S., Wang D., Lu S., Jiang Z. and Flanagan D. C. (2015) Modeling of the structure-specific kinetics of abiotic, dark reduction of Hg(II) complexed by O/N and S functional groups in humic acids while accounting for time-dependent structural rearrangement. *Geochim. Cosmochim. Acta* **154,** 151-167.

Kim M., Han S., Gieskes J. and Deheyn D. D. (2011) Importance of organic matter lability for monomethylmercury production in sulfate-rich marine sediments. *Sci. Total Environ.* **409,** 778-784.

King J. K., Kostka J. E., Frischer M. E. and Saunders F. M. (2000) Sulfate-reducing bacteria methylate mercury at variable rates in pure culture and in marine sediments. *Appl. Environ. Microbiol.* **66,** 2430-2437.

Kucharzyk K. H., Deshusses M. A., Porter K. A. and Hsu-Kim H. (2015) Relative contributions of mercury bioavailability and microbial growth rate on net methylmercury production by anaerobic mixed cultures. *Environ. Sci. Process. Impacts* **17,** 1568-1577.

Lambertsson L., Lundberg E., Nilsson M. and Frech W. (2001) Applications of enriched stable isotope tracers in combination with isotope dilution GC-ICP-MS to study mercury species transformation in sea sediments during in situ ethylation and determination. *J. Anal. At. Spectrom.* **16,** 1296-1301.

Liem-Nguyen V., Bouchet S. and Björn E. (2015) Determination of sub-nanomolar levels of low molecular mass thiols in natural waters by liquid chromatography tandem mass spectrometry after derivatization with p-(hydroxymercuri) benzoate and online preconcentration. *Anal. Chem.* **87,** 1089-1096.

Mason R. P., Choi A. L., Fitzgerald W. F., Hammerschmidt C. R., Lamborg C. H., Soerensen A. L. and Sunderland E. M. (2012) Mercury biogeochemical cycling in the ocean and policy implications. *Environ. Res.* **119,** 101-117.

Mayer L. M., Schick L. L. and Loder III T. C. (1999) Dissolved protein fluorescence in two maine estuaries. *Mar. Chem.* **64,** 171-179.

Mergler D., Anderson H. A., Chan L. H. M., Mahaffey K. R., Murray M., Sakamoto M. and Stern A. H. (2007) Methylmercury exposure and health effects in humans: A worldwide concern. *Ambio* **36,** 3-11.

Miller C. L., Mason R. P., Gilmour C. C. and Heyes A. (2007) Influence of dissolved organic matter on the complexation of mercury under sulfidic conditions. *Environ. Toxicol. Chem.* **26,** 624-633.

Mopper K. and Schultz C. A. (1993) Fluorescence as a possible tool for studying the nature and water column distribution of DOC components. *Mar. Chem.* **41,** 229-238.

Ndu U. C. (2011) The Mechanisms and Pathways of the Uptake of Inorganic Mercury and Methylmercury Species in Escherichia coli: Possible Implications for Mercury Cycling in the Marine Environment . Ph.D. thesis, University of Connecticut.

Para J., Coble P. G., Charrière B., Tedetti M., Fontana C. and Sempéré R. (2010) Fluorescence and absorption properties of chromophoric dissolved organic matter (CDOM) in coastal surface waters of the northwestern Mediterranean Sea, influence of the Rhône River. *Biogeosciences* **7,** 4083-4103.

Parks J. M., Johs A., Podar M., Bridou R., Hurt Jr. R. A., Smith S. D., Tomanicek S. J., Qian Y., Brown S. D., Brandt C. C., Palumbo A. V., Smith J. C., Wall J. D., Elias D. A. and Liang L. (2013) The genetic basis for bacterial mercury methylation. *Science* **339,** 1332-1335.

Schaefer J. K. and Morel F. M. M. (2009) High methylation rates of mercury bound to cysteine by Geobacter sulfurreducens. *Nat. Geosci.* **2,** 123-126.

Schaefer J. K., Szczuka A. and Morel F. M. M. (2014) Effect of divalent metals on Hg(II) uptake and methylation by bacteria. *Environ. Sci. Technol.* **48,** 3007-3013.

Schartup A. T., Mason R. P., Balcom P. H., Hollweg T. A. and Chen C. Y. (2013) Methylmercury production in estuarine sediments: Role of organic matter. *Environmental Science and Technology* **47,** 695-700.

Skyllberg U. (2011) Chemical speciation of mercury in soil and sediment. In *Environmental Chemistry and Toxicology of Mercury* (Anonymous). pp. 219-258.

Skyllberg U., Bloom P. R., Qian J., Lin C. -. and Bleam W. F. (2006) Complexation of mercury(II) in soil organic matter: EXAFS evidence for linear two-coordination with reduced sulfur groups. *Environmental Science and Technology* **40,** 4174-4180.

Slowey A. J. (2010) Rate of formation and dissolution of mercury sulfide nanoparticles: The dual role of natural organic matter. *Geochim. Cosmochim. Acta* **74,** 4693-4708.

Waples J. S., Nagy K. L., Aiken G. R. and Ryan J. N. (2005) Dissolution of cinnabar (HgS) in the presence of natural organic matter. *Geochim. Cosmochim. Acta* **69,** 1575-1588.

Yamashita Y. and Tanoue E. (2003) Chemical characterization of protein-like fluorophores in DOM in relation to aromatic amino acids. *Mar. Chem.* **82,** 255-271.

Zhang T., Kim B., Levard C., Reinsch B. C., Lowry G. V., Deshusses M. A. and Hsu-Kim H. (2012) Methylation of mercury by bacteria exposed to dissolved, nanoparticulate, and microparticulate mercuric sulfides. *Environmental Science and Technology* **46,** 6950-6958.

Zhang T., Kucharzyk K. H., Kim B., Deshusses M. A. and Hsu-Kim H. (2014) Net methylation of mercury in estuarine sediment microcosms amended with dissolved, nanoparticulate, and microparticulate mercuric sulfides. *Environ. Sci. Technol.* **48,** 9133-9141.

3.7. Supplementary Information

Dissolved organic matter (DOM) extraction. Marine DOM was extracted using solid phase extraction techniques following the procedure described by Dittmar et al. (2008). Seawater collected from Eastern Long Island Sound (ELIS) was filtered sequentially through a 0.45 µm Meissner cartridge filter and a 0.2 µm glass fiber filter (both pre-rinsed with 0.01 M HCl, > 1 L of ultrapure UV treated water and 1 L of sample water). The filtered seawater was then acidified to pH 2 to increase the extraction efficiency before loading it onto a modified benzene styrene polymer cartridge (pre-rinsed with 6 ml of methanol and 1 L of ultrapure UV treated water) at a rate of < 4ml/min. The cartridge was then rinsed with 40 ml of 0.01 M HCl and dried with Argon gas before the DOM was eluted with methanol followed by acetone. The DOM extract was dried using a Nitrogen evaporator (N-EVAP 111) at 40^{o}C and re-dissolved in purified water. The dissolved organic carbon (DOC) concentration was determined in an aliquot of the re-dissolved DOM.

Transmission electron microscopy (TEM). Samples for TEM were prepared by swirling the TEM grid in the nanoparticle suspension on and off for one hour and then rinsing the DOM from the grid by depositing 5 µL aliquots of ultrapure water a number of times and wicking excess water with a kimwipe. TEM images were captured using FEI –Talos high resolution microscope operated at an accelerating voltage of 200 KV. The size of the nanoparticles was determined to be 4.9 ± 1.2 nm (Fig. S1). All the particles displayed highly crystalline nature with clear lattice fringes as shown in the inset of Fig. S1. The lattice spacing of 0.356 nm corresponds to the (111) planes of Metacinnabar - HgS (ICDD No: 00-002-0439).

Calculating the limit of detection (LOD). As previously discussed by Jonsson et al. (2014) the concentration of added tracers in experimental systems with multiple tracers added are measured superimposed on a background from ambient Hg and smaller fraction of the other isotopically enriched Hg tracers (since these are not 100 % enriched in one single isotope). We thus calculated the LOD for the concentration of MeHg detected from each tracer and ambient Hg in each sample, as the concentration of MeHg that corresponds to 4.8% of the total intensity of the measured signal of the corresponding isotope. With the exception of the amount of MeHg determined from the β-HgS*(s)*$_{micro}$ and β-HgS*(s)*$_{nano}$ methylated

in the LOC 1 and HOC 2 sediment samples, the concentration of MeHg formed from all tracers in all samples (t > 0 h) were above the calculated LOD. The signal contribution of the MeHg from Hg^{II} tracers in the remaining samples were on average 60±20% of the total signal intensity of enriched isotope measured by the ICPMS.

To assure the k_m calculated from samples incubated for 12 h were truly reflecting Hg^{II} methylation, we further compared the fraction methylated in t=12 h samples with the fraction methylated in samples terminated by flash freezing immediately after mixing the sediment and tracer (t=0 h samples). Using the concentration of MeHg found in the t=0 h samples for each sediment (n=1 per site and assay) and the relative standard deviation (RSD) of the fraction of the tracer 'methylated' in these (in total 4) samples, we calculated the LOD for the k_m in each site as 'the fraction methylated in t = 0h x 2 RSD. The calculated LOD for k_m values are given in Table S4.

Ancillary parameters. The concentration of total mercury (HgT) and organic matter (%LOI) were determined on freeze-dried and homogenized un-spiked sediment slurries, using a direct mercury analyzer (DMA-80) and baking the sediment overnight at 550 °C, respectively (Balcom, et al., 2015). Pore water was extracted in a N_2 filled glove bag from the top 4 cm sections of bulk sediment cores using direct vacuum filtration with 0.2-µm Nalgene filter units. The concentration of HgT and MeHg was determined in collected pore water as described elsewhere (Balcom, et al., 2015). Dissolved sulfide was determined using an ion-selective electrode (Orion) in pore water preserved with sulfide antioxidant buffer (Brouwer and Murphy, 1994). Samples for dissolved organic carbon (DOC) analysis were preserved by freezing and were analyzed using a Shimadzu TOC analyzer (TOC-VCPN).

Fluorescence measurements. Fluorescence spectroscopy was performed on pore water samples using a Hitachi F2000 fluorometer with 1 cm quartz cell. All samples were first diluted using UV oxidized purified water to an absorption of < 0.05 cm^{-1} at 220 nm so as to reduce inner filter effects (Burdige, et al., 2004). Excitation and emission matrices (EEM) for samples and blanks were obtained by varying λ_{ex} every 5 nm starting from 220 to 450 nm and recording emissions every 1 nm from 230 to 700 nm. The intensity of the

blank EEM was subtracted from the sample EEM and corrected fluorescence intensities were normalized to the water Raman peak area determined daily at λ_{ex} of 350 nm and λ_{em} of 371-428nm (Lawaetz and Stedmon, 2009). To remove Raman and Rayleigh scattering, we included fluorescence signals starting 40 nm beyond λ_{ex} up to where second order Rayleigh scattering occurs, at 2 times λ_{ex}.

Thermodynamic modelling of dissolved inorganic mercury species. To determine the potential for β-HgS*(s)* precipitation in our sediment systems, we modelled the speciation of Hg^{II} in the dissolved phase. In our model, we included the measured concentration of Hg^{II}, dissolved sulfide, pH and salinity, and estimated the concentration of thiols based on the measured pore water DOC concentration (Hollweg, et al., 2010). The thermodynamic constants used in the modelling are presented in Table S7 and were adjusted to the ionic strength of seawater. In all sediment systems studied, the reaction quotient (Q) was lower than the solubility product of HgS*(s)*, indicating that precipitation of Hg as β- HgS*(s)* will not occur at the conditions specified.

Supplementary Figures

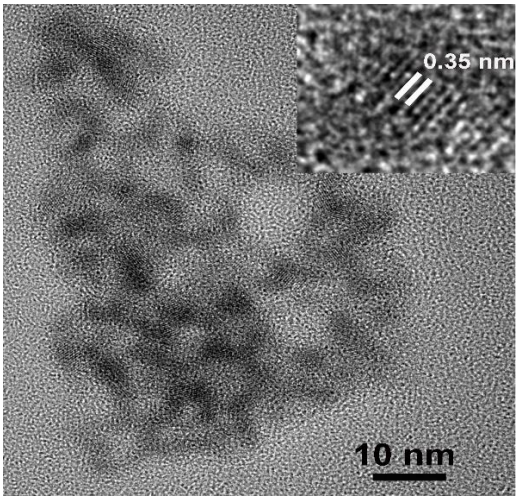

Fig. S1. Transmission electron microscopy (TEM) images of HgS*(s)* nanoparticles precipitated for 3 days in purified water containing 1.3 µmoles of Hg^{II}, 1.3 µmoles of S^{2-}, and 1.3 mg of marine derived dissolved organic carbon (DOC).

Fig. S2. Map showing the sampling locations in Barn Island and Goshen Cove, CT, USA (maps are from Google Earth).

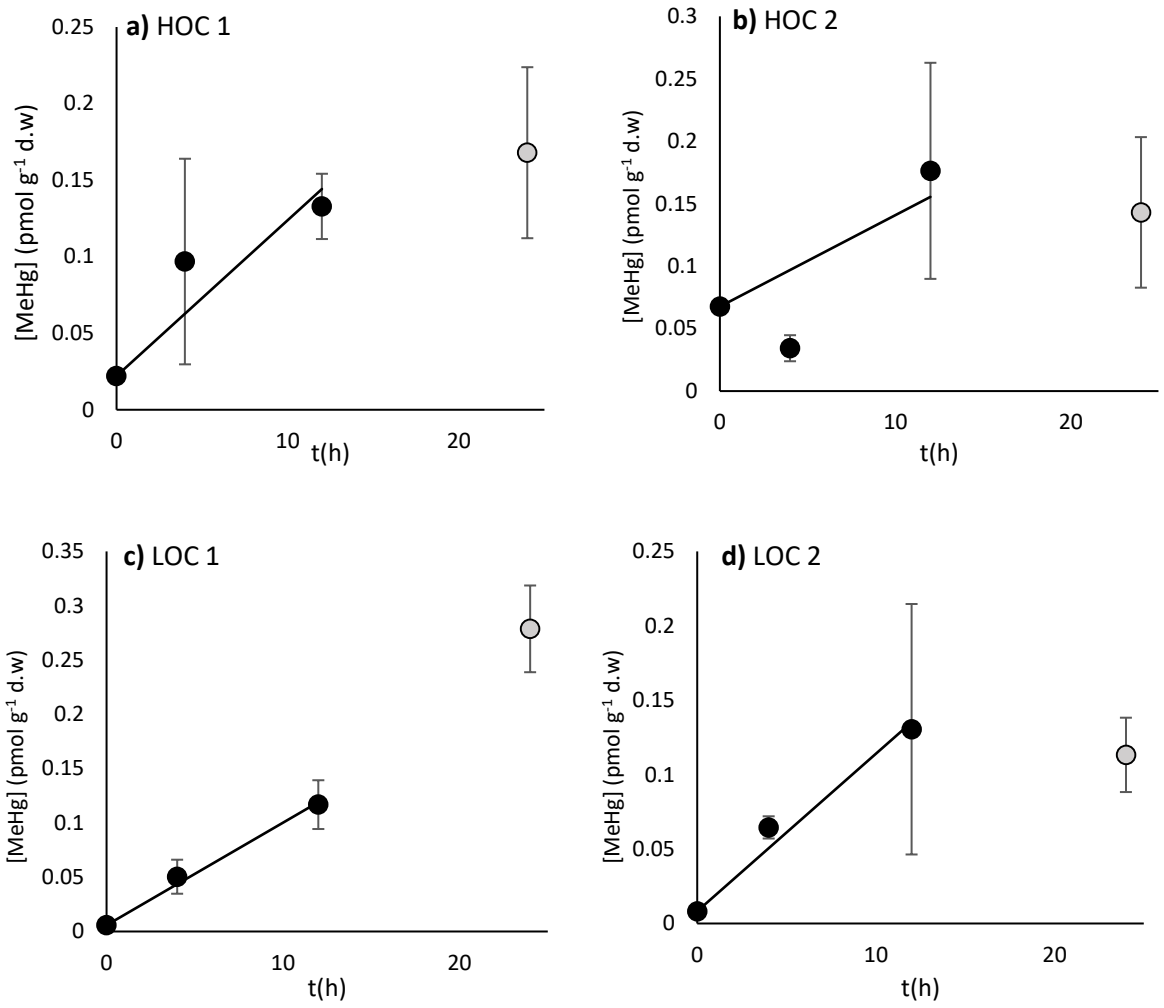

Fig. S3. Concentration of MeHg (pmol g^{-1} d.w., ±SE, n=3) formed as a function of incubation time (up to 12 h shown as black circles, t=24 h shown as gray circles) from added $^{200}Hg^{II}$*(aq)* tracer in the four different sediments; (a) HOC 1, (b) HOC 2, (c) LOC 1, and (d) LOC 2. The linear regression line was fitted for data up to 12 h.

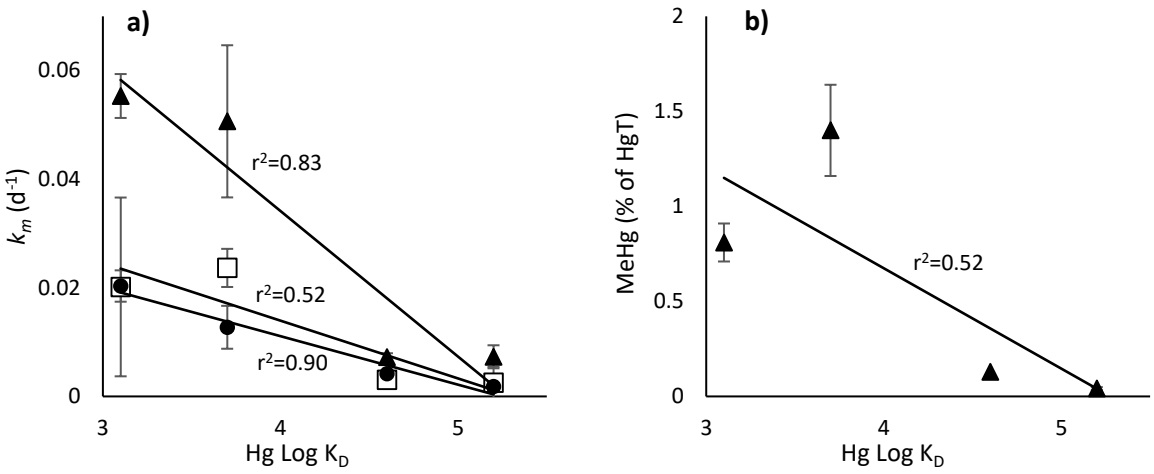

Fig. S4. Relation between the partitioning coefficient (K_D) for Hg (x-axis) and (**a**) the methylation rate constant (k_m, d^{-1}, ±SD, n=3) for Hg^{II}*(aq)* (white squares), Hg^{II}-POM (black circles) and Hg^{II}-DOM (black triangles) tracers, and (**b**) fraction ambient MeHg (% of HgT, ±SD, n=45).

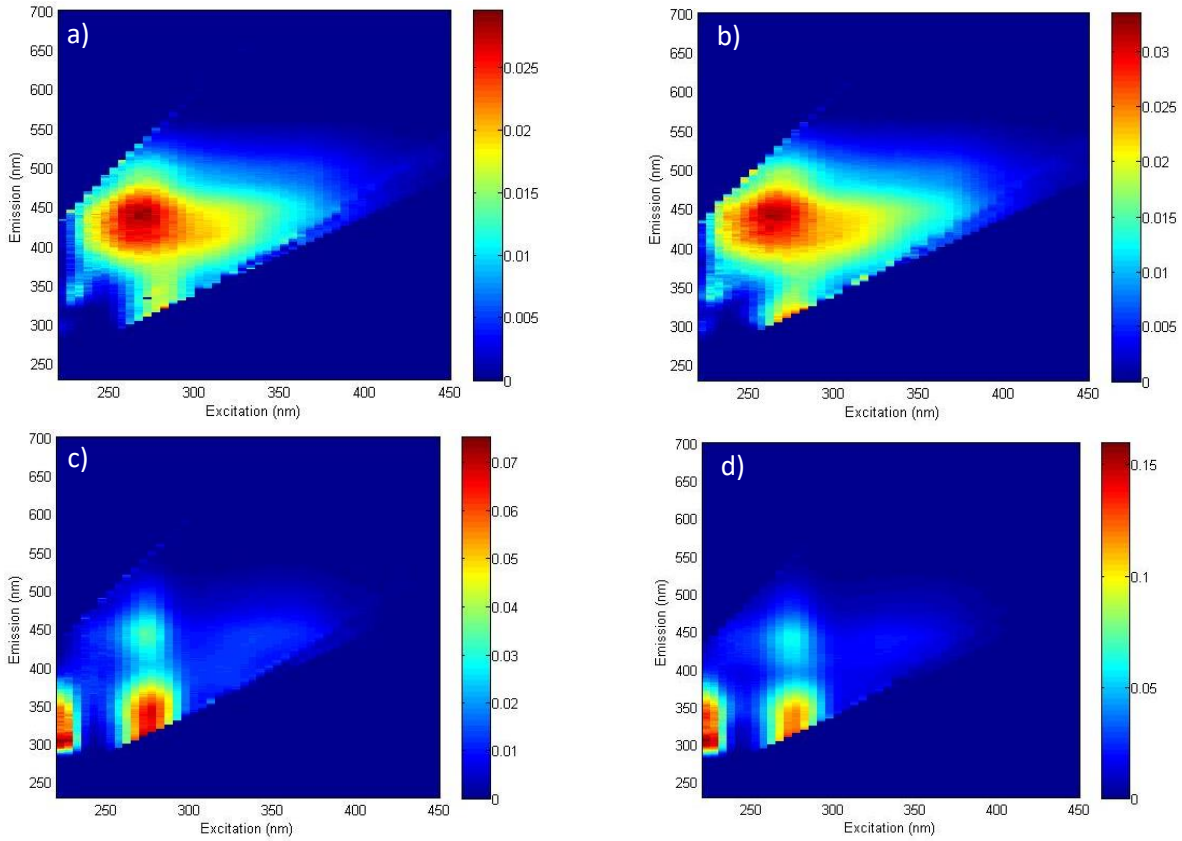

Fig. S5. Excitation and emission matrices (EEM) of colored dissolved organic matter in pore water samples collected from (a) HOC 1, (b) HOC 2, (c) LOC 1 and (d) LOC 2. Fluorescence intensities are given in Raman Units (R.U). Proteinaceous fluorescence occurs in the region where tyrosine and tryptophan emit light (λ_{em} 300-350 following two excitations at λ_{ex} 220 nm and 270 nm) (Para, et al., 2010; Yamashita and Tanoue, 2003; Coble, et al., 1990).

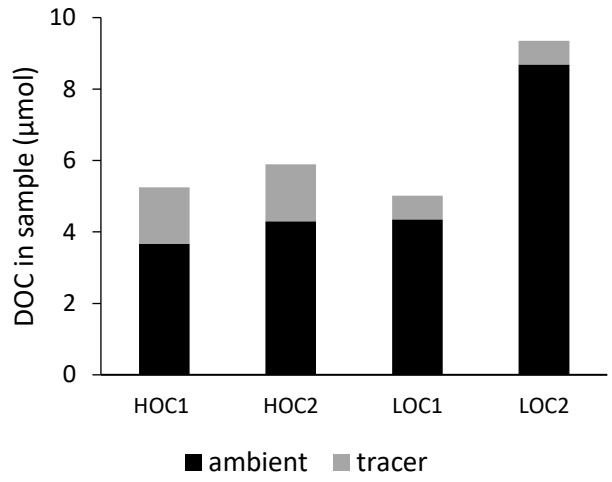

Fig. S6. Amount of DOC (µmol) in sediment assays containing the DOM originating from ambient DOM (black bar) and from the added Hg^{II}-DOM tracer (gray bar)**.**

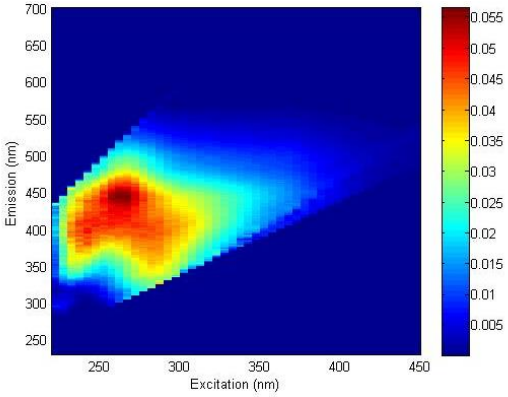

Fig. S7. Excitation and emission matrices (EEM) of colored dissolved organic matter extracted from Eastern Long Island Sound (used to synthesize the Hg^{II}-DOM tracer). Fluorescence intensities are given in Raman Units (R.U).

Supplementary Tables

Table S1: Average (±SD) concentration of total Hg (HgT), MeHg, organic carbon (measured as the loss on ignition, %) and total sulfur of freeze-dried sediments collected in 2013 from Barn Island high and low organic carbon sites (BI_HOC and BI_LOC). The two sediments were used to prepare the Hg^{II}-$HOC_{sediment}$ and Hg^{II}-$LOC_{sediment}$ tracers, respectively.

Freeze-dried Sediment	HgT (nmol/g)	MeHg (pmol/g)	% LOI	TS (mmol/g)
BI_HOC	0.34 (0.077)	0.54 (0.33)	17 (4.8)	0.43 (0.022)
BI_LOC	0.030 (0.017)	0.79(0.39)	1.3 (0.36)	0.02 (0.004)

Table S2: Average concentration of Hg^{II} tracers added (nmol Hg^{II} g^{-1} d.w.) to sampled sediments (HOC 1, HOC 2, LOC 1 and LOC 2). Percent increase of ambient HgT concentration due to the tracer addition is given in parenthesis.

Sediment	Hg^{II}*(aq)*	Hg^{II} -POM	β-HgS*(s)*$_{micro}$	β-HgS*(s)*$_{nano}$	Hg^{II} -DOM
HOC 1	0.083 (27%)	0.41 (140%)	1.53 (510%)	0.53 (180%)	0.069 (23%)
HOC 2	0.065 (7%)	0.32 (37%)	1.26 (140%)	0.44 (50%)	0.051 (6%)
LOC 1	0.0092 (18%)	0.048 (94%)	0.17 (330%)	0.058 (110%)	0.0089 (17%)
LOC 2	0.011 (26%)	0.053 (130%)	0.18 (420%)	0.062 (150%)	0.0084 (20%)

Table S3: Temperature of overlying water (°C) at time of sampling.

Sediment Slurry	Temperature (°C)
HOC 1	27.9
HOC 2	26.5
LOC 1	24.0
LOC 2	26.3

Table S4: Calculated limit of detection (LOD) for k_m (d^{-1}) of the different tracers used.

Sediment	Hg^{II}*(aq)*	Hg^{II}-POM	Hg^{II}-DOM	Hg^{II}-$LOC_{sediment}$	Hg^{II}-$HOC_{sediment}$
HOC 1	0.00096	0.00051	0.0012	0.00084	0.0021
HOC 2	0.0058	0.00054	0.0011	0.0016	0.0027
LOC 1	0.0029	0.00035	0.0016	-	0.0062
LOC 2	0.0051	0.00078	0.0025	0.0036	0.0081

Table S5: Average (±SD) concentration of HgT (pM), MeHg (pM), sulfide (µM) and DOC (µM) in sediment pore water collected from HOC 1, HOC 2, LOC 1 and LOC 2 sites.

Sediment	HgT (pM)	MeHg (pM)	% MeHg	Sulfide (µM)	DOC (µM)
HOC 1	7.4 (2.4)	1.4 (1.5)	20 (19)	8.9 (14)	700 (250)
HOC 2	5.1 (1.5)	0.73(0.55)	17 (15)	0.26 (0.11)	700 (230)
LOC 1	10 (6.7)	0.87 (0.2)	12 (9)	0.37 (0.24)	2500
LOC 2	31 (6)	1.8	6	1.4 (1.6)	3100 (3800)

Table S6: The k_m (d^{-1}) values determined for the different tracers in the four sediments investigated (HOC 1, HOC 2, LOC 1 and LOC 2)

	$Hg^{II}(aq)$	Hg^{II}-POM	$Hg^{II}(aq)$ + POM	β-HgS $(s)_{micro}$	β-HgS $(s)_{nano}$	Hg^{II} (aq) + β-HgS $(s)_{nano}$	Hg^{II}-DOM	Hg^{II} (aq) + DOM	Hg^{II} - $LOC_{sediment}$	Hg^{II} - $HOC_{sediment}$
HOC 1	0.0023	0.0041	0.0050	<0.00097	0.0071	0.0024	0.0077	0.0037	0.0028	0.0024
	0.0037	0.0035	0.0040	<0.00026	0.0019	0.0019	0.0064	0.0031	0.0031	0.0025
	0.0032	0.0049		<0.0011	0.0028		0.0076		0.0030	0.0025
HOC 2	0.00071	0.0018	<0.0058	<0.00029	<0.0058	<0.0058	0.0058	0.0063	0.0039	0.0056
	0.0010	0.0015	<0.0058	<0.00015	<0.0058	<0.0058	0.0088	0.0079	0.0036	0.010
	0.0059	0.0021		<0.00031	<0.0058		n.a.		0.0038	n.a.
LOC 1	0.024	0.012	0.019	<0.00012	<0.0029	<0.0029	0.037	0.023	0.011	0.016
	0.020	0.0092	0.024	<0.00019	<0.0029	<0.0029	0.065	0.011	0.0096	0.012
	0.027	0.017		<0.000099	<0.0029		0.050		0.0058	0.019
LOC 2	0.0085	0.017	0.024	<0.0021	0.011	0.0051	0.053	0.032	0.025	0.019
	0.013	0.022	0.023	<0.0022	0.016	0.0072	0.053	0.024	0.040	0.019
	0.039	0.022		<0.0012	0.0085		0.060		0.024	0.012

Table S7: Thermodynamic stability constants used for speciation modelling of Hg^{II} complexes in sediment pore water.(Drott, et al., 2013; Skyllberg, 2008; Stumm and Morgan, 1996)

Reaction	**log K**	**Reference**
$Hg^{2+} + Cl^- = HgCl^+$	7.2	Stumm and Morgan (1996)
$Hg^{2+} + 2Cl^- = Hg(Cl)_2^0$	14	Stumm and Morgan (1996)
$Hg^{2+} + 3Cl^- = HgCl_3^-$	15.1	Stumm and Morgan (1996)
$Hg^{2+} + 4Cl^- = HgCl^{2-}_4$	15.4	Stumm and Morgan (1996)
$Hg^{2+} + 2HS^- = Hg(SH)_2^0$	39.1	Drott et al. (2013)
$Hg^{2+} + 2HS^- = HgS_2H^- + H^+$	32.5	Drott et al. (2013)
$Hg^{2+} + 2HS^- = HgS_2^{2-} + 2H^+$	23.2	Drott et al. (2013)
$HgS_{(s)} + H^+ = Hg^{2+} + HS^-$	-36.8	Drott et al. (2013)
$Hg^{2+} + 2RS^- = Hg(SR)_2$	42	Skyllberg et al. (2008)
$H_2S = HS^- + H^+$	7	

References

Balcom P. H., Schartup A. T., Mason R. P. and Chen C. Y. (2015) Sources of water column methylmercury across multiple estuaries in the Northeast U.S. *Mar. Chem.* **177,** 721-730.

Brouwer H. and Murphy T. P. (1994) Diffusion method for the determination of acid-volatile sulfides (AVS) in sediment. *Environ. Toxicol. Chem.* **13,** 1273-1275.

Burdige D. J., Kline S. W. and Chen W. (2004) Fluorescent dissolved organic matter in marine sediment pore waters. *Mar. Chem.* **89,** 289-311.

Coble P. G., Green S. A., Blough N. V. and Gagosian R. B. (1990) Characterization of dissolved organic matter in the Black Sea by fluorescence spectroscopy. *Nature* **348,** 432-435.

Dittmar T., Koch B., Hertkorn N. and Kattner G. (2008) A simple and efficient method for the solid-phase extraction of dissolved organic matter (SPE-DOM) from seawater. *Limnol. Oceanogr. Methods* **6,** 230-235.

Drott A., Björn E., Bouchet S. and Skyllberg U. (2013) Refining thermodynamic constants for mercury(II)-sulfides in equilibrium with metacinnabar at sub-micromolar aqueous sulfide concentrations. *Environ. Sci. Technol.* **47,** 4197-4203.

Hollweg T. A., Gilmour C. C. and Mason R. P. (2010) Mercury and methylmercury cycling in sediments of the mid-Atlantic continental shelf and slope. *Limnol. Oceanogr.* **55,** 2703-2722.

Jonsson S., Skyllberg U., Nilsson M. B., Lundberg E., Andersson A. and Björn E. (2014) Differentiated availability of geochemical mercury pools controls methylmercury levels in estuarine sediment and biota. *Nature Communications* **5,** 4624.

Lawaetz A. J. and Stedmon C. A. (2009) Fluorescence intensity calibration using the Raman scatter peak of water. *Appl. Spectrosc.* **63,** 936-940.

Para J., Coble P. G., Charrière B., Tedetti M., Fontana C. and Sempéré R. (2010) Fluorescence and absorption properties of chromophoric dissolved organic matter (CDOM) in coastal surface waters of the northwestern Mediterranean Sea, influence of the Rhône River. *Biogeosciences* **7,** 4083-4103.

Skyllberg U. (2008) Competition among thiols and inorganic sulfides and polysulfides for Hg and MeHg in wetland soils and sediments under suboxic conditions: Illumination of controversies and implications for MeHg net production. *Journal of Geophysical Research: Biogeosciences* **113,** - G00C03.

Stumm W. and Morgan J. (1996) *Aquatic chemistry: chemical equilibria and rates in natural waters.* John Wiley & Sons, Inc, United States of America.

Yamashita Y. and Tanoue E. (2003) Chemical characterization of protein-like fluorophores in DOM in relation to aromatic amino acids. *Mar. Chem.* **82,** 255-271.

4. Dimethylmercury Formation Mediated by Inorganic and Organic Reduced Sulfur Species

This study was published in *Scientific Reports* (open access) on 06/15/2016. It is reproduced here, with permission from the authors.

Jonsson, S.; Mazrui, N.M.; Mason, R.P. Dimethylmercury Formation Mediated by Inorganic and Organic Reduced Sulfur Surfaces. *Sci. Rep.* **2016,** *6*; 10.1038/srep27958.

4.1. Introduction

Methylmercury (MeHg) bioaccumulates in aquatic food webs and is the main form of mercury found in fish (>95 %). For many fresh and marine system's worldwide, the concentration of MeHg found in the top of the aquatic food web is so high that it poses a neurotoxic risk to fish eating humans and wildlife.[1] Like Hg^{II}, MeHg has a strong affinity for reduced sulfur sites. In vivo, MeHg can form a MeHg-L-cysteine complex, which is structurally similar to methionine.[2] This structural similarity allows the complex to cross the blood-brain barrier and placenta through the amino acid transport system and get to the brain where it damages the central nervous system.[2] MeHg is mostly produced in anoxic marine sediments though recent research suggests MeHg production can also occur in anoxic microenvironments within the water column.[3-8] The MeHg is transported from the sediment to the water column via diffusion or through its association with particles, from where exposure to marine organisms occurs through particle ingestion, passive diffusion or active transport.[9-11]

The concentration of MeHg in sediments is typically around 1 % or less of the total mercury and the concentrations is in principal governed by the relative rates of methylation and demethylation.[9,12] Methylation involves the conversion of Hg^{II} to MeHg and occurs during the microbial degradation of organic matter by sulfate and iron reducing bacteria.[13-16] As such, methylation depends on the microbial activity and the bioavailability of Hg^{II} complexes.[17,18] Less is known about demethylation than methylation, though it is recognized that both biotic and abiotic mechanisms occurring in aerobic and anaerobic settings

contribute to the demethylation process.[19-23] The biotic demethylation pathway happens through oxidative and reductive demethylation. In oxidative demethylation, done for metabolic purposes, microorganisms oxidize the methyl group to CO_2 and MeHg is transformed to Hg^{II}.[20,24,25] Reductive demethylation on the other hand, occurs for detox purposes and is conducted by mercury resistant microorganisms carrying the mer operon genes (merA and merB). The enzyme organomercurial lyase, encoded by the merB gene breaks the Hg-C bond to form CH_4 and Hg^{II}, while the mercury reductase, encoded by the merA gene, reduces Hg^{II} to Hg^0.[20,26-28]

The abiotic demethylation pathways known to degrade MeHg in the environment include a photochemical reaction mediated by reactive oxygen species and a chemical reaction between MeHg and H_2S. During photo-degradation, MeHg is converted to Hg^{II} and this process contributes significantly to demethylation when light penetration is substantial.[29-31] In chemical degradation, MeHg has been shown to react with H_2S to form a white unstable intermediate known as bismethylmercury sulfide ($(CH_3Hg)_2S$), which degrades to dimethylmercury (DMeHg) and $HgS_{(s)}$.[32] It has also been shown that the addition of MeHg to pure cultures of sulfate reducing bacteria (SRB) (*Desulfovibrio desulfuricans* strain LS) produced a white intermediate identified as $(CH_3Hg)_2S$ which degraded to DMeHg and $HgS_{(s)}$.[33] In the same study MeHg was spiked into fresh sediment together with pyruvate — a carbon source for SRB — and after 9 days of incubation the concentration of DMeHg was found to be higher than in the control.[33] Sulfate reducing bacteria oxidize organic matter (represented here as CH_2O) using sulfate; converting SO_4^{2-} to H_2S as follows:

$$2CH_2O + SO_4^{2-} \rightarrow H_2S + 2HCO_3^- \qquad (1)$$

In their work, Baldi *et. al.*, concluded that MeHg was unstable in presence of biologically produced H_2S.[33] Similar to Baldi's proposed reaction between MeHg and H_2S, a reaction involving MeHg and (seleno) amino acids has been suggested to occur in vivo during the degradation of MeHg by (seleno) amino acids.[34,35] Though the intermediate complexes, $(CH_3Hg)_2S$ and $(CH_3Hg)_2Se$, expected to form from the reaction of MeHg with (seleno) amino acids are unstable in biological media and have not been detected in

vivo, presence of HgS and HgSe particles has been observed in rat plasma, liver, brain and other organs following administration of MeHg in the diet.[34,36] As the products of the chemical/biochemical degradation pathways discussed above are DMeHg and HgS/HgSe*(s)*, these pathways both methylate and demethylate MeHg.

In marine anaerobic sediments, some of the H_2S produced during the oxidation of organic matter by sulfate reducing bacteria, reacts with metals to form metal sulfide solids, with iron sulfides being the most abundant.[37] The precipitation of Fe^{II} by H_2S occurs via the reaction described in equation 2 below; where m stands for mackinawite — the first iron sulfide phase to form in nature.[38]

$$Fe^{II} + HS^- \rightarrow FeS_m\,(s) + H^+ \qquad (2)$$

Iron sulfides adsorb and co-precipitate with various metals during their formation.[37] Mercury has a high affinity for particles and with a log K_D (the partitioning coefficient between the solid and aqueous phase), of 3 – 6 and 2 – 5 L kg^{-1} for Hg and MeHg respectively, both species are found mostly bound to the solid phase.[39-42] In fact, it has been shown that reduced sulfur containing solids control the partitioning of Hg and MeHg between the sediment and pore water.[40,43,44] Thus, the association of Hg and MeHg with iron sulfide solids is expected and has been shown in previous studies.[45]

In this work, we investigate if the reaction of MeHg adsorbed on FeS_m*(s)* is similar to that of MeHg with dissolved reduced sulfur shown in previous studies.[32,35] One of the products expected from the reaction is volatile and highly toxic DMeHg. This form of mercury is ubiquitous in the marine environment and is commonly found in areas of high productivity or in regions with low oxygen concentrations.[3,5,7,46,47] It has been suggested that the biotic methylation of Hg^{II} to DMeHg could be a source of DMeHg; however, few studies have explored this option and the mechanism of formation remains unknown.[48,49] Unlike H_2S with a sulfide oxidation half-life of 2 days in oxic waters, metal sulfides have much longer oxidation half-lives (weeks to years).[50-52] For example, sub-micron pyrite (FeS_2) was found to oxidize at a rate of 10^{-5} µM day^{-1} suggesting that the iron sulfide mineral can persist in oxygenated waters for years.[53] The degradation of

MeHg from its reaction with FeS_m*(s)* has therefore important implications on the biogeochemistry and mobility of mercury in oxic and anoxic conditions. In this study, we hypothesize that: (1) the adsorption and subsequent degradation of MeHg on FeS_m*(s)* will result in the production of DMeHg; (2) since the inorganic Hg product will precipitate faster in presence of FeS_m*(s)* than in a solution of dissolved sulfide, the reaction of MeHg with FeS_m*(s)* will produce more DMeHg than that of MeHg with dissolved reduced sulfur species; (3) reaction of MeHg with thiols in organic matter could lead to the production of DMeHg; and (4) the reaction of MeHg with FeS_m*(s)* or thiols can occur in seawater and in presence of organic matter, though the complexation of MeHg to organic matter could potentially inhibit the reaction.

4.2 Methodology

4.2.1. Synthesis and Characterization of Metal Sulfide Particles

FeS_m*(s)*, CdS*(s)*, and HgS*(s)* particles were prepared under low O_2 conditions in a N_2 filled glove bag by adding 0.6 M sodium sulfide to 0.6 M $(NH_4)_2Fe(II)(SO_4)_2{\cdot}6H_2O$, $Cd(NO_3)_2{\cdot}4H_2O$, and $HgCl_2$, respectively. All solutions were prepared using ultra-pure water (Ω<18.2), degassed by boiling under N_2 for 20 min. Particles were allowed to age for 0, 1, and 7 days, after which they were washed at least 3 times then collected by centrifugation. Since the $HgCl_2$ salt was first dissolved in 700 µl HCl, the particles were washed until the pH of the solution was about neutral. As the purification of the particles took almost 1 hour to complete, particles that were washed immediately upon precipitation were actually aged for 1 h. The resultant slurries after centrifugation were re-suspended in a known volume of degassed utra-pure water and aliquots transferred to smaller vials and stored frozen at -80°C until use. One vial was freeze-dried and used to determine the final concentration (g/g) of the FeS_m*(s)* in the vials. The crystal structure and specific surface area were determined by X-ray Diffraction Crystallography (XRD) and Brunauer–Emmett–Teller (BET), respectively.

X-ray diffraction studies were conducted by Rigaku UltimaIV diffractometer with Cu Kα radiation (λ = 1.5418 Å) operating at a beam voltage of 40 kV and beam current of 45 mA. The patterns were acquired

at a scan rate of 2° min^{-1}, from 0 to 80 degrees in the 2θ range. Brunauer-Emmett-Teller (BET) surface-area measurements were performed using nitrogen sorption experiments conducted on a Quantochrome Nova 2000e instrument. All the samples were degassed for 5 h before analysis. Specific surface area was calculated using the adsorption isotherm within $0.05 < P/P_0 < 0.3$ range, where P/P_0 is the relative pressure.

4.2.2. The Adsorption of MeHg on $FeS_m(s)$ Particles

The adsorption of MeHg on $FeS_m(s)$ was investigated by adding 2.8 µmol of $FeS_m(s)$ to 0.7, 2.8 or 11 nmol of MeHg and incubating the mixtures for various times up to 1 h. The samples were filtered through 0.02 µm syringe filters after 0 to 60 min and the filtrate was analyzed for MeHg. The experiment was repeated at 10 min, 60 min, and 24 h using 0.068 nmol MeHg/µmol $FeS_m(s)$ and filtered through a 0.05 µm membrane filter. The filtrates were frozen immediately and analyzed within 48 h. Aliquots of the filtrates were diluted in ultra-pure water and the MeHg in solution was converted to methylethylmercury using sodium tetraethylborate ($Na(C_2H_5)_4BO_4$). Using the automated Tekran 2700, volatile methylethylmercury was bubbled from the solution, pyrolitically decomposed to Hg^0 and analyzed by Cold Vapor Atomic Fluorescence Spectroscopy, following EPA's method 1630.

4.2.3. Reactions of MeHg with Reduced Sulfur Species

The production of DMeHg from the reaction between MeHg and reduced sulfur was monitored by adding an aliquot of MeHg to a solution/suspension containing one of the reduced sulfur forms: precipitated metal sulfides ($FeS_m(s)$, $CdS(s)$, and $HgS(s)$), inorganic dissolved sulfide (added as an aqueous solution of Na_2S) and thiols (cysteine, mercaptopropionic acid, 1,2-ethanedithiol, and 1,3-propanedithiol). In each test, one form of reduced sulfur was reacted with MeHg and this was compared to the reaction of MeHg with $FeS_m(s)$ done in parallel with the test (Table 1). The MeHg was diluted from a 1000 ppm stock solution (Alfa Aeser) and the pH of the diluted solutions were adjusted to about 7 before use. With the exception of experiments done in artificial seawater and with the thiols, all other experiments were conducted in ultra-

pure water. The dithiols were first dissolved in acetone and then diluted in ultrapure water. To account for the effect that acetone might have had on the experiment, and also so we can compare the fraction of MeHg converted to DMeHg when MeHg was reacted with the different thiols or with $FeS_m(s)$ in the thiol test (Table 1), an equivalent amount of acetone (4µL) was added to the monothiols and to $FeS_m(s)$ conducted alongside the thiols. Blank experiments were done where MeHg was added to degassed ultra-pure water and to the filtrate of $FeS_m(s)$ slurry. Solutions were incubated for a specified time in a sealed acid cleaned glass vial under anoxic conditions. The concentrations of reactants and the MeHg to reduced sulfur ratio (nmol/µmol) is summarized in Table 1. Experiments conducted at temperatures other than room temperature (0, 40, and 60°C) were done by incubating the reaction vials for 30 min in an ice or heated water bath maintained at the desired temperature. Since the production of DMeHg at 0°C was below the detection limit (except when high concentrations of MeHg were used), these experiments were terminated by cooling all vials in ice for 30 min before analysis. We determined the detection limit for each test by quantifying the DMeHg in blank experiments containing equal concentrations of MeHg in the matrix of the test (i.e. ultra-pure water, 0.7 % by volume acetone solution or artificial seawater). The detection limit was calculated as average concentration of DMeHg in the blanks (n=3) ± 2 standard deviations.

4.2.4. Experiments in Seawater and in Presence of Thalassiosira Weissflogii

Artificial seawater was prepared according to the formula published by Kester *et al*.[54] The solution was filtered through a 0.2 µm cartridge filter and degassed before use. Diatom cultures were obtained from the National Oceanic and Atmospheric Administration in Milford, US. A subsample of the cultures was sonicated to break the cells and then centrifuged at 754G to separate cellular organelles (cell wall, nuclei and mitochondrion) from the cytoplasm. The supernatant consisting of the cytoplasm was removed and the organelles re-suspended in artificial seawater. Aliquots containing whole cells, cell organelles or the cytoplasm were diluted in seawater before amending each with 9.6 nmol of MeHg and 2.8 µmol $FeS_m(s)$.

Table 1. Summary of experimental details. Form and amount of sulfide used to mediate the conversion of MeHg to DMeHg, the initial amount of MeHg and the final total volume of the aqueous solution used.

Test	**Sulfide form name**	**(μmol)**	**MeHg (nmol)**	**MeHg:sulfide form (nmol umol^{-1})**	**Volume (ml)**
Initial test (Table 3)	FeS_m*(s)*	5.6	2.3	0.41	1.1
Varying MeHg (Fig. 2 & 3)	FeS_m*(s)*	2.8	0.7, 2.8, 11	0.25, 1.0, 3.9	0.6
Varying FeS_m*(s)* (Fig. 4)	FeS_m*(s)*	0.0028 to 280	9.6	3400 to 0.034	0.6
FeS_m*(s)* aging (Table 4)	FeS_m*(s)* (aged 1h, 1d, 7d)	2.8	9.6	3.4	0.6
Different sulfide minerals (Table 5)	CdS*(s)*	0.93	9.6	10	0.6
	FeS_m*(s)*	2.0	9.6	4.8	0.6
	HgS*(s)*	2.2	9.6	4.4	0.6
pH and ionic strengh (Fig. 6)	FeS_m*(s)*	2.8	8	2.9	0.6
FeS_m*(s)* and S^{-II}*(aq)* (Fig. 7)	FeS_m*(s)*	2.8	12	4.3	0.6
	S^{-II}*(aq)*	2.8, 0.13, 0.013, 0.0063	12	4.3, 92, 920, 1900	0.6
Temperature effect (Fig. 8)	FeS_m*(s)*	2.8	7.5	2.7	0.6
	S^{-II}*(aq)*	0.38	390	1000	0.6
Test of thiols (Fig. 9)	FeS_m*(s)*	2.8	9.6	3.4	0.6
	Cysteine	0.2	200	1000	0.6
	3-mercaptopropionic acid	0.2	200	1000	0.6
	1,2-ethanedithiol	0.1	200	2000	0.6
	1,3-propanedithiol	0.1	200	2000	0.6
Artificial sea water and *t.w.* (Fig. 10)	FeS_m*(s)*	2.8	9.6	3.4	2.5

4.2.5. Collection and Analysis of Dimethylmercury

The DMeHg produced in the reaction vials was collected on a Carbotrap™ (Supelco) adsorbent via two methods; for experiments where the rate was quantified, solutions were stirred continuously and the headspace purged with argon gas at a rate of 200 mL/min. In this case, the collected gas was dried on a soda lime trap placed before the Carbotrap. In all other experiments, 0.1–5 mL of the headspace was sampled using a syringe and injected via a valve with continuous gas flow on to the adsorbent. When the

headspace was sampled, the total concentration of DMeHg was calculated using the Henry's constant for DMeHg (0.3 at 25˚C) and the relative volume of liquid and gas in the reaction vial. The DMeHg adsorbed on the Carbotrap was thermally desorbed and separated from other Hg species using a packed gas chromatographic column heated to ~70˚C, then pyrolytically decomposed to elemental mercury (Hg^0) and analyzed by Cold Vapor Atomic Fluorescence Spectroscopy, using a Tekran 2500 instrument.

An external calibration curve was prepared daily from an isotopically enriched dilute solution of DMeHg synthesized in the lab using $^{200}HgCl_2$ and 3 M methyl magnesium chloride as described elsewhere.[55] Aliquots of the headspace were drawn from the vial containing the dilute solution of DMeHg, injected onto a Carbotrap and analyzed as described above for the samples. The concentration of DMeHg in the headspace was determined (standardized) daily using a calibration curve made from 10-200 µL of Hg^0 *(g)* trapped on gold traps. Three types of commercially available adsorbents are commonly used for trapping volatile Hg species. Carbotrap is mostly suitable for DMeHg, Tenax for methylethylmercury (MeHg derivatized with $Na(C_2H_5)_4BO_4$) and a gold trap for all Hg species.[46,56] Mercury is desorbed from Au by heating the trap to a temperature of 450-500°C. During the desorption process, the Hg species are decomposed to Hg^0 *(g)*, thus the speciation of Hg (DMeHg, MeHg, Hg^{II}, Hg^0) cannot be determined when Au traps are used. Since no other Hg species was detected in the headspace of the vial containing the isotopically enriched dilute solution of DMeHg, either when using the Carbotrap or in a gold trap placed after the Carbotrap; the standardization was done by collecting headspace gas aliquots of isotopically enriched DMeHg on gold traps.

All the data was *log* transformed and tested for normality using SPSS. For normally distributed *log* transformed data, differences between sets were verified through analysis of variance and *Tukey's* post-hoc test. For *log* transformed data not normally distributed, a median test and a pairwise t-test were used to determine statistical differences.

4.3. Results

FeS_m*(s)*, CdS*(s)*, or HgS*(s)* was precipitated on addition of an aqueous solution of Na_2S to $(NH_4)_2Fe(II)(SO_4)_2{\cdot}6H_2O$, $Cd(NO_3)_2{\cdot}4H_2O$, and $HgCl_2$, respectively. The crystalline structures of the solids matched that of tetragonal mackinawite for FeS_m*(s)*, hexatetrahedral hawleyite for CdS*(s)*, and cubic metacinnabar for HgS*(s)*, when indexed to known XRD spectra in the literature (Fig.1).[57,58] The FeS_m*(s)* diffractogram shows broader and less intense peaks than seen for the other metal sulfides prepared here. The specific surface areas for FeS_m*(s)*, CdS*(s)*, or HgS*(s)* precipitated with equimolar amounts of metal ion and S^{-II}, were found to be 55.3, 73.9, and 19.29 m^2g^{-1}, respectively (Table 2).

Table 2. **Surface area of FeS_m*(s)*, CdS*(s)* and HgS*(s)*.** Specific surface areas of precipitated crystals determined using BET.

	Specific surface area (m^2 g^{-1})
FeS_m*(s)*[1]	34.9
FeS_m*(s)*[2]	55.3
CdS*(s)*	73.9
HgS*(s)*	19.29

1) *FeS_m(s) batch used for all experiments except data presented in Table 5.*
2) *FeS_m(s) batch used for data presented in Table 5.*

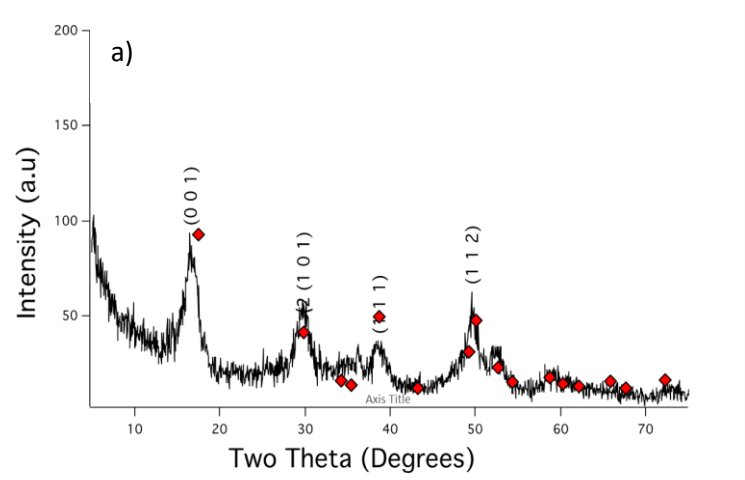

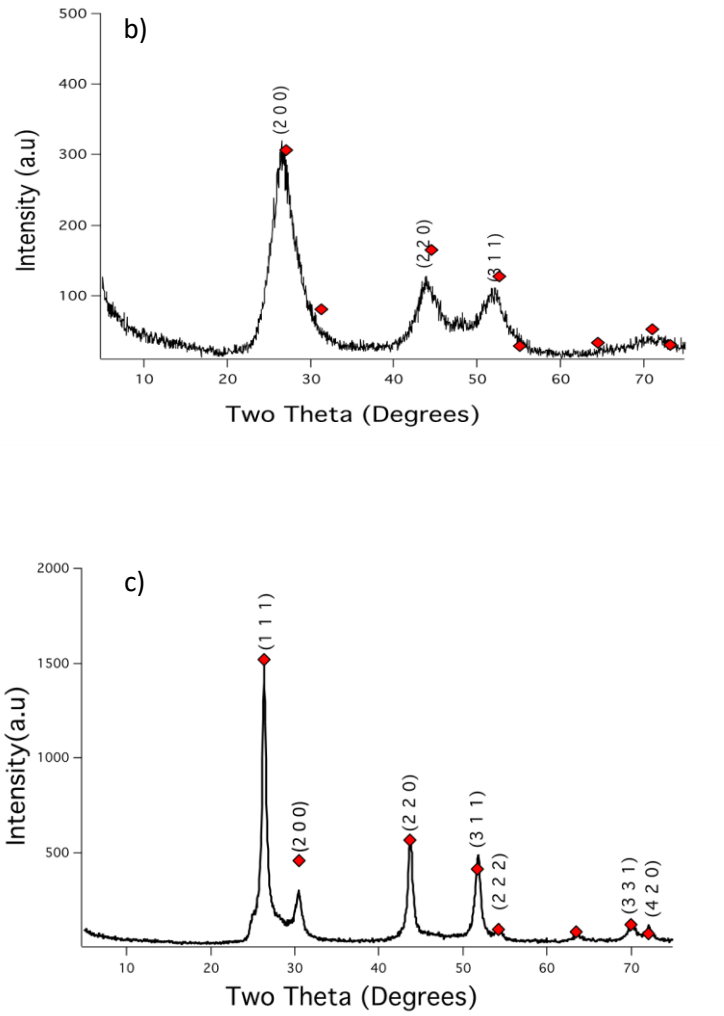

Fig. 1. Characterization of crystal structure. X-ray diffractograms of synthesized a) FeS_m*(s)*, b) CdS*(s)* and c) HgS*(s)* with diffraction patterns (red diamonds) for ordered tetragonal mackinawite, hexatetrahedral Hawleyite and cubic metacinnabar, respectively.[57,58]

The reaction between MeHg and FeS_m*(s)* resulted in the production of DMeHg. The volatile compound was first detected in experiments where 2.3 nmol of MeHg were added to a slurry containing 5.6 µmol FeS_m*(s)* in degassed ultra-pure water. During the first 20 min of reaction, 0.37 ± 0.08 pmol of DMeHg were formed. The formation decreased in the next two 20 min period and became 0.16 ±0.07 pmol at 40-60 min. (Table 3). In similar experiments where the same amount of MeHg was added to degassed

ultra-pure water or to the filtrate of the FeS_m*(s)* slurry (0.02 µm filtered), the DMeHg produced was lower than the detection limit.

Table 3. Production of DMeHg*(g)* from MeHg*(aq)* added to filtered and unfiltered FeS_m*(s)* slurries. Amount of DMeHg *(g)* (pmol) formed from 2.3 nmol of MeHg*(aq)* added to 0.2 µm filtrated and unfiltered FeS_m*(s)* slurries. The unfiltered FeS_m*(s)* slurry contained 5.6 µmol FeS_m*(s)* giving a MeHg:FeS_m*(s)* ratio of 0.41 (nmol $umol^{-1}$).

Sample	Purging interval (min)	DMeHg*(g)* (pmol)
Filtrated slurry	0-20	<0.038
FeS_m*(s)*	0-20	0.37 ± 0.08
	20-40	0.21 ± 0.07
	40-60	0.16 ± 0.07

The adsorption of MeHg on FeS_m*(s)* was studied by adding 0.7, 2.8, and 11 nmol of MeHg to 2.8 µmol of FeS_m*(s)*. The ratios of MeHg: FeS_m*(s)* were chosen based on the results of our initial experiments. It was desired to have the concentration of MeHg as close as possible to environmental concentrations but high enough to produce a quantifiable amount of DMeHg. The adsorption was initially rapid with more than 50% of the MeHg immobilized on the FeS_m*(s)* particles within the first 2 min (Fig. 2). This was followed by a gradual increase in adsorption with up to 90% of the MeHg adsorbed onto the FeS_m*(s)* after 1 h (Fig. 2). An additional adsorption experiment was conducted for 10 min, 60 min and 24 h at a much lower ratio of MeHg to FeS_m*(s)* (0.068 nmol MeHg/µmol FeS_m*(s)*). The adsorption followed a similar pattern as the previous test and after 24 h, 96% of the MeHg was immobilized on the FeS_m*(s)* particles (Fig. 2).

Using results from our adsorption experiments and the surface area of the FeS_m*(s)* particles (Fig. 2 and Table 2), we calculated the fraction of mono coordinated sulfide sites ($\equiv Fe_1S_1^-$) saturated with MeHg at each time point in the adsorption experiment. Though the FeS_m*(s)* surface is predominantly composed of both mono and tri coordinated sulfide sites, the mono coordinated sites have stronger anionic properties and can be expected to dominate the complexation of MeHg.[38] It was thus assumed that the $\equiv Fe_1S_1^-$ sites, existing on the FeS_m*(s)* surface at a concentration of two sites per nm^2, were the main MeHg binding sites

present.[38] When the ratio of MeHg:FeS_m*(s)* was 3.9 nmol MeHg/µmol FeS_m*(s)*, up to 35% of the binding sites were saturated after 1 h of adsorption while only less than 5% were saturated after 1 h when the ratio was 0.25 nmol MeHg/µmol FeS_m*(s)* (Fig. 3).

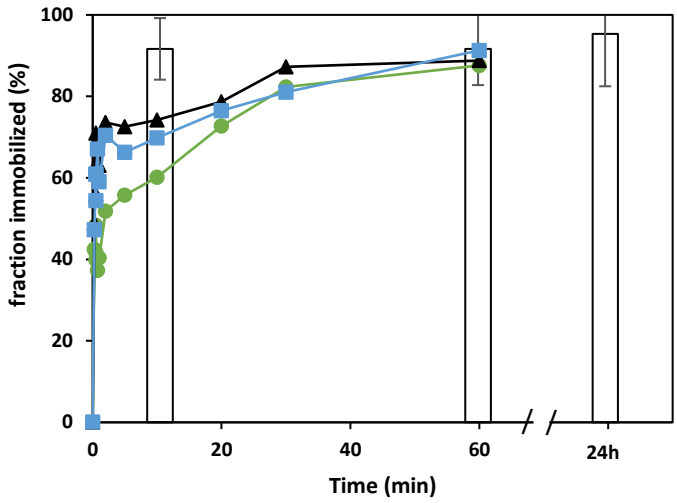

Fig. 2. Adsorption of MeHg*(aq)* on FeS_m*(s)*. Fraction MeHg immobilized by FeS_m*(s)* as a function of time in an experiment using 0.02 µm syringe filters and MeHg:FeS_m ratios (nmol μmol^{-1}) of 3.9 (blue squares), 1.0 (green circles) and 0.25 (black triangles) or using 0.05 µm membrane filters (bar graph) and a MeHg:FeS_m ratio of 0.068 nmol μmol^{-1}.

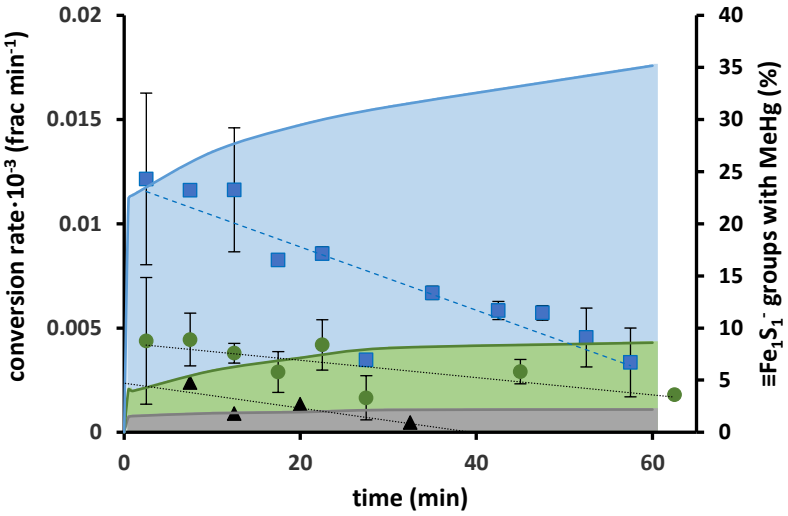

Fig. 3. Conversion rate of MeHg to DMeHg at different MeHg:FeS_m*(s)* ratios. Conversion rate of MeHg (fraction min^{-1}, scatter plot, left hand axis) and percent of $\equiv Fe_1S_1^-$ groups on the FeS_m*(s)* surface with MeHg adsorbed (background area graph, right hand axis) at MeHg:FeS_m*(s)* ratios (nmol µmol^{-1}) of 3.9 (blue squares, upper blue area), 1.0 (green circles, middle green area) and 0.25 (black triangles, lower gray area). Conversion rates at the three MeHg:FeS_m*(s)* ratios tested were significantly different ($p<0.05$, Analysis of Covariance).

The conversion rate (methylation rate) of MeHg to DMeHg was also measured in experiments done in parallel to the adsorption studies and using the same three MeHg:FeS_m*(s)* ratios (0.25, 1, and 3.9 nmol MeHg/µmole of FeS_m*(s)*). Similar to the initial experiment, the conversion rate decreased with time for each ratio, though there was no systematic trend between the ratios and the rate of decrease (Fig. 3). It was also found that the rate increased with an increase in the MeHg:FeS_m ratio (Fig. 3). Additional experiments covering a wider ratio from 0.034 to 3400 nmol MeHg/µmol of FeS_m*(s)* were conducted. Here, the amount of MeHg added was held constant at 9.6 nmol while the amount of FeS_m*(s)* was varied. We found that the fraction of MeHg converted to DMeHg increased with increase in the fraction of the $\equiv Fe_1S_1^-$ sites saturated with MeHg up to where all the $\equiv Fe_1S_1^-$ sites were theoretically saturated. Beyond this theoretical saturation point, the fraction of MeHg converted to DMeHg reduced (Fig. 4).

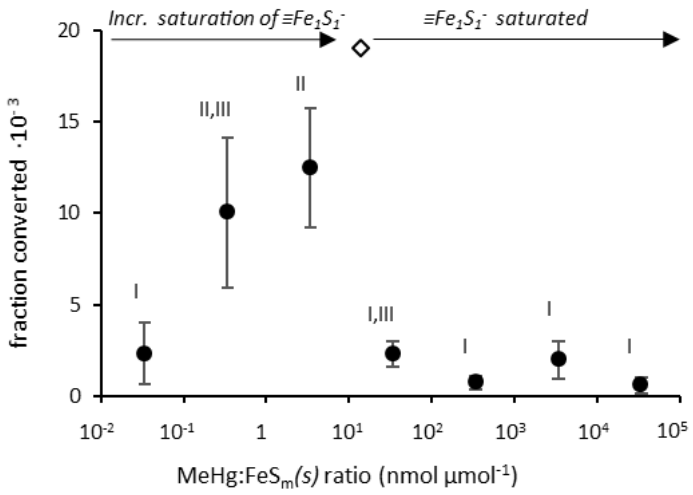

Fig. 4. **Conversion of MeHg to DMeHg at different MeHg:FeS_m*(s)* ratios**. Fraction of MeHg methylated at MeHg:FeS_m*(s)* ratios (nmol µmol^{-1}) of $3.4\cdot10^{-2}$ to $3.4\cdot10^{4}$ and the theoretical saturation point of $\equiv Fe_1S_1^-$ groups on the FeS_m*(s)* surface (diamond). Roman numbers indicate significant differences ($p<0.05$).

Since the crystallinity of iron sulfide solids has been shown to increase over time, the reaction of MeHg with FeS_m*(s)* was examined in experiments using FeS_m*(s)* aged for 1 h, 1 d, and 7 d.[59-61] In our experiments, there was no statistical difference in the fraction of MeHg converted to DMeHg when MeHg was reacted with FeS_m*(s)* aged for the different times (Table 4). Consistent with this, experiments using thermodynamically more stable metal sulfides (HgS*(s)* and CdS*(s)*) yielded a similar fraction of DMeHg as obtained from the reaction of MeHg with FeS_m*(s)* (Table 5). In these latter experiments, the amount of FeS_m*(s)*, HgS*(s)*, and CdS*(s)* used was adjusted according to their specific surface area to give a MeHg to metal sulfide surface ratio of 970 nmol MeHg m^{-2} metal sulfide surface.

Table 4. **Conversion of MeHg to DMeHg on FeS_m*(s)* of different age.** Fraction of MeHg methylated when the reaction was mediated by FeS_m*(s)*, aged for 1hour, 1day or 7 days. The amounts of MeHg and FeS_m*(s)* reacted was 9.6 nmol and 2.8 µmol respectively, giving a final MeHg:FeS_m*(s)* ratio of 3.4 nmol µmol^{-1}. No statistical differences between the reactions with the FeS_m*(s)* of different ages ($p>0.05$) was observed.

	Fraction converted ·10^{-3}
FeS_m*(s)* aged 1h	16 ± 4.6
FeS_m*(s)* aged 1d	17 ± 14
FeS_m*(s)* aged 7d	12 ± 3.3

Table 5. **Conversion of MeHg to DMeHg on FeS_m*(s)*, CdS*(s)* and HgS*(s)*.** Fraction of MeHg methylated on CdS*(s)*, FeS*(s)* and HgS*(s)* at equal MeHg to specific surface area ratios (9.6 nmol MeHg, 970 nmol MeHg m^{-2} mineral surface). No significant differences were found for the methylation on the sulfide minerals tested (ANOVA, $p>0.05$).

	Fraction converted $\cdot 10^{-3}$	**MeHg:(Fe/Cd/Hg)S*(s)* ratio**	
		nmol µmol^{-1}	**nmol surface area $(m^2)^{-1}$**
FeS_m*(s)*	8.3 ± 3.6	4.8	970
CdS*(s)*	2.2 ± 1.3	10	970
HgS*(s)*	4.0 ± 1.9	4.4	970

The effect of pH and ionic strength on the production of DMeHg was also tested. Fig. 5 shows the speciation of the FeS_m*(s)* surface sites modeled by Wolther *et al*.[38] As the figure shows, the $\equiv Fe_1S_1^-$ sites are fully protonated at pH 6; while at pH 8 they are fully deprotonated.[38] We varied the pH of our solutions from 6 to 8 to investigate if the degree of protonation of $\equiv Fe_1S_1^-$ sites affected the reaction between MeHg and FeS_m*(s)*. The fraction of MeHg converted to DMeHg (or pmol of DMeHg produced) was found not to change with pH (Fig. 6). Moreover, the conversion of MeHg to DMeHg was not affected when experiments were performed in a solution of 0.02 or 0.20 M NaCl (Fig. 6).

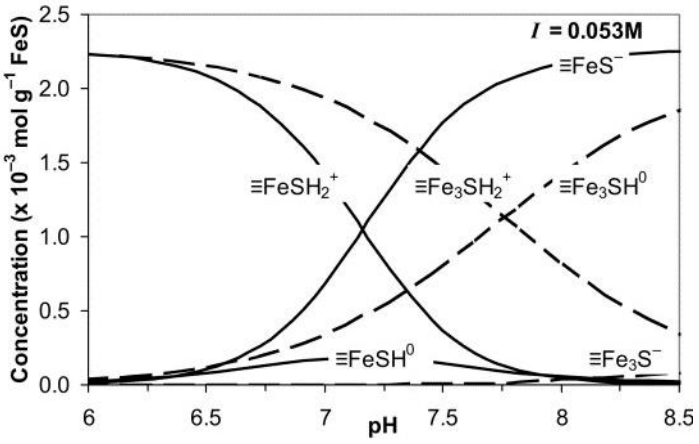

Fig. 5. **Speciation of $\equiv Fe_1S_1^-$ groups on the FeS_m*(s)* surface, modelled by Wolthers *et al*.[61]** Figure reprinted from 'Surface chemistry of disordered mackinawite (FeS)' by Wolthers *et al.*, 2005, *Geochimica Cosmochimica Acta, 69* (14) Pages 3469-3481.Copyright (2005) Elsevier.

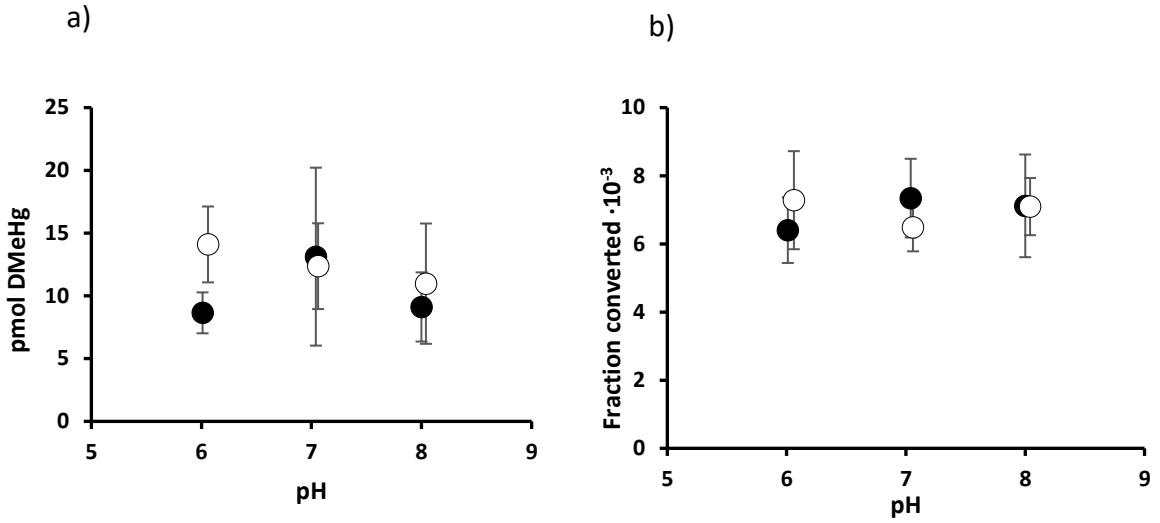

Fig. 6. Conversion of MeHg to DMeHg on FeS_m*(s)* at different pH and ionic strengths. Formation of DMeHg when adsorbing MeHg on FeS_m*(s)* at pH of 6, 7 or 8 and ionic strength of 0.02 (white circles) or 0.20 M (black circles) in a) short term and b) long term experiments. No significant differences (two-way ANOVA, $p>0.05$) were found for the amount of DMeHg formed in a) or b).

The reaction between MeHg and FeS_m*(s)* was compared to that of MeHg and dissolved inorganic sulfide (shown in previous studies).[32,33] As the pK_{a1} of H_2S is equal to 7, the speciation of sulfide at the pH of our experimental solutions (~7) was dominated by H_2S and HS^-. However, we henceforth use S^{-II} to refer to the dissolved inorganic sulfide; bearing in mind that the S^{-II} representation stands for the oxidation state of the sulfide in solution rather than the speciation of sulfide. Experiments were conducted using MeHg:S^{-II} ratios starting from 4.3 to 1900 nmol MeHg/µmol S^{-II}. The fraction of MeHg converted to DMeHg was found to be at least 6 times lower for S^{-II} than for FeS_m*(s)* tested at a ratio of 4.3 nmol/µmol FeS_m*(s)* (Fig. 7).

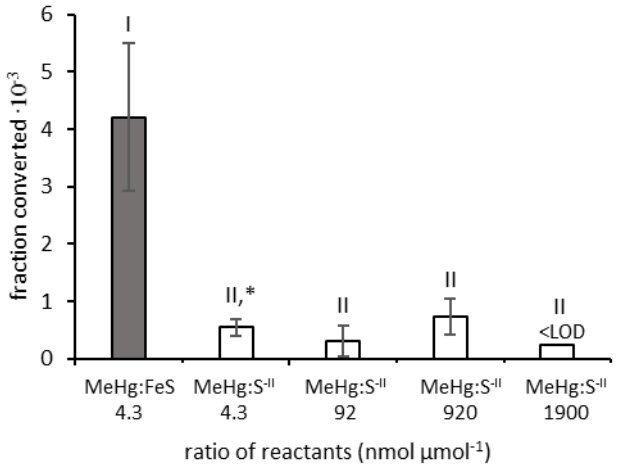

Fig. 7. Conversion of MeHg to DMeHg from reaction of MeHg with S^{-II}*(aq)*. Fraction of MeHg methylated on FeS_m*(s)* (±SD, n=3) at a MeHg:FeS_m*(s)* ratio of 4.3 (nmol µmol^{-1}) or with dissolved sulfide at MeHg:S^{-II} ratios of 4.3 to 1900 (nmol µmol^{-1}). LOD = Limit of detection. Roman numbers indicate significant differences ($p<0.05$). *One outlier removed (n=2).

To better explain the difference in the production of DMeHg between the two forms of sulfide used, we determined the activation energy for the two reactions assuming pseudo first order reaction kinetics and using the Arrhenius equation:

$$\ln k = \ln A_e - E_a/RT \qquad (3)$$

where: k is the rate constant, A_e is the frequency factor, E_a the activation energy, R gas constant, and T is the temperature in kelvin.

Experiments were conducted at 0, 18, 40, and 60ºC. For the reaction between MeHg and FeS_m*(s)*, the production of DMeHg was below detection at 0ºC and the activation energy was calculated from the results obtained at 18, 40, and 60ºC. For the reaction between MeHg and S^{-II}, a higher concentration of MeHg was used to ensure that the amount of DMeHg produced from the reaction was above the detection limit. The production of DMeHg at 0 and 18ºC was similar, hence only the results at 40 and 60 ºC were used to

calculate the activation energy. The activation energy for the reaction with FeS_m*(s)* was found to be 91±4.6 kJ mol^{-1}, while the reaction with S^{-II} had an activation energy of 41±6.8 kJ mol^{-1} (Fig. 8).

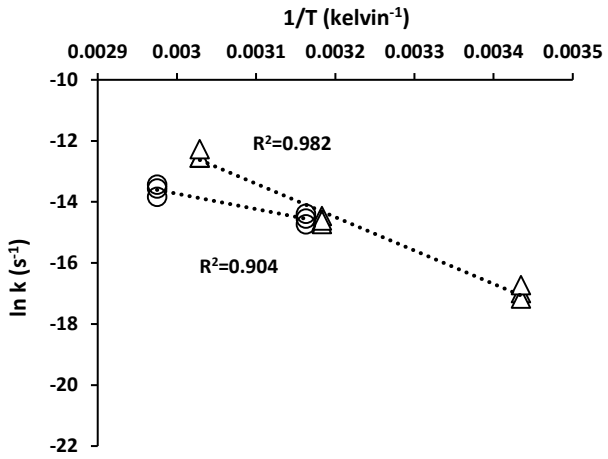

Fig. 8. Conversion of MeHg to DMeHg on FeS_m*(s)* at different temperatures. Effect of temperature (1/T (kelvin^{-1})) on the reaction rate constant (k, s^{-1}) for 7.5 nmol MeHg added to 2.8 µmol FeS_m*(s)* (triangles) and 390 nmol MeHg reacted with 380 nmol S^{-II}*(aq)* (circles). Both regression models were statistically significant (linear regression, ANOVA, $p<0.05$).

To investigate if DMeHg will be produced when MeHg is reacted with reduced sulfur sites on organic compounds (thiols), MeHg was reacted with monothiols and dithiols at a ratio of 1000 nmol MeHg/µmol thiol group. While the reaction of MeHg with the dithiols produced detectable amounts of DMeHg, the production of DMeHg from the reaction of MeHg with the monothiols was below the detection limit. Additionally, the fraction of MeHg converted to DMeHg was almost 20 times more when MeHg was reacted with 1,2-ethanedithiol than when 1,3-propanedithiol was reacted. Compared to the reaction with FeS_m*(s)* when tested at a ratio of 3.4 nmol MeHg/µmol FeS_m*(s)*, the fraction of MeHg converted to DMeHg by the reaction of MeHg with 1,2-ethanedithiol was 100 times less than that converted when MeHg was reacted with FeS_m*(s)* (Fig. 9).

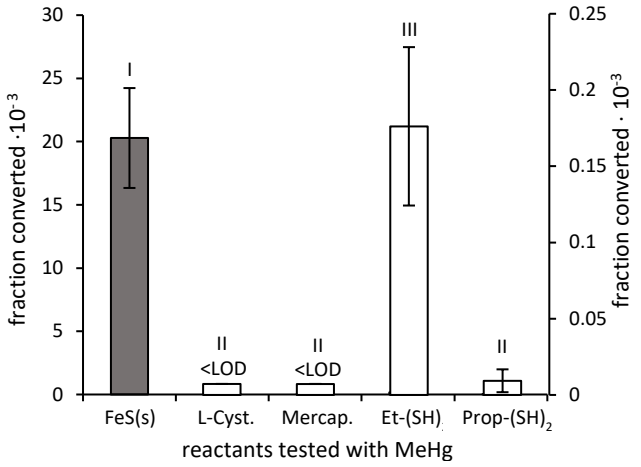

Fig. 9. **Conversion of MeHg to DMeHg from reaction of MeHg with organic thiols**. Fraction of MeHg methylated (±SD, n=3) on FeS_m*(s)* (MeHg:FeS_m*(s)* ratio of 3.4 nmol μmol^{-1}, left hand axis) or with L-Cysteine (L-Cyst.), 3-mercaptopropionic acid (Mercap.), 1,2-ethanedithiol (Et-$(SH)_2$) or 1,3-propanedithiol (Prop-$(SH)_2$) (MeHg:thiol ratio of 1000 and 2000 nmol μmol^{-1} for mono- and dithiols respectively giving a MeHg:R-SH ratio of 1 for both mono and di-thiols, right hand axis). LOD = Limit of detection. Roman numbers indicate significant differences ($p<0.05$).

To investigate the production of DMeHg under conditions more representative of the natural environment, MeHg was reacted with FeS_m*(s)* in artificial seawater with and without the algae *Thalassiosira weissflogii*. The reaction was also studied in presence of different constituents of the algae cells — cell membrane and organelles vs cytoplasm. The fraction of MeHg converted to DMeHg was highest in seawater without any organic material and lowest when intact algae cells were added (Fig. 10). Further, the difference between the amounts of DMeHg produced when no organic material was present and when whole cells were present was in agreement to sum of differences between experiments with seawater vs. seawater with organelles and seawater vs. seawater with cytoplasm.

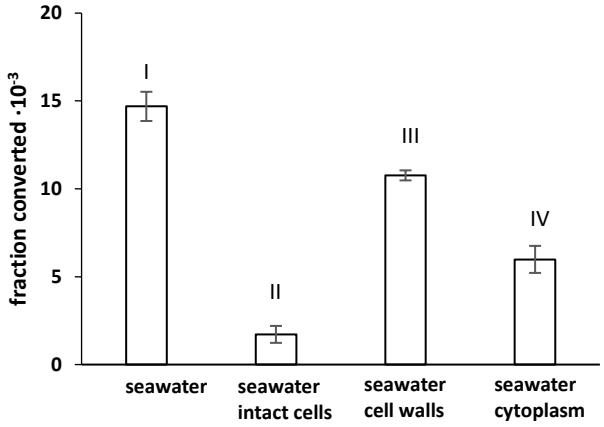

Fig. 10. Conversion of MeHg to DMeHg on FeS_m*(s)* in sea water and in the presence of organic material. Fraction of MeHg methylated when adsorbing MeHg on FeS_m*(s)* in artificial sea water, and in artificial sea water with whole cells, cell walls (pellet obtained at 754 G for 15 min) or the cytoplasm (remaining in solution after centrifugation at 754 G, 15 min) of $1.2 \cdot 10^6$ cells of *Thalassiosira weissflogii*. Roman letters indicate significantly differences ($p<0.05$, ANOVA followed by Tukey's post-hoc test).

4.4. Discussion

4.4.1. Mechanism for DMeHg Formation

The adsorption of MeHg on FeS_m*(s)* using three different ratios of MeHg to FeS_m*(s)* resulted in about 90 % of the MeHg adsorbed on the FeS_m*(s)* particles for all three experiments after 1 h of reaction (Fig. 2). Additionally, all three ratios produced detectable amounts of DMeHg. As MeHg was the only methyl containing group in our solutions, the reaction to produce DMeHg must have involved two MeHg ions. We suggest that the reaction must have involved two adsorbed MeHg ions rather than one MeHg ion adsorbed and the other one in solution. If the reaction had involved one MeHg ion adsorbed and one in solution, the fraction of MeHg converted to DMeHg would be constant for all three MeHg:FeS_m*(s)* ratios used as the fraction of MeHg immobilized on FeS_m*(s)* was constant among the ratios. This was however not the case. Our results show that the fraction of MeHg converted (methylated) to DMeHg (and conversion rate) increased with increase in MeHg:FeS_m*(s)* ratio and with the fraction of $\equiv Fe_1S_1^-$ sites saturated (Fig. 3); suggesting that the reaction involves two adsorbed MeHg groups and that the fraction of MeHg converted

to DMeHg depends on the fraction of binding sites saturated with MeHg. Additional experiments where the concentration of MeHg was held constant and the concentration of FeS_m*(s)* was varied, show that the fraction of MeHg converted to DMeHg increased with increased saturation of $\equiv Fe_1S_1^-$ sites, up to the point where all the sites were theoretical saturated at about 10 nmol MeHg/µmol FeS_m*(s)* (Fig. 4). At MeHg:FeS_m*(s)* ratios of 10 nmol MeHg/µmol FeS_m*(s)* and below, the number of $\equiv Fe_1S_1^-$ sites was greater than the amount of MeHg added to the experiment (9.6 nmol), thus the amount (and fraction) of MeHg adsorbed on the $\equiv Fe_1S_1^-$ sites was equal in these experiments. The increase in the fraction of MeHg converted to DMeHg with increased saturation of $\equiv Fe_1S_1^-$ sites seen in the first half of Fig. 4, therefore confirms the involvement of two adsorbed MeHg groups in the reaction mechanism and suggests that the proximity of the adsorbed groups is important for the reaction. At ratios greater than 10 nmol MeHg/µmol FeS_m, the $\equiv Fe_1S_1^-$ sites available were less than 9.6 nmol, i.e. less than the amount of MeHg added to the solutions. The decrease in the fraction of MeHg converted to DMeHg at MeHg:FeS_m*(s)* ratios greater than 10 nmol MeHg/µmol FeS_m (Fig. 4), was thus likely due to the decrease in the fraction of MeHg adsorbed on the $\equiv Fe_1S_1^-$ sites as the number of $\equiv Fe_1S_1^-$ sites present were now less than the amount of MeHg added to the solutions.

From the results of the above experiments, we suggest that an S_N2-type of reaction is occurring on the FeS_m*(s)* mineral surface. The reaction begins when a $\equiv Fe_1S_1^-$ site acts as a nucleophile and forms a bond with the Hg atom of a MeHg ion adsorbed on a neighboring $\equiv Fe_1S_1^-$ site. A nucleophilic substitution follows where the nucleophilic $\equiv Fe_1S_1^-$ site replaces the methyl group on the Hg atom. The methyl leaving group then combines with the MeHg ion adsorbed initially on the nucleophilic $\equiv Fe_1S_1^-$ site and forms DMeHg (Fig. 11).

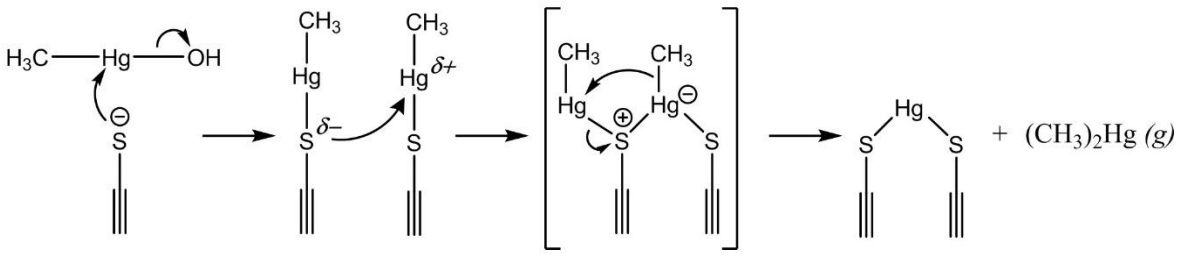

Fig. 11. Proposed reaction mechanism. The proposed S_N2-type reaction mechanism for the formation of $(CH_3)_2Hg$ (DMeHg) from CH_3Hg (MeHg) mediated by inorganic or organic surfaces with neighboring reduced sulfur groups.

The reaction is bound to proceed faster when the adsorbed groups are closer together; hence the increase in conversion of MeHg to DMeHg with increase in saturation of $\equiv Fe_1S_1^-$ sites. As for the Hg atom remaining on the surface of $FeS_m(s)$, previous studies investigating the sorption mechanism of Hg^{II} by $FeS_m(s)$ show that β-HgS*(s)* is the dominant product formed when Hg^{II} reacts with $FeS_m(s)$, though mixed Hg chlorosulfide-like surface precipitates also form at lower Hg concentrations.[62] We suggest that the Hg atom that remains on the surface bound to sulfur forms β-HgS*(s)* or mixed surface precipitates of Hg.[45,62] In our experiments, we did not investigate the nature of the solid products of our reaction. The ratio of Hg:$FeS_m(s)$ used here is much lower than used in previous studies and only about 0.1% of the MeHg is converted to DMeHg in 24 h. Nonetheless, the overall reaction between MeHg and $FeS_m(s)$ to form DMeHg and β-HgS*(s)* (Eqn. 4) is thermodynamically feasible at the concentrations defined in our experiments and assuming the dissolved Fe^{II} concentration is set by the solubility product of $FeS_m(s)$ at pH 7. At standard temperature and pressure, a highly favorable reaction with a log K and ΔG value of 31.5 and -107 kJ mol^{-1} respectively, were calculated using the stability constants given by Stumm and Morgan.[63]

$$2\ CH_3HgOH + 2H^+ + FeS_m(s) \rightarrow HgS(s) + (CH_3)_2Hg + Fe^{2+} + 2H_2O \qquad (4)$$

4.4.2. Reactions of MeHg with Metal Sulfide Solids

The first iron sulfide phase to precipitate in nature from an aqueous solution of Fe^{II} and S^{-II} is mackinawite.[38,59] This mineral phase of iron sulfide also precipitated in our experiments when Fe^{II} was reacted with S^{-II} (Fig. 1). With time and under excess sulfide concentrations or mildly reducing conditions, mackinawite is transformed to the more stable and crystalline phase of pyrite (FeS_2) via the intermediate greigite (Fe_3S_4).[38,64] As this is a solid state transformation, mixed phases containing mackinawite, greigite and pyrite are encountered in the environment.[64] In anoxic non-sulfidic sediments, mackinawite can exist for a relatively long time; and though the mineral is not transformed to other iron sulfide phases under these conditions, its crystallinity increases over time.[60,61,65] Where iron sulfide precipitates form, there is also the potential for other metal sulfides (HgS, PbS, CdS, and ZnS) to form.[37] For other metals such as Co^{2+}, Cu^{2+}, Ni^{2+} and Cr^{+2}, co-precipitation with the iron sulfide solids is more likely to happen than the formation of a pure metal sulfide phase.[37,66] Whether a metal ion co-precipitates or not depends on the kinetics and thermodynamics of the reaction between the metal ions and S^{-II}. For metal sulfides of lower thermodynamic stability or slower reaction kinetics, relative to those of $FeS_m(s)$, the metal ion is likely to co-precipitate with $FeS_m(s)$ rather than form its own metal sulfide solid.[37,66] In natural settings therefore, various forms and compositions of metal sulfides exist. To study how the variability of the metal sulfide pool found in nature can impact the formation of DMeHg, we examined DMeHg formation using two metal sulfide species ($HgS(s)$ and $CdS(s)$) thermodynamically more stable than $FeS_m(s)$, and using $FeS_m(s)$ aged for 1h, 1d and 7d. Our results show that neither the aging of $FeS_m(s)$ nor the stability of the metal sulfides changes the production of DMeHg (Table 4 and 5). The thermodynamic stability and crystallinity of the sulfide mineral thus do not seem to affect the production of DMeHg; further supporting the proposed surface mediated reaction mechanism.

4.4.3. Reactions of MeHg with Dissolved Reduced Sulfur

The formation of DMeHg from the abiotic degradation of MeHg was first reported by Craig and Bartlett.[32] In their study, H_2S was purged through aqueous solutions and sediments spiked with MeHg at a concentration of 5-3000 µM and 0.5µg/g, respectively.[32] At high concentrations of MeHg, the researchers observed a white precipitate identified as bismethylmercurysulfide ($(CH_3Hg)_2S$), which with time, degraded to a black solid. The final products of the reaction were identified as DMeHg and $HgS(s)$.[32] More recent studies have reported the abiotic degradation of MeHg with selenocysteine via the formation of the intermediate $(CH_3Hg)_2Se$ and final products DMeHg and HgSe nanoparticles.[35] Density Functional Theory calculations support the reaction of MeHg with thiol amino acids or their selenium analogues to produce DMeHg and $HgS(s)$ or HgSe via the intermediate $(CH_3Hg)_2S(s)$ or $(CH_3Hg)_2Se(s)$, respectively.[34] The reaction is proposed to proceed through either of two mechanisms (Fig. 12) with comparable thermodynamic favorability. The first one involves the reaction of two MeHg-thiol (selenol) complexes with a third molecule of thiol (seleno) amino acid; and the second one involves one MeHg-thiol (selenol) complex and one MeHgOH complex. The former reaction is in line with experimental observations.[35]

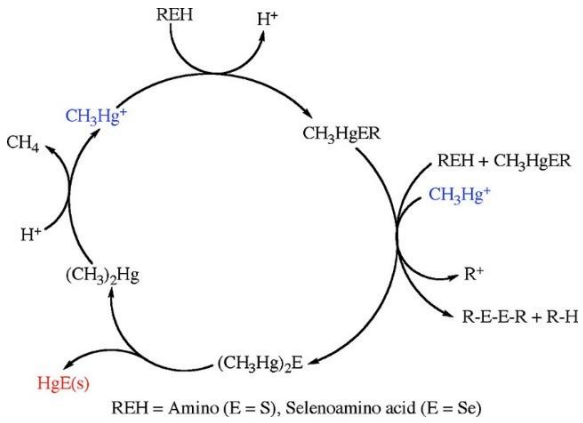

Fig. 12. Proposed mechanism for the formation of DMeHg from the reaction of MeHg with amino and selenoaminoacids. Figure reprinted from 'Degradation Mechanism of Methyl Mercury Selenoamino Acid Complexes: A computational Study' with permission from Asaduzzaman and Schreckenbach, *Inorg. Chem.* **2011,** 50, 2366-2372. Copyright (2011) American Chemical Society.

In our experiments where MeHg was reacted with S^{-II} and thiols, we did not detect the intermediate, $(CH_3Hg)_2S$, possibly because of the lower concentrations of MeHg used in our experiments. However, the fraction of MeHg converted to DMeHg when S^{-II} or thiols was used was at least 6 times less than when FeS_m*(s)* was used, respectively (Fig. 7 and Fig. 9). Additionally, the reaction of MeHg with dithiols produced detectable amounts of DMeHg while the monothiols did not; and 20 times more DMeHg was detected when MeHg was reacted with 1,2-ethanedithiol than when reacted with 1,3-propanedithiol (Fig. 9). These results suggest that more DMeHg is produced where the adsorbed MeHg groups are closer together, and thus support a reaction mechanism involving the transfer of MeHg groups attached on neighboring sulfide sites. The higher activation energy calculated for the reaction between MeHg and FeS_m*(s)* (91 kJ mol^{-1}) relative to the reaction with S^{-II} (41 kJ mol^{-1}) suggests that the latter reaction is not hindered by a high A*e*.

The reaction between MeHg and S^{-II} may be hindered by the formation of soluble Hg-sulfide complexes. In the S^{-II} system, 4.9 pmol of organic mercury (DMeHg) were produced, meaning the same amount of inorganic mercury were also produced from the reaction of 12 nmol of MeHg with 2.8 µmol of S^{-II}. Our speciation modeling results suggest that 71 % of the inorganic mercury produced from the reaction will exists as HgS_2H^- *(aq)* at pH 7; and under these conditions, the solubility product of HgS*(s)* is not exceeded. In the FeS_m*(s)* system on the other hand, if we assume the dissolved sulfide concentration is set by the Ksp of FeS_m*(s)*, the mere production of 4.9 pmol of inorganic mercury will cause the precipitation of HgS*(s)*. The removal of the inorganic mercury product from solution via the precipitation of HgS*(s)* will favor the forward reaction and promote the formation of more DMeHg as shown in equation 4 above. Just like Hg-Sulfide aqueous complexes, Hg-thiol complexes can form in presence of thiols and these also inhibit the precipitation of HgS*(s)*.[67] Indeed, in earlier experiments, cysteine inhibited the precipitation of HgS*(s)* from the reaction of MeHg with S^{-II}. While solutions containing 150 µM MeHg and 150 µM S^{-II} precipitated HgS*(s)* particles after 7 days, particles were only noticed after 1 month in solutions containing 150 µM MeHg, 150 µM S^{-II} and 150 µM cysteine. It seems like a plausible explanation that if S^{-II} and thiols inhibit the precipitation of HgS*(s)*, the reaction will be hindered from moving forward and less DMeHg

will be produced. However, the thermodynamic favorability of the reaction between MeHg and S^{-II} (Eqn. 5) to form soluble Hg-sulfide species and DMeHg, is similar to the reaction between MeHg and FeS_m*(s)* forming HgS*(s)*and DMeHg. The reaction in equation 5 under the experimental conditions yields a log K and ΔG value of 28.8 and ~-112 kJ/mole respectively, slightly more than for the reaction between MeHg and FeS_m*(s)* in equation 4 above.

$$2\ CH_3HgOH + H^+ + 2HS^- \rightarrow HgS_2H^- + (CH_3)_2Hg + 2H_2O \qquad (5)$$

For the reaction between MeHg and the thiols, assuming the reaction follows a similar mechanism as that of MeHg and S^{-II}, one of the products will be Hg-thiol complexes as shown in equation 6 below. At the concentrations used in our experiments and using Hg-thiol stability constants determined by Skyllberg,[68] the log K and ΔG value for reaction 6 is 38.3 and ~ -130 kJ/mole respectively. Our value of ΔG^o (~ -200 kJ/mole) for the reaction between MeHg and thiols is lower than that reported by Asaduzzaman (-276 kJ/mole) using density functional calculations.[34] Thus, the reaction of MeHg with the thiols is more feasible than that with either FeS_m*(s)* or S^{-II}.

$$2\ CH_3HgOH + 2H^+ + 2RS^- \rightarrow Hg(SR)_2 + (CH_3)_2Hg + 2H_2O \qquad (6)$$

We propose that while the reaction between MeHg and S^{-II} or thiols is thermodynamically more favorable, these reactions are instead inhibited by a lower probability of occurrence for the nucleophilic attack initiated by the sulfide site on the MeHg ion adsorbed on a neighboring sulfide site (as demonstrated in Fig. 11). For these reactions, once MeHg and S^{-II} or MeHg and thiol complexes form, at least two of these must collide for the reaction to happen. The adsorbed MeHg groups are further apart when in solution and the reaction is hindered by the diffusion of the complexes. In the case of 1,2-ethanedithiol, even though the adsorbed MeHg groups are on sulfide sites situated on adjacent carbon atoms, the reaction of MeHg with 1,2-ethanedithiol produced 100 times less DMeHg than the reaction between MeHg and FeS_m*(s)*. The

higher productivity of the latter reaction is likely because of a higher density of electrons on the FeS_m*(s)* surface than on the organic dithiol molecule. The presence of coordinatively unsaturated sulfur atoms on the surface of the FeS_m*(s)* can also be expected to increase the reactivity of the sulfide sites on the FeS_m*(s)* relative to the sites on the dithiol molecule. This also means that the production of DMeHg would occur even faster when MeHg is adsorbed on metal sulfide NPs.

4.4.4. DMeHg Formation in Seawater and in Presence of Thalassiosira Weissflogii

The reaction between MeHg and FeS_m*(s)* was examined under environmental conditions with the reaction medium consisting of artificial seawater and the algae *Thalassiosira weissflogii*. When FeS_m*(s)* and MeHg were added to solutions containing intact algae cells, cell organelles only or the cytoplasm only, the production of DMeHg was less than when FeS_m*(s)* and MeHg were added to seawater without any organic matter addition (Fig. 10). The change in the production of DMeHg when the intact cells were added to seawater compared to when no organic material was added, was comparable to the sum of change in DMeHg production witnessed when the organelles only and the cytoplasm only were added (Fig. 10). This suggests that the reduced production of DMeHg when the intact cells were added was due to the complexation of MeHg to ligands, likely thiol ligands, present in the cytoplasm and in the cell organelles. As we did not see a difference in the reaction of MeHg with FeS_m*(s)* at a pH of 6, 7 or 8, and in solutions of 0.02 M or 0.20M NaCl (Fig. 6), the reactions should not have been affected by the higher pH or ionic strength of the seawater. Our results showing reduced DMeHg production when MeHg and FeS_m*(s)* are reacted in presence of organic matter, likely caused by the binding of MeHg to thiol sites (Fig. 10), agree with the reduced production of DMeHg when MeHg was reacted with thiols compared to when reacted with FeS_m*(s)* (Fig. 9). The experiments in seawater and in the presence of algae cells were conducted in order to determine the potential for abiotic degradation of MeHg by the intracellular reaction of MeHg with iron-sulfur clusters present in some proteins (e.g. ferredoxins). These iron- sulfur clusters mediate many redox reactions in biochemical processes and are found in many organisms including photosynthetic

organisms.[59] The known structures of the clusters consist of $Fe_2S_2(SR)_2$, $Fe_3S_4(SR)_3$, and $Fe_4S_4(SR)_4$, with Fe_2S_2 reported as having a core similar to that of mackinawite.[59] Though here we do not show the degradation of MeHg by iron-sulfur clusters, we show the potential for the reaction to happen intracellularly in photosynthetic marine organisms.

4.5. Conclusions and Environmental Implications

This work is the first demonstration on the production of DMeHg from the degradation of MeHg on metal sulfide surfaces (FeS*(s)*, CdS*(s)* and HgS*(s)*) as well as from the reaction of MeHg with dithiols. In comparison to the production of DMeHg from the reaction of MeHg with S^{-II} or with monothiols (previously shown), the reaction with solid metal sulfides is at least 6 times faster.[32,35] Additionally, although the reaction of MeHg with FeS*(s)* is inhibited in presence of organic matter, it is not prevented from occurring. As far as the degradation of MeHg is concerned, our mechanism may not seem to be an important pathway for the demethylation of MeHg in sediments. Typical demethylation rates measured in estuarine sediments range from 0.4–9.6 d^{-1}, much higher than the 0.02 d^{-1} measured in our experiments (as twice the conversion rate of MeHg to DMeHg in Fig. 3).[40] However, here we only measured the production of DMeHg from the degradation of MeHg on reduced sulfur sites. Also, the amount of DMeHg determined might be an underestimation of the actual amount produced in our experiments as some might have degraded to methane and MeHg (Eqn. 7) as suggested in previous studies examining the degradation of MeHg by dissolved sulfur species.[32,33,35]

$$(CH_3)_2Hg + H_2O \rightarrow CH_3HgOH + CH_4\,(g) \qquad (7)$$

The degradation of DMeHg by H^+ is also suggested by the mechanism outlined in Fig. 12.

A major implication of our work is the identification of a possible source of DMeHg in the ocean. DMeHg has been detected in various compartments of the ocean including in the sediment, in the water column and near hydrothermal vent systems.[3,5,42,69-71] Its presence in the water column has been correlated

to regions of high primary production and organic matter degradation.[3,5,7,46,47,72,73] In some locations, the dissolved concentration of DMeHg is comparable to that of MeHg. As it is a volatile compound, it can be evaded out of the ocean and into the atmosphere where it then undergoes photo-degradation to MeHg and gets re-deposited to another location. DMeHg evaded to the atmosphere during upwelling events has been suggested to be a source of MeHg deposition to coastal areas in Monterey Bay, California.[74] Another example is the high concentrations of methylated Hg (MeHg +DMeHg) detected in the pristine Arctic ocean, where it has been suggested that DMeHg evaded from the open ocean gets photo-degraded and redeposited to the region as MeHg.[56] As DMeHg is more hydrophobic (log K_{ow} = 2.6) than neutral MeHg complexes (e.g. CH_3HgCl, log K_{ow} = 0.23) and it also degrades to MeHg relatively fast via various mechanisms, it is suggested to be both a direct source and an indirect source of methylated Hg to marine organisms.[6,70] Additionally, in the ocean water column, degradation of DMeHg is an important source of MeHg.[68] The sources of DMeHg in the ocean, however, remain largely unknown.

In our experiments, we show the production of DMeHg from the reactions of MeHg with various reduced sulfur species. This pathway of DMeHg formation is not only relevant to sulfidic environments in marine sediments, but it also applies to surface and deep waters where DMeHg has been detected. A major source of sulfur to the ocean is reduced sulfur emanating from hydrothermal vents.[75] On contact with seawater rich in dissolved metal ions and organic matter, the sulfide precipitates as metal sulfide nanoparticles.[76-78] Indeed, nanoparticles of $ZnS_{(s)}$, $CdS_{(s)}$, $FeS_{2(s)}$ and $FeS_{m(s)}$ have been detected around hydrothermal systems, and as discussed in Chapter 2 and suggested by others, these can be transported far from their source without undergoing oxidation or aggregation.[53,76-79] It has also been shown that reducing conditions exists within aggregates forming from the coagulation of particles settling from the water column. Ortiz *et al*., for example, demonstrated that the methylation of Hg^{II} to MeHg, likely from the degradation of organic matter by sulfate reducing bacteria (SRB), occurs in these anoxic microenvironments.[8] The production of H_2S from dissimulative sulfate reduction by SRB could cause the precipitation of metal sulfide particles within these regions. Thus, the presence of both MeHg and reduced sulfur in these aggregates makes them suitable zones for the formation of DMeHg via the mechanism

demonstrated here. MeHg and DMeHg are also commonly found in regions of high primary production, suggesting environments rich in low molecular weight thiols.[3,5,47] The production of DMeHg from the reaction of MeHg with thiols or intracellularly from the reaction of MeHg with iron-sulfur clusters present in certain proteins is also possible here. Last but not least, the precipitation of Cd, Zn and Cu by sulfide produced in oxygen deficient zones of ocean waters has been documented.[80] It is important to note that higher concentrations of methylated Hg are found in these waters and that the concentrations of methylated mercury has been correlated to apparent oxygen utilization, or other proxies of organic matter degradation, such as nutrient concentrations, within the ocean's water column.[6,7,72,73,81]

While higher concentrations of MeHg were used in our experiments than found in the water column of the ocean, the ratio of MeHg:FeS*(s)* used here (nmol MeHg per µmol FeS*(s)*) is similar to the ratio of MeHg:sulfide particles in the environment or to the ratio of MeHg:Fe found inside the cells of phytoplanktons.[10,82,83] Thus, the production of DMeHg via our proposed mechanism is possible from the reaction of MeHg with metal sulfides or thiols in surface, intermediate or deep waters as well as within phytoplankton cells with iron-sulfur clusters.

References

1. Mergler, D.; Anderson, H.A.; Chan, L.H.M.; Mahaffey, K.R.; Murray, M.; Sakamoto, M.; Stern, A.H. Methylmercury exposure and health effects in humans: A worldwide concern. *Ambio* **2007,** *36* (1), 3-11; 10.1579/0044-7447(2007)36[3:MEAHEI]2.0.CO;2.

2. Aschner, M.; Aschner, J.L. Mercury neurotoxicity: Mechanisms of blood-brain barrier transport. *Neurosci. Biobehav. Rev.* **1990,** *14* (2), 169-176; 10.1016/S0149-7634(05)80217-9.

3. Mason, R.P.; Fitzgerald, W.F. Alkylmercury species in the equatorial Pacific. *Nature* **1990,** *347* (6292), 457-459.

4. Sunderland, E.M.; Krabbenhoft, D.P.; Moreau, J.W.; Strode, S.A.; Landing, W.M. Mercury sources, distribution, and bioavailability in the North Pacific Ocean: Insights from data and models. *Global Biogeochem. Cycles* **2009,** *23* (2).

5. Heimbürger, L.-.; Cossa, D.; Marty, J.-.; Migon, C.; Averty, B.; Dufour, A.; Ras, J. Methyl mercury distributions in relation to the presence of nano- and picophytoplankton in an oceanic water column (Ligurian Sea, North-western Mediterranean). *Geochim. Cosmochim. Acta* **2010,** *74* (19), 5549-5559; 10.1016/j.gca.2010.06.036.

6. Lehnherr, I.; St. Louis, V.L.; Hintelmann, H.; Kirk, J.L. Methylation of inorganic mercury in polar marine waters. *Nat. Geosci.* **2011,** *4* (5), 298-302; 10.1038/ngeo1134.

7. Cossa, D.; Heimbürger, L.-.; Lannuzel, D.; Rintoul, S.R.; Butler, E.C.V.; Bowie, A.R.; Averty, B.; Watson, R.J.; Remenyi, T. Mercury in the Southern Ocean. *Geochim. Cosmochim. Acta* **2011,** *75* (14), 4037-4052; 10.1016/j.gca.2011.05.001.

8. Ortiz, V.L.; Mason, R.P.; Evan Ward, J. An examination of the factors influencing mercury and methylmercury particulate distributions, methylation and demethylation rates in laboratory-generated marine snow. *Mar. Chem.* **2015,** *177*, 753-762; 10.1016/j.marchem.2015.07.006.

9. Karlsson, T.; Skyllberg, U. Bonding of ppb Levels of Methyl Mercury to Reduced Sulfur Groups in Soil Organic Matter. *Environ. Sci. Technol.* **2003,** *37* (21), 4912-4918; 10.1021/es034302n.

10. Mason, R.P.; Reinfelder, J.R.; Morel, F.M.M. Uptake, toxicity, and trophic transfer of mercury in a coastal diatom. *Environ. Sci. Technol.* **1996,** *30* (6), 1835-1845; 10.1021/es950373d.

11. Moye, H.A.; Miles, C.J.; Phlips, E.J.; Sargent, B.; Merritt, K.K. Kinetics and uptake mechanisms for monomethylmercury between freshwater algae and water. *Environ. Sci. Technol.* **2002,** *36* (16), 3550-3555; 10.1021/es011421z.

12. Campbell, L.M.; Norstrom, R.J.; Hobson, K.A.; Muir, D.C.G.; Backus, S.; Fisk, A.T. Mercury and other trace elements in a pelagic Arctic marine food web (Northwater Polynya, Baffin Bay). *Sci. Total Environ.* **2005,** *351-352*, 247-263; 10.1016/j.scitotenv.2005.02.043.

13. Gilmour, C.C.; Henry, E.A.; Mitchell, R. Sulfate stimulation of mercury methylation in freshwater sediments. *Environmental Science and Technology* **1992,** *26* (11), 2281-2287.

14. Gilmour, C.C.; Elias, D.A.; Kucken, A.M.; Brown, S.D.; Palumbo, A.V.; Schadt, C.W.; Wall, J.D. Sulfate-reducing bacterium Desulfovibrio desulfuricans ND132 as a model for understanding bacterial mercury methylation. *Appl. Environ. Microbiol.* **2011,** *77* (12), 3938-3951; 10.1128/AEM.02993-10.

15. Yu, R.-; Adatto, I.; Montesdeoca, M.R.; Driscoll, C.T.; Hines, M.E.; Barkay, T. Mercury methylation in Sphagnum moss mats and its association with sulfate-reducing bacteria in an acidic Adirondack forest lake wetland. *FEMS Microbiol. Ecol.* **2010,** *74* (3), 655-668; 10.1111/j.1574-6941.2010.00978.x.

16. Yu, R.-; Flanders, J.R.; MacK, E.E.; Turner, R.; Mirza, M.B.; Barkay, T. Contribution of coexisting sulfate and iron reducing bacteria to methylmercury production in freshwater river sediments. *Environ. Sci. Technol.* **2012,** *46* (5), 2684-2691; 10.1021/es2033718.

17. Jonsson, S.; Skyllberg, U.; Nilsson, M.B.; Westlund, P.-; Shchukarev, A.; Lundberg, E.; Björn, E. Mercury methylation rates for geochemically relevant HgII species in sediments. *Environmental Science and Technology* **2012,** *46* (21), 11653-11659.

18. Mazrui, N.M.; Jonsson, S.; Thota, S.; Zhao, J.; Mason, R.P. Enhanced availability of mercury bound to dissolved organic matter for methylation in marine sediments. *Geochim. Cosmochim. Acta* **2016,** *194*, 153-162; 10.1016/j.gca.2016.08.019.

19. Compeau, G.C.; Bartha, R. Sulfate-reducing bacteria: Principal methylators of mercury in anoxic estuarine sediment. *Appl. Environ. Microbiol.* **1985,** *50* (2), 498-502.

20. Marvin-Dipasquale, M.C.; Oremland, R.S. Bacterial methylmercury degradation in Florida everglades peat sediment. *Environ. Sci. Technol.* **1998,** *32* (17), 2556-2563; 10.1021/es971099l.

21. Spangler, W.J.; Spigarelli, J.L.; Rose, J.M.; Flippin, R.S.; Miller, H.H. Degradation of methylmercury by bacteria isolated from environmental samples. *Appl. Microbiol.* **1973,** *25* (4), 488-493.

22. Radosevich, M.; Klein, D.A. Bacterial enumeration and mercury volatilization in deep subsurface sediment samples. *Bull. Environ. Contam. Toxicol.* **1993,** *51* (2), 226-233; 10.1007/BF00198885.

23. Weber, J.H.; Evans, R.; Jones, S.H.; Hines, M.E. Conversion of mercury(II) into mercury(0), monomethylmercury cation, and dimethylmercury in saltmarsh sediment slurries. *Chemosphere* **1998,** *36* (7), 1669-1687; 10.1016/S0045-6535(97)10042-X.

24. Oremland, R.S.; Culbertson, C.W.; Winfrey, M.R. Methylmercury decomposition in sediments and bacterial cultures: Involvement of methanogens and sulfate reducers in oxidative demethylation. *Appl. Environ. Microbiol.* **1991,** *57* (1), 130-137.

25. Oremland, R.S.; Miller, L.G.; Dowdle, P.; Connell, T.; Barkay, T. Methylmercury oxidative degradation potentials in contaminated and pristine sediments of the Carson River, Nevada. *Appl. Environ. Microbiol.* **1995,** *61* (7), 2745-2753.

26. Barkay, T.; Miller, S.M.; Summers, A.O. Bacterial mercury resistance from atoms to ecosystems. *FEMS Microbiol. Rev.* **2003,** *27* (2-3), 355-384; 10.1016/S0168-6445(03)00046-9.

27. Barkay, T.; Turner, R.R.; VandenBrook, A.; Liebert, C. The relationships of Hg(II) volatilization from a freshwater pond to the abundance of mer genes in the gene pool of the indigenous microbial community. *Microb. Ecol.* **1991,** *21* (1), 151-161; 10.1007/BF02539150.

28. Drott, A.; Lambertsson, L.; Björn, E.; Skyllberg, U. Potential demethylation rate determinations in relation to concentrations of MeHg, Hg and pore water speciation of MeHg in contaminated sediments. *Mar. Chem.* **2008,** *112* (1-2), 93-101; 10.1016/j.marchem.2008.07.002.

29. Hammerschmidt, C.R.; Fitzgerald, W.F. Methylmercury cycling in sediments on the continental shelf of southern New England. *Geochim. Cosmochim. Acta* **2006,** *70* (4), 918-930; http://dx.doi.org/10.1016/j.gca.2005.10.020.

30. Zhang, T.; Hsu-Kim, H. Photolytic degradation of methylmercury enhanced by binding to natural organic ligands. *Nat. Geosci.* **2010,** *3* (7), 473-476; 10.1038/ngeo892.

31. Jeremiason, J.D.; Portner, J.C.; Aiken, G.R.; Hiranaka, A.J.; Dvorak, M.T.; Tran, K.T.; Latch, D.E. Photoreduction of Hg(II) and photodemethylation of methylmercury: The key role of thiol sites on dissolved organic matter. *Environ. Sci. Process. Impacts* **2015,** *17* (11), 1892-1903; 10.1039/c5em00305a.

32. Craig, P.J.; Bartlett, P.D. The role of hydrogen sulphide in environmental transport of mercury. *Nature* **1978,** *275* (5681), 635-637.

33. Baldi, F.; Parati, F.; Filippelli, M. Dimethylmercury and dimethylmercury-sulfide of microbial origin in the biogeochemical cycle of HG. *Water Air Soil Pollut.* **1995,** *80* (1-4), 805-815; 10.1007/BF01189732.

34. Asaduzzaman, A.M.; Schreckenbach, G. Degradation mechanism of methyl mercury selenoamino acid complexes: a computational study. *Inorg. Chem.* **2011,** *50* (6), 2366-2372; 10.1021/ic1021406; 10.1021/ic1021406.

35. Khan, M.A.; Wang, F. Chemical demethylation of methylmercury by selenoamino acids. *Chem. Res. Toxicol.* **2010,** *23* (7), 1202-1206; 10.1021/tx100080s; 10.1021/tx100080s.

36. Fang, S.C.; Fallin, E. Uptake and subcellular cleavage of organomercury compounds by rat liver and kidney. *Chem. -Biol. Interact.* **1974,** *9* (1), 57-64; 10.1016/0009-2797(74)90067-2.

37. Morse, J.W.; Luther III, G.W. Chemical influences on trace metal-sulfide interactions in anoxic sediments. *Geochim. Cosmochim. Acta* **1999,** *63* (19-20), 3373-3378.

38. Wolthers, M.; Charlet, L.; van Der Linde, P.R.; Rickard, D.; van Der Weijden, C.H. Surface chemistry of disordered mackinawite (FeS). *Geochim. Cosmochim. Acta* **2005,** *69* (14), 3469-3481; 10.1016/j.gca.2005.01.027.

39. Hammerschmidt, C.R.; Fitzgerald, W.F.; Balcom, P.H.; Visscher, P.T. Organic matter and sulfide inhibit methylmercury production in sediments of New York/New Jersey Harbor. *Mar. Chem.* **2008,** *109* (1-2), 165-182.

40. Hollweg, T.A.; Gilmour, C.C.; Mason, R.P. Mercury and methylmercury cycling in sediments of the mid-Atlantic continental shelf and slope. *Limnol. Oceanogr.* **2010,** *55* (6), 2703-2722.

41. Schartup, A.T.; Mason, R.P.; Balcom, P.H.; Hollweg, T.A.; Chen, C.Y. Methylmercury production in estuarine sediments: Role of organic matter. *Environmental Science and Technology* **2013,** *47* (2), 695-700.

42. Mason, R.P.; Lawson, N.M.; Lawrence, A.L.; Leaner, J.J.; Lee, J.G.; Sheu, G.-. Mercury in the Chesapeake Bay. *Mar. Chem.* **1999,** *65* (1-2), 77-96.

43. Schartup, A.T.; Balcom, P.H.; Mason, R.P. Sediment-porewater partitioning, total sulfur, and methylmercury production in estuaries. *Environ. Sci. Technol.* **2014,** *48* (2), 954-960; 10.1021/es403030d; 10.1021/es403030d.

44. Benoit, J.M.; Gilmour, C.C.; Mason, R.P.; Heyes, A. Sulfide controls on mercury speciation and bioavailability to methylating bacteria in sediment pore waters. *Environ. Sci. Technol.* **1999,** *33* (6), 951-957; 10.1021/es9808200.

45. Jeong, H.Y.; Klaue, B.; Blum, J.D.; Hayes, K.F. Sorption of mercuric ion by synthetic nanocrystalline mackinawite (FeS). *Environ. Sci. Technol.* **2007,** *41* (22), 7699-7705.

46. Fitzgerald, W.F.; Lamborg, C.H.; Hammerschmidt, C.R. Marine biogeochemical cycling of mercury. *Chem. Rev.* **2007,** *107* (2), 641-662; 10.1021/cr050353m.

47. Pongratz, R.; Heumann, K.G. Production of methylated mercury and lead by polar macroalgae - A significant natural source for atmospheric heavy metals in clean room compartments. *Chemosphere* **1998,** *36* (9), 1935-1946; 10.1016/S0045-6535(97)10078-9.

48. Benoit, J.M.; Gilmour, C.C.; Mason, R.P. Aspects of bioavailability of mercury for methylation in pure cultures of Desulfobulbus propionicus (1pr3). *Appl. Environ. Microbiol.* **2001,** *67* (1), 51-58.

49. Baldi, F.; Pepi, M.; Filippelli, M. Methylmercury resistance in Desulfovibrio desulfuricans strains in relation to methylmercury degradation. *Appl. Environ. Microbiol.* **1993,** *59* (8), 2479-2485.

50. Rozan, T.F.; Benoit, G. Geochemical factors controlling free Cu ion concentrations in river water. *Geochim. Cosmochim. Acta* **1999,** *63* (19-20), 3311-3319; 10.1016/S0016-7037(99)00253-7.

51. Luther III, G.W.; Rickard, D.T. Metal sulfide cluster complexes and their biogeochemical importance in the environment. *Journal of Nanoparticle Research* **2005,** *7* (6), 389-407.

52. Mullaugh, K.M.; Luther III, G.W. Growth kinetics and long-term stability of CdS nanoparticles in aqueous solution under ambient conditions. *Journal of Nanoparticle Research* **2011,** *13* (1), 393-404.

53. Gartman, A.; Luther, G.W. Oxidation of synthesized sub-micron pyrite (FeS2) in seawater. *Geochim. Cosmochim. Acta* **2014,** *144*, 96-108; 10.1016/j.gca.2014.08.022.

54. KESTER, D.R.; DUEDALL, I.W.; CONNORS, D.N.; PYTKOWICZ, R.M. PREPARATION OF ARTIFICIAL SEAWATER. *Limnol. Oceanogr.* **1967,** *12* (1), 176-179; 10.4319/lo.1967.12.1.0176.

55. Jonsson, S.; Mazrui, N.M.; Mason, R.P. Dimethylmercury Formation Mediated by Inorganic and Organic Reduced Sulfur Surfaces. *Sci. Rep.* **2016,** *6*; 10.1038/srep27958.

56. Baya, P.A.; Gosselin, M.; Lehnherr, I.; St. Louis, V.L.; Hintelmann, H. Determination of monomethylmercury and dimethylmercury in the arctic marine boundary layer. *Environ. Sci. Technol.* **2015,** *49* (1), 223-232; 10.1021/es502601z.

57. Downs, R.; Hall-Wallace, M. The American Minerologist Crystal Structure Database. **2003,** *88*, 247-250.

58. NIST Standard Reference Database. **1984,** .

59. Rickard, D.; Luther III, G.W. Chemistry of iron sulfides. *Chem. Rev.* **2007,** *107* (2), 514-562; 10.1021/cr0503658.

60. Csákberényi-Malasics, D.; Rodriguez-Blanco, J.D.; Kis, V.K.; Recnik, A.; Benning, L.G.; Pósfai, M. Structural properties and transformations of precipitated FeS. *Chem. Geol.* **2012,** *294-295*, 249-258; 10.1016/j.chemgeo.2011.12.009.

61. Wolthers, M.; Van Der Gaast, S.J.; Rickard, D. The structure of disordered mackinawite. *Am. Mineral.* **2003,** *88* (11-12 PART 2), 2007-2015.

62. Jeong, H.Y.; Sun, K.; Hayes, K.F. Microscopic and spectroscopic characterization of Hg(II) immobilization by mackinawite (FeS). *Environ. Sci. Technol.* **2010,** *44* (19), 7476-7483; 10.1021/es100808y.

63. Stumm, W.; Morgan, J. *Aquatic chemistry: chemical equilibria and rates in natural waters.* John Wiley & Sons, Inc: United States of America, 1996.

64. Lan, Y.; Butler, E.C. Monitoring the transformation of mackinawite to greigite and pyrite on polymer supports. *Appl. Geochem.* **2014,** *50*, 1-6; 10.1016/j.apgeochem.2014.07.020.

65. Berner, R.A. A new geochemical classification of sedimentary environments. *J. Sediment. Petrol.* **1981,** *51* (2), 359-366.

66. Morgan, B.; Rate, A.W.; Burton, E.D. Trace element reactivity in FeS-rich estuarine sediments: Influence of formation environment and acid sulfate soil drainage. *Sci. Total Environ.* **2012,** *438*, 463-476; 10.1016/j.scitotenv.2012.08.088.

67. Deonarine, A.; Hsu-Kim, H. Precipitation of mercuric sulfide nanoparticles in NOM-containing water: Implications for the natural environment. *Environmental Science and Technology* **2009,** *43* (7), 2368-2373.

68. Drott, A.; Lambertsson, L.; Björn, E.; Skyllberg, U. Importance of dissolved neutral mercury sulfides for methyl mercury production in contaminated sediments. *Environmental Science and Technology* **2007,** *41* (7), 2270-2276.

69. Conaway, C.H.; Black, F.J.; Gault-Ringold, M.; Pennington, J.T.; Chavez, F.P.; Flegal, A.R. Dimethylmercury in coastal upwelling waters, Monterey Bay, California. *Environ. Sci. Technol.* **2009,** *43* (5), 1305-1309; 10.1021/es802705t.

70. Mason, R.P.; Rolfhus, K.R.; Fitzgerald, W.F. Methylated and elemental mercury cycling in surface and deep ocean waters of the North Atlantic. *Water Air Soil Pollut.* **1995,** *80* (1-4), 665-677; 10.1007/BF01189719.

71. Bowman, K.L.; Hammerschmidt, C.R.; Lamborg, C.H.; Swarr, G. Mercury in the North Atlantic Ocean: The U.S. GEOTRACES zonal and meridional sections. *Deep-Sea Res. Part II Top. Stud. Oceanogr.* **2015,** *116*, 251-261; 10.1016/j.dsr2.2014.07.004.

72. Cossa, D.; Averty, B.; Pirrone, N. The origin of methylmercury in open mediterranean waters. *Limnol. Oceanogr.* **2009,** *54* (3), 837-844.

73. Wang, F.; MacDonald, R.W.; Armstrong, D.A.; Stern, G.A. Total and methylated mercury in the beaufort sea: The role of local and recent organic remineralization. *Environ. Sci. Technol.* **2012,** *46* (21), 11821-11828; 10.1021/es302882d.

74. Weiss-Penzias, P.S.; Ortiz, C.; Acosta, R.P.; Heim, W.; Ryan, J.P.; Fernandez, D.; Collett, J.L.; Flegal, A.R. Total and monomethyl mercury in fog water from the central California coast. *Geophys. Res. Lett.* **2012,** *39* (3); 10.1029/2011GL050324.

75. Oppenheimer, C.; Scaillet, B.; Martin, R.S. Sulfur degassing from volcanoes: Source conditions, surveillance, plume chemistry and earth system impacts. *Reviews in Mineralogy and Geochemistry* **2011,** *73*, 363-421.

76. Hsu-Kim, H.; Mullaugh, K.M.; Tsang, J.J.; Yucel, M.; Luther III, G.W. Formation of Zn- and Fe-sulfides near hydrothermal vents at the Eastern Lau Spreading Center: Implications for sulfide bioavailability to chemoautotrophs. *Geochem. Trans.* **2008,** *9*; 10.1186/1467-4866-9-6.

77. Hatton, B.; Rickard, D. Nucleic acids bind to nanoparticulate iron (II) monosulphide in aqueous solutions. *Orig. Life Evol. Biosph.* **2008,** *38* (3), 257-270; 10.1007/s11084-008-9132-7.

78. Yücel, M.; Gartman, A.; Chan, C.S.; Luther III, G.W. Hydrothermal vents as a kinetically stable source of iron-sulphide-bearing nanoparticles to the ocean. *Nature Geoscience* **2011,** *4* (6), 367-371.

79. Gartman, A.; Findlay, A.J.; Luther, G.W. Nanoparticulate pyrite and other nanoparticles are a widespread component of hydrothermal vent black smoker emissions. *Chem. Geol.* **2014,** *366*, 32-41.

80. Janssen, D.J.; Conway, T.M.; John, S.G.; Christian, J.R.; Kramer, D.I.; Pedersen, T.F.; Cullen, J.T. Undocumented water column sink for cadmium in open ocean oxygen-deficient zones. *Proc. Natl. Acad. Sci. U. S. A.* **2014,** *111* (19), 6888-6893; 10.1073/pnas.1402388111.

81. Schartup, A.T.; Balcom, P.H.; Soerensen, A.L.; Gosnell, K.J.; Calder, R.S.D.; Mason, R.P.; Sunderland, E.M.; St. Louis, V.L. Freshwater discharges drive high levels of methylmercury in Arctic marine biota. *Proc. Natl. Acad. Sci. U. S. A.* **2015,** *112* (38), 11789-11794; 10.1073/pnas.1505541112.

82. Luengen, A.C.; Flegal, A.R. Role of phytoplankton in mercury cycling in the San Francisco Bay estuary. *Limnol. Oceanogr.* **2009,** *54* (1), 23-40.

83. Eisler, R. Compendium of Trace Metals and Marine Biota, In *Compendium of Trace Metals and Marine Biota*, Anonymous ;2010; .

5. Overall Conclusions

The primary aims of this work were to provide a better understanding of the reactions between Hg^{II} and MeHg with inorganic and organic reduced sulfur species and how these reactions affect the transformation of one Hg form to another. As Hg preferentially binds to reduced sulfur, the transformation (and biogeochemistry) of Hg involves and is driven by the chemistry between Hg and reduced S. The work presented in this thesis, provides new insights that lead to a deeper understanding of the interactions of Hg^{II} and MeHg with reduced sulfur and highlights the implications of these reactions on the conversion of Hg^{II} to its methylated forms.

5.1 Overview and Implications of Findings

The research was focused by a number of specific aims that were detailed and discussed in Chapter 1, and are reiterated here. The overall specific aims were:

1. To study the formation of β-HgS*(s)*$_{nano}$ in solutions containing DOM extracted from the marine environment and from the overall dynamics of the interaction of Hg^{II} with metal sulfide nanoparticles.
2. To study the methylation rates, in multiple estuaries, for Hg^{II} complexed to different reduced sulfur species that are commonly found in the sediment.
3. To study if MeHg adsorbed onto FeS_m*(s)*, other metal sulfide minerals, as we all as on low molecular weight thiols, can degrade to form DMeHg, similar to the known reaction of MeHg with H_2S.

The overall results and conclusions from the study and how these demonstrate achievement of the specific aims are detailed below.

To fulfil Specific Aim 1, we examined in Chapter 2 of this thesis, the reaction of Hg^{II} with S^{-II} in presence of marine DOM under conditions where β-HgS*(s)* should precipitate. We demonstrated that by DOM adsorbing on the surface of the growing β-HgS*(s)* sub-micron particles, DOM inhibits aggregation

and growth of β-HgS*(s)*, thereby leading to the stable formation of β-HgS*(s)* nanoparticles. The size and stability of the β-HgS$(s)_{nano}$ were found to vary with the type and concentration of the DOM. The DOM extracted from offshore marine environments and characterized by organic molecules with less humic character was less effective in controlling the growth of β-HgS*(s)* while DOM extracted from a coastal location and characterized by having more humic substances effectively controlled the growth of β-HgS*(s)*. Both types of DOM however, led to the formation of nano-sized β-HgS*(s)*. Additionally, we found that upon increasing the Hg^{II}:DOM ratio by reducing the concentration of DOM in the experimental solutions, β-HgS*(s)* particles grew in size likely by oriented attachment. However, only at very high Hg^{II}:DOM ratios (>41 μmol Hg^{II}/ mg C; >0.49 Hg/C (molar ratio)), much higher than molar ratios of Hg/C found in coastal sediments (10^{-5}-$10^{-7.5}$) did rapid aggregation and sedimentation of the particles occur.[1] Our results suggest that in both pristine and contaminated marine sediments, under conditions of supersaturation with respect to β-HgS*(s)*, it is β-HgS$(s)_{nano}$ and not microparticles (β-HgS$(s)_{micro}$) that will precipitate. The size of the particles precipitating under these natural conditions will likely be about 5 nm, meaning almost 50% of the atoms will be on the surface of the particles. The formation of β-HgS$(s)_{nano}$ has been shown before in solutions containing DOM extracted from a terrestrial or fresh water source.[2-5] Here, we show formation of β-HgS$(s)_{nano}$ using DOM extracted from offshore environments and from two coastal locations, and that these should form over the range of expected Hg^{II} and DOM concentrations in regions of intermediate sulfide concentration.

In Chapter 3, examining Specific Aim 2, we studied the methylation rate of Hg^{II} added as β-HgS$(s)_{nano}$ relative to Hg^{II} added as Hg^{II} complexed to reduced sulfur forms, as well as to $Hg^{II}(aq)$ and β-HgS$(s)_{micro}$ in different sediments. These rates were also compared to those for Hg^{II} bound to organic matter, likely via binding to thiols groups in the DOM. We found that in some sediment slurries, the methylation of β-HgS$(s)_{nano}$ was comparable to that of $Hg^{II}(aq)$, and always higher than the methylation of β-HgS$(s)_{micro}$. While previous studies have compared the methylation of β-HgS$(s)_{nano}$ capped with Suwanee River Humic Acid to commercially available β-HgS$(s)_{micro}$, our study compares methylation of β-HgS$(s)_{nano}$ to that of β-HgS$(s)_{micro}$ precipitated under similar conditions and aged for the same amount of time.[6,7] The higher

fraction and lability of surface atoms on β-HgS*(s)*$_{nano}$ relative to β-HgS*(s)*$_{micro}$ means that the dissolution kinetics of β-HgS*(s)*$_{nano}$ will be faster than those of β-HgS*(s)*$_{micro}$; and as the methylating bacteria are thought to take up only dissolved Hg^{II} complexes, the methylation rate of β-HgS*(s)*$_{nano}$ can be expected to be higher than that of β-HgS*(s)*$_{micro}$. It is also possible for the dissolution kinetics of β-HgS*(s)*$_{nano}$ to be reduced to a rate similar to that of β-HgS*(s)*$_{micro}$ based on the prevailing conditions in the sediment. For example, the presence of metal ions that can adsorb or precipitate on the reactive β-HgS*(s)*$_{nano}$ surface could reduce the presence of labile surface Hg^{II} atoms on the β-HgS*(s)*$_{nano}$, and hinder dissolution. In such a case, the bioavailability of β-HgS*(s)*$_{nano}$ to methylating bacteria will be lower than that of Hg^{II}*(aq)* and maybe similar to that of β-HgS*(s)*$_{micro}$. As the surface of the β-HgS*(s)*$_{micro}$ is less reactive than that of β-HgS*(s)*$_{nano}$ and as the methylation of β-HgS*(s)*$_{micro}$ is already very low, metal ions that adsorb or precipitate on the surface of β-HgS*(s)*$_{micro}$ may not cause an observable change in the methylation of β-HgS*(s)*$_{micro}$.

Overall, our results suggest that the precipitation of β-HgS*(s)* in marine sediments, which is predicted to occur under measured conditions based on thermodynamic calculations, will not always limit the availability of Hg^{II} to methylating bacteria. Results from this work can be used to interpret field data, and provide information needed to construct better thermodynamic models of Hg speciation in sediments. For example, in a study by Schartup *et al.*, sediment total Hg was normalized to organic carbon across a range of Hg^{II} and DOM concentrations from pristine to contaminated sites (Fig.1), and the methylation rate found to be higher at low pHg/C (- log Hg/C).[1] In our experiments where the formation of β-HgS*(s)*$_{nano}$ was investigated using different Hg^{II}:DOM ratios, the pHg/C at the lowest ratio used in our work (1.5 nmol/ mg C) was about 5 — close to the values for some of the sites examined by Schartup *et al*.[1]

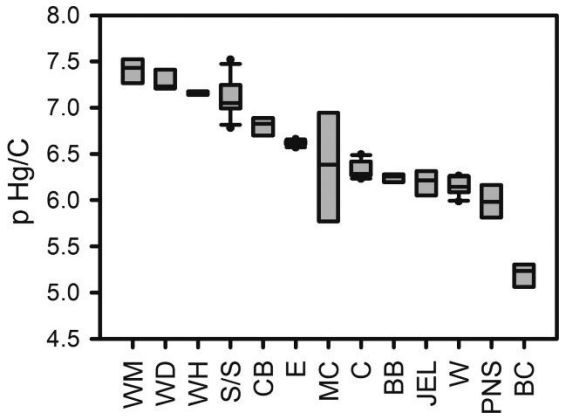

Fig. 1 Sediment total Hg concentration normalized to organic carbon across a range of Hg^{II} and DOM concentrations from pristine to contaminated sites. Each bar is an average of 2-3 sediment cores with the top and bottom of the bars representing the 25th and 75th percentile. Figure reprinted from 'Methylmercury Production in Estuarine Sediments: Role of Organic Matter', with permission from Schartup et al., *Environ. Sci. Technol.* **2013,** 47, 695-700. Copyright (2012) American Chemical Society.

In Chapter 3, we also found that Hg^{II} complexed to thiol groups in DOM was more available for methylation than all the other Hg^{II} tracers tested here. Previous studies done in pure bacterial cultures have shown that the bacteria can take up Hg-thiol complexes by active transport; however, not all types of thiols that form complexes with Hg^{II} could be taken up by the bacteria.[8,9] In this work, we have shown, in sediment slurries, that Hg-thiol complexes in DOM are taken up by the bacteria and were methylated more than two times the methylation of Hg^{II} *(aq)*. As reduced sulfur groups on DOM are associated with multiple components of the DOM, our results suggest that certain Hg-thiol complexes in DOM might be more available than others to the methylating bacteria. The presence and concentration of these thiol complexes with enhanced availability to the methylating bacteria might be a potential factor affecting mercury methylation rates in sediments.

In chapter 4, to investigate Specific Aim 3, we determined if the adsorption of MeHg on the iron sulfide phase mackinawite (FeS_m*(s)*) and on other metal sulfide minerals (HgS*(s)* and CdS*(s)*) as well as on low molecular weight thiols can degrade to form β-HgS*(s)* and DMeHg, similar to the reaction of MeHg with H_2S shown in previous studies.[10-12] We found that indeed DMeHg formed from the adsorption of MeHg on metal sulfide solids and on low molecular weight thiols. The fraction of MeHg converted to DMeHg was comparable when MeHg was reacted with the metal sulfide solids and at least 6 times greater

than when MeHg was reacted with dissolved reduced sulfur. Additionally, though the reaction of MeHg and $FeS_m(s)$ was inhibited in the presence of organic material (phytoplankton) in seawater, it was not prevented from proceeding. Based on our results, we propose a mechanism for the formation of DMeHg from the reaction of two MeHg groups adsorbed on reduced sulfur species. We suggest that DMeHg in the ocean can be formed via our proposed mechanism where MeHg reacts with low molecular weight thiols in areas of high primary production or from the reaction of MeHg with metal sulfide nanoparticles released from e.g. hydrothermal vents or those forming in low oxygen intermediate waters.[13-16] The sources of DMeHg to the ocean are not well known. Here, we propose a possible pathway, which has not been demonstrated before, for the formation of DMeHg in ocean waters.

5.2 Future Work

While the results of this thesis can be used to interpret trends in Hg^{II} methylation rates and the net production of MeHg observed in different systems, more research is needed to further elucidate the complex relation between Hg^{II} and MeHg with reduced sulfur. Some research areas that warrant further studies include:

1) Studies looking at the fraction of Hg^{II} precipitating as nanoparticulate in solutions containing Hg^{II}, S^{-II} and DOM. The mechanism of precipitation is suggested to involve first the formation of molecular clusters which then transform to nanoparticles and then to bulk precipitates.[17,18] The clusters are defined in classical nucleation theory as a group of molecules that eventually lead to the formation of a condensed phase.[17] DOM may also stabilize molecular clusters of Hg-S preventing the formation of $\beta\text{-HgS}(s)_{nano}$ just as it stabilizes $\beta\text{-HgS}(s)_{nano}$ preventing formation of $\beta\text{-HgS}(s)_{micro}$. In this case, this would mean that some Hg^{II} in the $\beta\text{-HgS}(s)_{nano}$ solutions exists in the dissolved phase as Hg-S clusters and the bioavailability of the Hg-S clusters to methylating bacteria relative to the $\beta\text{-HgS}(s)_{nano}$ would likely be enhanced. It has also been suggested that Hg

clusters can also form with polysulfides (e.g. $Hg(S_6)_2^{2-}$.[17] The bioavailability of these clusters would be a function of size and surface charge. Ultimately, knowing the fraction of Hg^{II} that actually precipitates as a micro solid phase under conditions of supersaturation would shed more light on the importance of the formation of β-HgS*(s)*$_{nano}$ for methylation in the environment.

2) Studies should be performed using porewater DOM to form β-HgS*(s)*$_{nano}$ to examine the methylation rates of β-HgS*(s)*$_{nano}$ and Hg^{II}-DOM species in sediments. In this study, we have used DOM extracted from the water column, since the extraction efficiency of the current DOM isolation techniques are low and require large volumes of water. As the collection of large amounts of porewater can be logistically challenging, we opted to extract DOM from seawater. The use of porewater DOM however, would be more representative of Hg-S-DOM conditions typically found in sediments where higher methylation rates of mercury occur.[19-21]

3) In this work, we have shown that Hg^{II}-DOM complexes are taken up by methylating bacteria preferentially over other Hg^{II} complexes commonly found in the sediment. However, reduced sulfur compounds in DOM are associated with different components of the DOM. Currently, it is analytically challenging to measure the low concentration of individual DOM components, though emerging analytical techniques hold great promise for future studies.[22] Recent studies have suggested that low molecular weight thiols, predominantly cysteine and glutathione, exist in ocean surface waters at nM concentrations and are likely present in porewaters at higher concentrations.[23] The better detection of individual thiol complexes in DOM would help in determining which Hg-thiol components in DOM form bioavailable Hg^{II} complexes and the concentration and importance of each complex to mercury methylation.

4) Studies looking at other products of the reaction between MeHg and metal sulfide solids should also be done. Here we have quantified the rate of DMeHg formation from the reaction of MeHg

with reduced sulfur species. Results from previous studies suggest that in addition to DMeHg, β-HgS*(s)* and CH_4*(g)* are other possible products that can form from the reaction of MeHg with reduced dissolved sulfur.[11,12,24,25] Future studies that quantify all the products of the reaction of MeHg with reduced sulfur species will help in determining the importance of this pathway also as a degradation mechanism for MeHg in addition to its importance for the formation of DMeHg.

References

1. Schartup, A.T.; Mason, R.P.; Balcom, P.H.; Hollweg, T.A.; Chen, C.Y. Methylmercury production in estuarine sediments: Role of organic matter. *Environmental Science and Technology* **2013,** *47* (2), 695-700.

2. Deonarine, A.; Hsu-Kim, H. Precipitation of mercuric sulfide nanoparticles in NOM-containing water: Implications for the natural environment. *Environmental Science and Technology* **2009,** *43* (7), 2368-2373.

3. Pham, A.L.T.; Morris, A.; Zhang, T.; Ticknor, J.; Levard, C.; Hsu-Kim, H. Precipitation of nanoscale mercuric sulfides in the presence of natural organic matter: Structural properties, aggregation, and biotransformation. *Geochim. Cosmochim. Acta* **2014,** *133*, 204-215; 10.1016/j.gca.2014.02.027.

4. Slowey, A.J. Rate of formation and dissolution of mercury sulfide nanoparticles: The dual role of natural organic matter. *Geochim. Cosmochim. Acta* **2010,** *74* (16), 4693-4708.

5. Gerbig, C.A.; Kim, C.S.; Stegemeier, J.P.; Ryan, J.N.; Aiken, G.R. Formation of nanocolloidal metacinnabar in mercury-DOM-sulfide systems. *Environ. Sci. Technol.* **2011,** *45* (21), 9180-9187; 10.1021/es201837h.

6. Zhang, T.; Kim, B.; Levard, C.; Reinsch, B.C.; Lowry, G.V.; Deshusses, M.A.; Hsu-Kim, H. Methylation of mercury by bacteria exposed to dissolved, nanoparticulate, and microparticulate mercuric sulfides. *Environmental Science and Technology* **2012,** *46* (13), 6950-6958.

7. Zhang, T.; Kucharzyk, K.H.; Kim, B.; Deshusses, M.A.; Hsu-Kim, H. Net methylation of mercury in estuarine sediment microcosms amended with dissolved, nanoparticulate, and microparticulate mercuric sulfides. *Environ. Sci. Technol.* **2014,** *48* (16), 9133-9141; 10.1021/es500336j.

8. Schaefer, J.K.; Rocks, S.S.; Zheng, W.; Liang, L.; Gu, B.; Morel, F.M.M. Active transport, substrate specificity, and methylation of Hg(II) in anaerobic bacteria. *Proc. Natl. Acad. Sci. U. S. A.* **2011,** *108* (21), 8714-8719; 10.1073/pnas.1105781108.

9. Schaefer, J.K.; Morel, F.M.M. High methylation rates of mercury bound to cysteine by Geobacter sulfurreducens. *Nat. Geosci.* **2009,** *2* (2), 123-126; 10.1038/ngeo412.

10. Baldi, F.; Pepi, M.; Filippelli, M. Methylmercury resistance in Desulfovibrio desulfuricans strains in relation to methylmercury degradation. *Appl. Environ. Microbiol.* **1993,** *59* (8), 2479-2485.

11. Baldi, F.; Parati, F.; Filippelli, M. Dimethylmercury and dimethylmercury-sulfide of microbial origin in the biogeochemical cycle of HG. *Water Air Soil Pollut.* **1995,** *80* (1-4), 805-815; 10.1007/BF01189732.

12. Craig, P.J.; Bartlett, P.D. The role of hydrogen sulphide in environmental transport of mercury. *Nature* **1978,** *275* (5681), 635-637.

13. Hsu-Kim, H.; Mullaugh, K.M.; Tsang, J.J.; Yucel, M.; Luther III, G.W. Formation of Zn- and Fe-sulfides near hydrothermal vents at the Eastern Lau Spreading Center: Implications for sulfide bioavailability to chemoautotrophs. *Geochem. Trans.* **2008,** *9*; 10.1186/1467-4866-9-6.

14. Yücel, M.; Gartman, A.; Chan, C.S.; Luther III, G.W. Hydrothermal vents as a kinetically stable source of iron-sulphide-bearing nanoparticles to the ocean. *Nature Geoscience* **2011,** *4* (6), 367-371.

15. Gartman, A.; Findlay, A.J.; Luther, G.W. Nanoparticulate pyrite and other nanoparticles are a widespread component of hydrothermal vent black smoker emissions. *Chem. Geol.* **2014,** *366*, 32-41.

16. Janssen, D.J.; Conway, T.M.; John, S.G.; Christian, J.R.; Kramer, D.I.; Pedersen, T.F.; Cullen, J.T. Undocumented water column sink for cadmium in open ocean oxygen-deficient zones. *Proc. Natl. Acad. Sci. U. S. A.* **2014,** *111* (19), 6888-6893; 10.1073/pnas.1402388111.

17. Rickard, D.; Luther III, G.W. Metal sulfide complexes and clusters. *Reviews in Mineralogy and Geochemistry* **2006,** *61*, 421-504.

18. Mullaugh, K.M.; Luther III, G.W. Growth kinetics and long-term stability of CdS nanoparticles in aqueous solution under ambient conditions. *Journal of Nanoparticle Research* **2011,** *13* (1), 393-404.

19. Compeau, G.C.; Bartha, R. Sulfate-reducing bacteria: Principal methylators of mercury in anoxic estuarine sediment. *Appl. Environ. Microbiol.* **1985,** *50* (2), 498-502.

20. Capone, D.G.; Kiene, R.P. Comparison of microbial dynamics in marine and freshwater sediments: Contrasts in anaerobic carbon catabolism. *Limnol. Oceanogr.* **1988,** *33* (4part2), 725-749; 10.4319/lo.1988.33.4part2.0725.

21. Mason, R.P.; Lawson, N.M.; Lawrence, A.L.; Leaner, J.J.; Lee, J.G.; Sheu, G.-. Mercury in the Chesapeake Bay. *Mar. Chem.* **1999,** *65* (1-2), 77-96.

22. Liem-Nguyen, V.; Bouchet, S.; Björn, E. Determination of sub-nanomolar levels of low molecular mass thiols in natural waters by liquid chromatography tandem mass spectrometry after derivatization with p-(hydroxymercuri) benzoate and online preconcentration. *Anal. Chem.* **2015,** *87* (2), 1089-1096; 10.1021/ac503679y.

23. Swarr, G.J.; Kading, T.; Lamborg, C.H.; Hammerschmidt, C.R.; Bowman, K.L. Dissolved low-molecular weight thiol concentrations from the U.S. GEOTRACES North Atlantic Ocean zonal transect. *Deep-Sea Res. Part I Oceanogr. Res. Pap.* **2016,** *116*, 77-87; 10.1016/j.dsr.2016.06.003.

24. Khan, M.A.; Wang, F. Chemical demethylation of methylmercury by selenoamino acids. *Chem. Res. Toxicol.* **2010,** *23* (7), 1202-1206; 10.1021/tx100080s; 10.1021/tx100080s.

25. Asaduzzaman, A.M.; Schreckenbach, G. Degradation mechanism of methyl mercury selenoamino acid complexes: a computational study. *Inorg. Chem.* **2011,** *50* (6), 2366-2372; 10.1021/ic1021406; 10.1021/ic1021406.